UNIVERSITÀ DEGLI STUDI DI MILANO

CORSO DI DOTTORATO

AGRICULTURE, ENVIRONMENT AND BIOENERGY
*XXX*VI CICLO

DIPARTIMENTO DI SCIENZE AGRARIE E AMBIENTALI

TESI DI DOTTORATO DI RICERCA

NOVEL PERSPECTIVES IN THE CONTROL OF PLANT PATHOGENIC OOMYCETES

AGR12

Demetrio MARCIANÒ

Matricola: R12861

Tutor: Prof.ssa Silvia Laura TOFFOLATTI

Co-tutor e coordinatore del corso di dottorato: Prof. Piero Attilio BIANCO

A.A. 2022-2023

Contents

Abstract

Plant pathogenic oomycetes pose significant threats to the productivity, quality and sustainability of agricultural production. Traditionally, the control of oomycete-borne diseases is achieved by means of chemical control based on fungicides. However, the negative impact of these molecules on the environment and the increase of resistant strains in the pathogen populations put stakeholders and government agencies in demand for new solutions characterized by high specificity towards the target species and low impact on human health and the environment. However, the effective development of such solutions requires overcoming interdisciplinary challenges by integrating various skills and research expertise. Moreover, it has to face some limitations caused by the biotrophic adaptation of several oomycetes species, which greatly hampers pathogen handling thus limiting the study of their biology and the efficacy screenings for new antifungals. In the present study, methods for characterizing the biology and epidemiology, and quantifying infections caused by oomycetes have been developed and/or implemented to assess the efficacy of innovative, target-specific fungicides (peptide aptamers) in limiting the growth and infection by important oomycetes such as Phytophthora infestans, Phytophthora capsici, Pythium ultimum, and Plasmopara viticola. An innovative protocol combining flow cytometry and cell sorting was successfully designed and employed to analyze the composition and efficiency of the secondary inoculum of the oomycete pathogen Plasmopara viticola, offering new insights into the epidemiology of this important pathogen and offering a new paradigm for the study of its biology. Moreover, an accessible and open-source solution for disease severity estimation at the laboratory level using digital imagery and supervised machine learning was developed and tested across three different oomycete pathosystems. The pipeline effectively detected and quantified disease symptoms with high reproducibility, offering a cost-effective and accessible solution to the plant pathology community. Lastly, the potential use of peptide aptamers targeting proteins involved in oomycete cell wall biosynthesis was investigated as a novel tool for controlling oomycete-borne diseases such as potato late blight, blight and fruit rot of cucurbits, Phytium root rot and grapevine downy mildew. Out of the 77 compounds tested, two promising molecules showed a consistently high efficacy and were characterized for their antimicrobial activity and mode of action. Overall, this research provides novel perspectives in the study of plant pathogenic oomycetes, introducing novel techniques, tools, and approaches to better understand, assess, and control plant diseases caused by oomycetes.

Riassunto

Gli oomiceti fitopatogeni rappresentano una minaccia significativa per la resa, la qualità e la sostenibilità delle produzioni agricole. Tradizionalmente, il controllo delle malattie causate da oomiceti è prevalentemente basato sul controllo chimico a base di fungicidi. Tuttavia, i rischi associati all'utilizzo di queste molecole e l'aumento di ceppi resistenti nelle popolazioni dei patogeni determinano una richiesta crescente da parte di agenzie governative e della filiera agricola di nuove soluzioni per la difesa, che siano caratterizzate da elevata specificità verso le specie bersaglio e da basso impatto sulla salute umana e sull'ambiente. Perché le nuove soluzioni siano efficaci, si devono tuttavia superare sfide importanti che richiedono un approccio interdisciplinare alla ricerca, in grado di integrare varie competenze che comprendono, tra le altre, la biologia, l'epidemiologia e la chimica. Per quanto riguarda i patogeni, si devono affrontare importanti limitazioni legate all'adattamento biotrofico di diverse specie di oomiceti, che ostacolano notevolmente la manipolazione dei ceppi, lo studio della loro biologia e l'esecuzione di saggi di efficacia per nuovi fungicidi. In questo studio sono stati sviluppati e/o implementati metodi per caratterizzare la biologia e l'epidemiologia, nonché per quantificare le infezioni causate dagli oomiceti, al fine di valutare l'efficacia di fungicidi innovativi e specifici (aptameri peptidici) nel limitare la crescita e l'infezione da importanti oomiceti quali *Phytophthora infestans*, *Phytophthora capsici*, *Pythium ultimum* e *Plasmopara viticola*.
La messa a punto di un protocollo innovativo che combina citometria a flusso e sorting cellulare ha consentito di analizzare la composizione e l'efficienza dell'inoculo secondario dell'oomicete patogeno Plasmopara viticola, ottenendo così nuove conoscenze sull'epidemiologia di questo importante patogeno e una nuova prospettiva per lo studio della sua biologia. Inoltre, è stata sviluppato e saggiato su tre diversi patosistemi comprendenti importanti oomiceti (*P. infestans*, *P. capsici* e *P. viticola*) un sistema liberamente accessibile per la stima della gravità della malattia a livello di laboratorio utilizzando immagini digitali e apprendimento automatico supervisionato. Il sistema è in grado di rilevare e quantificare i sintomi della malattia con elevata accuratezza e riproducibilità, offrendo una soluzione conveniente e accessibile alla comunità dei patologi vegetali. Infine, è stata valutata l'efficacia di fungicidi innovativi a base di aptameri peptidici selezionati per la loro capacità di inibire proteine coinvolte nella biosintesi della parete cellulare degli oomiceti. Delle 77 molecole saggiate, due hanno mostrato un elevato indice di protezione e sono quindi state caratterizzate per la loro attività antimicrobica e la loro modalità di azione. Nel complesso, questa ricerca apre una promettente prospettiva nello sviluppo di nuove strategie di controllo delle malattie causate degli oomiceti, fornendo strumenti innovativi per la caratterizzazione dei patogeni, la valutazione della gravità delle malattie, e nuove prospettive per la scoperta di fungicidi a basso impatto ambientale.

List of publications/manuscripts

Paper I

Massi, F.*****, Marcianò, D.*****, Russo, G., Stuknytė, M., Arioli, S., Mora, D., Toffolatti, S. L. (2022). Evaluation of the Characteristics and Infectivity of the Secondary Inoculum Produced by *Plasmopara viticola* on Grapevine Leaves by Means of Flow Cytometry and Fluorescence-Activated Cell Sorting. Applied and Environmental Microbiology, 88(21), e01010-22.

* Federico Massi and Demetrio Marcianò contributed equally to this article. Author order was determined in order of decreasing seniority.

Paper II

Marcianò, D., Lecchi, B., Maddalena G., Toffolatti, S. L. (2023). From the horse's mouth: an open-source platform to meet plant pathologists with computer vision and machine learning algorithms for efficient plant disease assessment. Manuscript.

Paper III

Marcianò, D *., Rosa, S.*, Colombo, M., Srivastava, V., Feni, L., Pellegrino, S., Toffolatti, S.L., Pesaresi, P., Masiero, S. (2023). CP20 and CP32 two novel antimicrobial peptide aptamers exhibiting strong anti-oomycete activity. Manuscript.

* Demetrio Marcianò and Stefano Rosa contributed equally to this article.

Author's contribution to the publications/manuscripts

Paper I

Demetrio Marcianò contributed to sample preparation, aided in cytometry experiments, contributed to manuscript's writing, and editing.

Paper II

Demetrio Marcianò designed and performed the artificial inoculation experiments, recorded the images, wrote the program code, classified the training data and supervised machine learning algorithms, performed the statistical analysis, wrote and edited the manuscript.

Paper III

Demetrio Marcianò carried out the experiments aiming to verify the efficacy and the mode of action of peptide aptamers, performed the statistical analysis, contributed to manuscript's writing, and editing.

Results disseminated in international conferences

Paper I

Oral presentation entitled: “Remodelling the anti-oomycetes efficacy screenings: exploring new frontiers and refining the existing” delivered at 16th European Conference on Fungal Genetics, Innsbruck Austria, 5-8th March 2023.

Paper II & III

Oral presentation entitled: “A step forward in the application and teaching of modern statistical methods for plant pathology” delivered at 12th International Congress of Plant Pathology (ICPP), Lyon, France, 20-25th August 2023.

Additional scientific publications not included in this thesis work

1. Toffolatti, S. L., Davillerd, Y., D'Isita, I., Facchinelli, C., Germinara, G. S., Ippolito, A., **Marcianò, D**... & Romanazzi, G. (2023). Are Basic Substances a Key to Sustainable Pest and Disease Management in Agriculture? An Open Field Perspective. Plants, 12(17), 3152. DOI: 10.3390/plants12173152.
2. Kumar, R., Meghwanshi, G. K., **Marcianò, D**., Ullah, S. F., Bulone, V., Toffolatti, S. L., & Srivastava, V. (2023). Sequence, structure and functionality of pectin methylesterases and their use in sustainable carbohydrate bioproducts: A review. International Journal of Biological Macromolecules, 125385. DOI: 10.1016/j.ijbiomac.2023.125385.
3. **Marcianò, D.***, Ricciardi, V.*, Maddalena, G., Massafra, A., Marone Fassolo, E., Masiero, S., ... & Toffolatti, S. L. (2023). Influence of Nitrogen on Grapevine Susceptibility to Downy Mildew. Plants, 12(2), 263. DOI: 10.3390/plants12020263.
4. **Marcianò, D**., & Toffolatti, S. L. (2023). Methods for Fungicide Efficacy Screenings: Multiwell Testing Procedures for the Oomycetes Phytophthora infestans and Pythium ultimum. Microorganisms, 11(2), 350. DOI: 10.3390/microorganisms11020350.
5. Marone Fassolo, E., Lecchi, B., **Marcianò, D.**, Maddalena, G., & Toffolatti, S. L. (2022). Pathogen Adaptation to American (Rpv3-1) and Eurasian (Rpv29) Grapevine Loci Conferring Resistance to Downy Mildew. Plants, 11(19), 2619. DOI: 10.3390/plants11192619.
6. **Marcianò, D***., Ricciardi, V*., Marone Fassolo, E., Passera, A., Bianco, P. A., Failla, O., ... & Toffolatti, S. L. (2021). RNAi of a putative grapevine susceptibility gene as a possible downy mildew control strategy. Frontiers in Plant Science, 12, 667319. DOI: 10.3389/fpls.2021.667319.
7. Ricciardi, V*., **Marcianò, D***., Sargolzaei, M., Maddalena, G., Maghradze, D., Tirelli, A., ... & De Lorenzis, G. (2021). From plant resistance response to the discovery of antimicrobial compounds: The role of volatile organic compounds (VOCs) in grapevine downy mildew infection. Plant Physiology and Biochemistry, 160, 294-305. DOI: 10.1016/j.plaphy.2021.01.035.

***Authors contributed equally to this article and share the first authorship.**

List of abbreviations

ABC: Adaptive Boosting Classifier
BA: Bland-Altman (plot)
BRM: beta regression model
CCC: concordance correlation coefficient
CesA: Cellulose synthase subunit A
CHAPS: 3-[(3-cholamidopropyl)dimethylammonio]-1-propanesulfonate
CP: cyclic peptide
Cpm: count per minutes
DA: Diseased Area
DCB: 2,6-Dichlorobenzonitrile
DE: detergent extracts
DMSO: dimetylsulphoxide
dpi: days post inoculation
DRA: dose-response analysis
DSI: disease severity index
DTC: Decision Tree Classifier
ECx: effective concentrations
EMMs: estimated marginal means
FACS: fluorescence activated cell sorting
FCM: flow cytometry
GAL4-AD: GAL4 Activating Domain
GAL4-BD: GAL4 Binding Domain
GIPL: Growth inhibition percentage (liquid medium)
GIPS: Growth inhibition percentage (solid medium)
Glc: glucose
GPU: Graphical Processing Unit
hpi: hours post inoculation
KNN: K-Nearest Neighbors
LOA: limits of agreement
MF: microsomal fractions
MLPC: Multi-layer Perceptron Classifier
NBC: Naive Bayes Classifier
PA: peptide aptamers
PAM: pea agar medium

PBS: Phosphate Buffered Saline

PCR: Polymerase chain reaction

PDA: Potato Dextrose Agar

PDB: Potato Dextrose Broth

PPI: Percentage Protection Index

QDA: Quadratic Discriminant Analysis

RFC: Random Forests Classifier

RP-HPLC: reverse phase high performance liquid cromatography

Skimage: Scikit-image

Sklearn: Scikit-learn

SML: supervised machine learning

SPPS: solid-phase peptide synthesis

TLC: Thin Layer Chromatography

UDP-Glc: Uridine diphosphate glucose

Y2H: Yeast two hybrid

Introduction

The oomycete phylum and phytopathogenic species lifestyles

Oomycetes are fungal-like organisms, and despite their morphological resemblance to filamentous fungi, they are phylogenetically related to diatoms and brown algae. As a result, they were recently classified within the TSAR eukaryotic supergroup [1]. The oomycete phylum comprises several genera that are widely recognized as phytopathogens and are notorious for causing devastating diseases in numerous plants and cultivated crops [2]. Oomycete borne diseases in plants cause annual losses in the order of tens of billions of dollars [3], and the multimillion market value associated on active ingredients available for oomycete control, suggests the relevant economic impact of these organisms [4]. Phytopathogenic oomycetes are adapted to terrestrial habitats, and according to recent studies parasitism on angiosperms has evolved independently in at least four lineages because of co-evolution with specific hosts. This fact resulted in variegated lifestyles and strategies adopted to infect plants which differ among taxa in terms of host, development, infection site, penetration mode, mycelium formation, and propagation [5]. Primary infections are usually originated by soilborne inoculum in the form of mycelium or sexual diploid spores (oospores) and can affects both roots and above ground organs (e.g. leaves, flowers or fruits). On the other hand, asexual spores (sporangia and zoospores) produced in large quantities from infected tissues are responsible for secondary infections through an efficient propagation often driven by wind and humid environments. Indeed, sporangia in several genera produce flagellate zoospores, devoid of cell wall, which reach the infection site, where they encyst (i.e. loose flagella and deposit cell wall) and penetrate the host tissues. Alternatively, sporangia can germinate directly, thus reducing their dependence on water, and a facultative switch between these two modes triggered by temperature has been described for some genera (e.g. *Phytophthora*). Mode of penetration is also variegated, indeed parasitic oomycetes can form appressoria to invade the inner tissues of the plant by direct penetration in roots (e.g. *Pythium*) or leaves (e.g. *Phytophthora, Peronospora*, *Bremia*) while others exploit natural openings in the plant as the entry point (e.g. *Plasmopara* viticola) [6]. After penetration, patterns of plant colonization depend on the lifestyle of the pathogen (Figure 1). Usually, phytopathogenic oomycetes are divided in three main groups according to their lifestyle. Necrotrophic pathogens kill host cells and consume the released nutrients with their hyphae growing intercellularly or intracellularly, acquiring the nutrients they need from dead and dying cells. On the contrary, biotrophic species feed and grow on the host's living tissues, therefore are highly adapted to the host, and generally secrete an arsenal of effectors to avoid plant defense mechanisms. Indeed, to establish a successful feeding relationship biotrophs must minimize the disruption of the host structures, therefore their hyphae ramify through the intercellular spaces, and acquire nutrients through the formation of haustoria. These are specific feeding structures formed through a localized degradation of the plant cell wall and the invagination

of the plant plasma membrane. Hemibiotrophs exploit both infection strategies, suppressing or avoiding plant defences during early stages of infection and then shifting to necrotrophy and rapidly killing the host tissues [7, 8, 9]. Necrotrophs and hemibiotrophs can usually be cultivated on artificial media based on energy-rich carbohydrates and other nutrients, whereas this is not possible for biotrophic oomycetes, which are so adapted to their host that they lost several metabolic pathways such as those related to nitrogen and sulfur assimilation [6, 8].

Figure 1: infection strategies and lifestyles of phytopathogenic oomycetes. (a) Typical asexual Phytophthora dispersal structures. (b) Leaf colonization. (c) Root colonization. Reprinted from "Oomycete interactions with plants: infection strategies and resistance principles", Fawke S et al., 2015 [5].

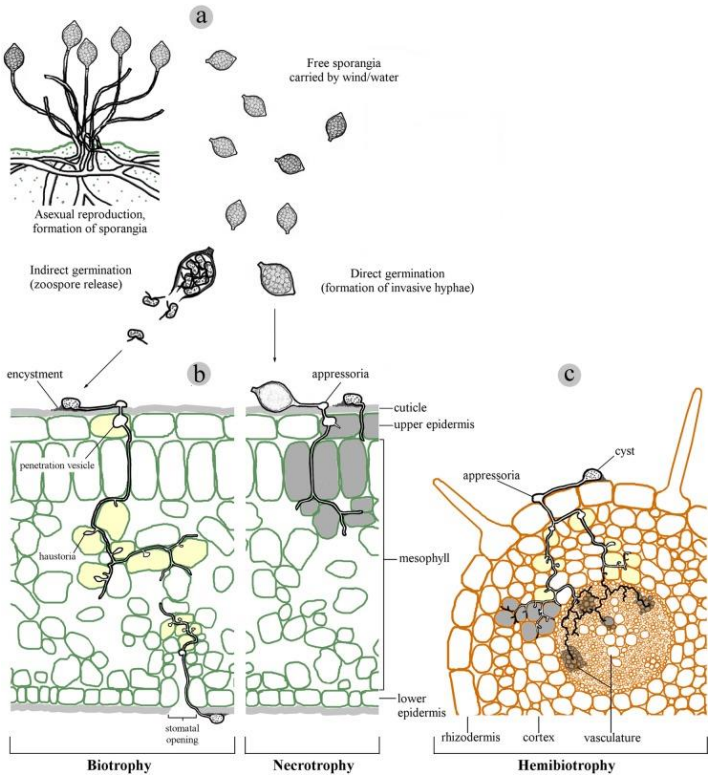

Phytopathogenic oomycetes control: state of the art and research needs

Integrated plant disease management is a paradigm approach to plant protection involving an extensive strategy incorporating all the suitable skills, practices, and techniques available to control harmful organisms [10]. However, despite the wide application of integrated approaches like monitoring, coupled with the adoption of agronomic practices and the exploitation of genetic and biological resources, the control of oomycete-borne diseases mostly relies on the use of fungicides, which still represent the most efficient control strategy [11, 12, 13]. The drawback side effects related to the large use of these compounds over the last 60 years resulted in harmful consequences to the environment and human health [14] (Figure 2). For this reason, to achieve greater sustainability

several international agencies advocate for the reduction of chemical pesticides, emphasizing the need to develop alternative strategies to maintain crop yields while simultaneously limiting the negative impacts of traditional pesticides [14]. In this context, the rapid emergence of fungicide resistance, and increasingly stringent environmental regulations significantly reduced the success rate of traditional methods for fungicide discovery. Consequently, stakeholders need to identify innovative approaches that can efficiently steer discovery efforts, allowing them to adapt swiftly to evolving market conditions [15]. Therefore, enhancing collaboration between industry and academia, encouraging the synergistic application of diverse expertise (pathogen cell biology, plant pathology, biotechnological approaches, synthetic organic chemistry and toxicology), with the goal of developing a new generation of fungicides characterized by high specificity towards target species and low environmental impact, will play a major role in global food security for the next years [16].

Figure 2: Global map of the number of agrochemicals posing risks to the environment. The map has a spatial resolution of 5 arcmin, which is approximately 10 km × 10 km at the Equator. The pie charts represent the fraction of agricultural land contaminated by different numbers of agrochemicals in each region, and the values in parentheses above the pie charts denote the total agricultural land in that region. Reprinted from "Risk of pesticide pollution at the global scale", Tang F.H. et al., 2021 [17].

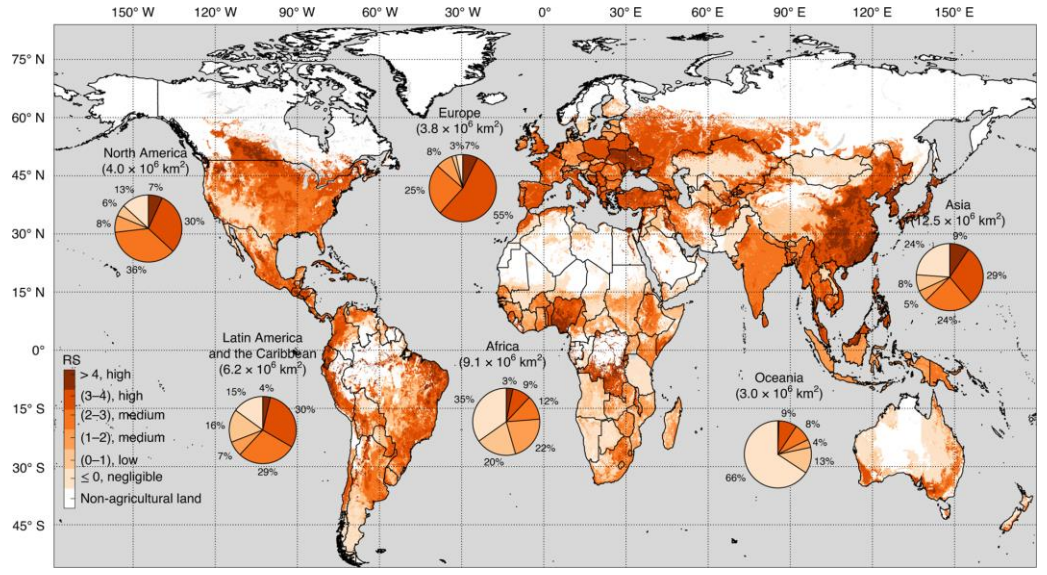

Oomycete species handling and study: current limitations and research needs

The biotrophic adaptation of several oomycete pathogens poses a significant negative impact on the cultivation of these organisms, and this badly reflects on the research practices. This situation highlights the need for the efficient development of high-throughput strategies to improve such pathogens characterization. For instance, in the case of *P. viticola*, a major pathogen affecting grapevines, all in vitro testing procedures currently rely on methods such as leaf disc inoculation or spore germination assessment. Since the cultivation of this pathogen is only feasible on grapevine

tissues, and sporangia represent the main source of material that can be easily isolated from the plant. However, the use of such techniques is highly resource-intensive and comes with certain limitations [18]. In recent years, significant advances in the development of single-cell analytical tools (e.g. flow cytometry and cell sorting) improved sample characterization and increased the availability of omics analyses (e.g. genomics, transcriptomics, and proteomics) at the cellular level, thus positively impacting drug discovery and development in the field of human medicine [19]. The successful transposition of these techniques to oomycete biology could support and improve traditional techniques and provide similar benefits to the study of *P. viticola* and oomycete biology meanwhile providing a new paradigm for efficacy screenings of new-generation fungicides.

Bioassays carried out on inoculated plant tissues, such as leaf disc bioassays, play a crucial role in evaluating plant pathogen interactions and in the development and validation of new active compounds. Disease severity estimation (i.e. measure of the amount of disease per sampling unit) is a key factor in the phenotyping tasks related to plant-pathogen interaction, both in the field and at the laboratory level (Figure 3) [20]. Traditionally, this activity is carried out by experts in the field of study, specifically plant pathologists, who conduct visual assessments of the diseased area, sometimes with the assistance of standard area diagrams. However, visual estimation is subjected to some drawbacks, including overestimating or underestimating the severity. These errors are often induced by the subjective traits associated with different raters or with the experimental set-up [21]. To overcome these issues and to ensure accurate measurements of severity, visible light photography and digital image analysis have become progressively more popular, and several tools for disease severity estimation have been developed [22]. Despite the great progress made over the last 20 years in developing tools and techniques for plant phenotyping, the performance and reliability of developed methods are frequently questioned by the potential users, particularly due to challenges in linking biological causes to machine learning features. Therefore, to bridge the gap between users and developers, special efforts must be undertaken, involving particular emphasis in intercommunication between the parts involved. For this reason, fostering stronger connections and coordination between plant pathologists and computer scientists is recommended and will play a pivotal role in the coming years. This collaboration aims to define common research perspectives and goals, and hopefully, contribute to the successful progress in both research and practice, even in the field of phytopathometry [23].

Figure 3: (A) Late blight symptoms caused by *P. infestans* on potato tuber; (B) Late blight symptoms caused by *P. infestans* on potato leaves (photograph by Rasback, distributed under a CC-BY 3.0 license); (C) *P. viticola* sporulation on grapevine leaves (photograph by Lucyin, distributed under a CC-BY 4.0 license); (D) *P. capsici* blight on sweet pepper stem (photograph by Don Ferrin, distributed under a CC-BY 3.0 license).

Aims of the thesis

The primary objective of this study was to develop an innovative protocol that integrates flow cytometry and cell sorting techniques to analyze both the composition and efficiency of the inoculum produced by the oomycete pathogen *P. viticola*, overcoming the limitations of traditional methods (Paper I). The second objective was to introduce an accessible and open-source solution for disease severity estimation at the laboratory level, utilizing digital imagery and supervised machine learning. Special emphasis was placed on providing a user-friendly tool for the plant pathology community, with experts in the field playing a central role in the decision-making process (Paper II). In the last work, the antimicrobial activity and mode of action of peptide aptamers targeting proteins involved in the biosynthesis of oomycete cell walls were evaluated as innovative low impact and target specific fungicides (Paper III).

References (Introduction)

1. Burki F, Roger AJ, Brown MW, Simpson AG. 2020. The new tree of eukaryotes. Trends in ecology & evolution 35:43–55.
2. Kamoun S, Furzer O, Jones JD, Judelson HS, Ali GS, Dalio RJ, Roy SG, Schena L, Zambounis A, Panabières F. 2015. The Top 10 oomycete pathogens in molecular plant pathology. Molecular plant pathology 16:413–434.
3. Tyler, B.M. 2010. Towards a systems-level understanding of oomycete-plant interactions. In Genome-Enabled Analysis of Plant-Pathogen Interactions; Wolpert, T., Shiraishi, T., Collmer, A., Akimitsu, K., Glazebrook, J., Eds.; American Phytopathological Society: St. Paul, MN, USA; pp. 161–174.
4. Gisi U, Sierotzki H. 2015. Oomycete fungicides: Phenylamides, quinone outside inhibitors, and carboxylic acid amides. Fungicide resistance in plant pathogens: principles and a guide to practical management 145–174.
5. Fawke S, Doumane M, Schornack S. 2015. Oomycete interactions with plants: infection strategies and resistance principles. Microbiology and Molecular Biology Reviews 79:263–280.
6. Spring O, Gomez-Zeledon J, Hadziabdic D, Trigiano RN, Thines M, Lebeda A. 2018. Biological characteristics and assessment of virulence diversity in pathosystems of economically important biotrophic oomycetes. Critical Reviews in Plant Sciences 37:439–495.
7. Hardham AR. 2007. Cell biology of plant–oomycete interactions. Cellular microbiology 9:31–39.
8. Baxter L, Tripathy S, Ishaque N, Boot N, Cabral A, Kemen E, Thines M, Ah-Fong A, Anderson R, Badejoko W. 2010. Signatures of adaptation to obligate biotrophy in the Hyaloperonospora arabidopsidis genome. science 330:1549–1551.
9. Ah-Fong AM, Kagda MS, Abrahamian M, Judelson HS. 2019. Niche-specific metabolic adaptation in biotrophic and necrotrophic oomycetes is manifested in differential use of nutrients, variation in gene content, and enzyme evolution. PLoS Pathogens 15:e1007729.
10. Khan SM, Ali S, Nawaz A, Bukhari SAH, Ejaz S, Ahmad S. 2019. Integrated pest and disease management for better agronomic crop production. Agronomic Crops: Volume 2: Management Practices 385–428.
11. Taxvig C, Hass U, Axelstad M, Dalgaard M, Boberg J, Andeasen HR, Vinggaard AM. 2007. Endocrine-disrupting activities in vivo of the fungicides tebuconazole and epoxiconazole. Toxicological Sciences 100:464–473.
12. Zubrod JP, Bundschuh M, Feckler A, Englert D, Schulz R. 2011. Ecotoxicological impact of the fungicide tebuconazole on an aquatic decomposer-detritivore system. Environmental Toxicology and Chemistry 30:2718–2724.
13. Thind TS, Hollomon DW. 2018. Thiocarbamate fungicides: reliable tools in resistance management and future outlook. Pest management science 74:1547–1551.
14. Rosa S, Pesaresi P, Mizzotti C, Bulone V, Mezzetti B, Baraldi E, Masiero S. 2022. Game-changing alternatives to conventional fungicides: Small RNAs and short peptides. Trends in Biotechnology 40:320–337.
15. Liu C, Guan A, Yang J, Chai B, Li M, Li H, Yang J, Xie Y. 2016. Efficient approach to discover novel agrochemical candidates: intermediate derivatization method. Journal of agricultural and food chemistry 64:45–51.
16. Steinberg G, Gurr SJ. 2020. Fungi, fungicide discovery and global food security. Fungal Genetics and Biology 144:103476.
17. Tang FH, Lenzen M, McBratney A, Maggi F. 2021. Risk of pesticide pollution at the global scale. Nature Geoscience 14:206–210.
18. Massi F, Torriani SF, Borghi L, Toffolatti SL. 2021. Fungicide resistance evolution and detection in plant pathogens: Plasmopara viticola as a case study. Microorganisms 9:119.
19. Heath JR, Ribas A, Mischel PS. 2016. Single-cell analysis tools for drug discovery and development. Nature reviews Drug discovery 15:204–216.
20. Nutter FW, Esker PD, Netto RAC. 2006. Disease assessment concepts and the advancements made in improving the accuracy and precision of plant disease data. European Journal of Plant Pathology 115:95–103.
21. Bock CH, Barbedo JG, Del Ponte EM, Bohnenkamp D, Mahlein A-K. 2020. From visual estimates to fully automated sensor-based measurements of plant disease severity: status and challenges for improving accuracy. Phytopathology Research 2:1–30.
22. Habib A, Abdullah A, Puyam A. 2022. Visual Estimation: A Classical Approach for Plant Disease Estimation. Trends in Plant Disease Assessment 19–45.
23. Kuska MT, Heim RH, Geedicke I, Gold KM, Brugger A, Paulus S. 2022. Digital plant pathology: A foundation and guide to modern agriculture. Journal of Plant Diseases and Protection 129:457–468.

Paper I

Introduction to paper I

Flow cytometry (FCM) is a powerful technique which allows the rapid multi-parametric analysis of single cells in suspensions. Thanks to a wide range of fluorescent reporters, both living or fixed cells can be stained to monitor metabolic processes or different cell compartments. Moreover, through fluorescence activated cell sorting (FACS), one can select cells for downstream experiments based on fluorescence and/or light scattering properties. Usually, applications in filamentous organisms are hampered by hyphal growth, therefore spores are commonly analyzed in conventional flow cytometers. Downy mildew, caused by the oomycete *P. viticola*, is a devastating disease that affects grapevines, leading to reduced yields and quality of grapes. The causal agent is a polycyclic organism capable of multiple secondary infection cycles within a single grapevine growing season. Therefore, secondary infections are mostly driven by the production of asexual spores (sporangia and zoospores), which play a vital role in the success of the pathogen. Current methods employed to study the secondary inoculum are based on visual observation under the microscope or at the spectrophotometer of zoospores' release. However, the reliability of such methods is limited to zoospore production and mobility and do not take into account the actual infection efficiency on grapevine tissues. In this context, during my PhD we developed a novel protocol combining FCM and FACS to analyze the composition and infection efficiency of the *P. viticola* secondary inoculum. In the following section, we introduce the first research article included in this thesis work, named paper I.

AMERICAN SOCIETY FOR MICROBIOLOGY | Applied and Environmental Microbiology®

Evaluation of the Characteristics and Infectivity of the Secondary Inoculum Produced by *Plasmopara viticola* on Grapevine Leaves by Means of Flow Cytometry and Fluorescence-Activated Cell Sorting

Federico Massi,[a] Demetrio Marcianò,[a] Giuseppe Russo,[b] Milda Stuknytė,[c] Stefania Arioli,[d] Diego Mora,[d] Silvia L. Toffolatti[a]

[a]Dipartimento di Scienze Agrarie e Ambientali, Università degli Studi di Milano, Milan, Italy
[b]Ordine dei Dottori Agronomi e dei Dottori Forestali di Milano, Milan, Italy
[c]Unitech COSPECT – Piattaforme Tecnologiche di Ateneo, Università degli Studi di Milano, Milan, Italy
[d]Dipartimento di Scienze per gli Alimenti, la Nutrizione e l'Ambiente, Università degli Studi di Milano, Milan, Italy

Federico Massi and Demetrio Marcianò contributed equally to this article. Author order was determined in order of decreasing seniority.

ABSTRACT

Plasmopara viticola, the oomycete causing grapevine downy mildew, is one of the most important pathogens in viticulture. *P. viticola* is a polycyclic pathogen, able to carry out numerous secondary cycles of infection during a single vegetative grapevine season, by producing asexual spores (zoospores) within sporangia. The extent of these infections is strongly influenced by both the quantity (density) and quality (infectivity) of the inoculum produced by the pathogen. To date, the protocols for evaluating all these characteristics are quite limited and time-consuming and do not allow all the information to be obtained in a single run. In this study, a protocol combining flow cytometry (FCM) and fluorescence-activated cell sorting (FACS) was developed to investigate the composition, the infection efficiency and the dynamics of the inoculum produced by *P. viticola* for secondary infection cycles. In our analyses, we identified different structures within the inoculum, including degenerated and intact sporangia. The latter have been sorted, and single sporangia were directly inoculated on grapevine leaf discs, thus allowing a thorough investigation of the infection dynamics and efficiency. In detail, we determined that, in our conditions, 8% of sporangia were able to infect the leaves and that on a susceptible variety, the time required by the pathogen to reach 50% of total infection is about 10 days. The analytical approach developed in this study could open a new perspective to shed light on the biology and epidemiology of this important pathogen.

IMPORTANCE

P. viticola secondary infections contribute significantly to the epidemiology of this important plant pathogen. However, the infection dynamics of asexual spores produced by this organism are still poorly investigated. The main challenges in dissecting the grapevine-*P. viticola* interaction in vitro are attributable to the biotrophic adaptation of the pathogen. This work provides new insights into the infection efficiency and dynamics imputable to *P. viticola* sporangia, contributing useful information on grapevine downy mildew epidemiology. Moreover, future applications of the sorting protocol developed in this work could yield a significant and positive impact in the study of *P. viticola*, providing unmatched resolution, precision, and accuracy compared with the traditional techniques.

KEYWORDS plant pathology, obligate parasite, fungal disease, epidemiology, infection dynamics

Editor Irina S. Druzhinina, Royal Botanic Gardens

Address correspondence to Silvia L. Toffolatti, silvia.toffolatti@unimi.it, or Stefania Arioli, stefania.arioli@unimi.it.

The authors declare no conflict of interest.

Received 17 June 2022

Accepted 20 September 2022
Published 17 October 2022

Grapevine downy mildew, caused by the phytopathogenic oomycete *Plasmopara viticola* (Berk. et Curtis) Berl. & De Toni (kingdom Chromista, phylum Oomycota, class Oomycetes, order Peronosporales, family Peronosporaceae), is one of the major threats to grapevine production worldwide. Indeed, severe disease epidemics caused by this oomycete are often associated with consistent quantitative and qualitative yield losses (1).

P. viticola is an obligate, biotrophic pathogen, able to undergo numerous infection cycles during a single grapevine-growing season (2). In autumn, the pathogen develops overwintering structures differentiated by sexual reproduction (oospores), through which it survives the winter period embedded in dead leaves on the vineyard floor (2–4). In spring, during favorable climatic conditions (5), oospores germinate producing macrosporangia that, in turn, produce zoospores. Receptive tissues of grapevine leaves are infected by zoospores through splashing by rain, which leads to the primary infections through stomata penetration (6, 7). The pathogen develops an intercellular mycelium with haustoria (feeding structures) and, in high humidity conditions, differentiates into sporangiophores that emerge from stomata and produce sporangia, which will originate secondary infections cycles through the emission of new zoospores (2).

Oospores are considered to play a principal role in triggering the epidemics in the early grapevine season, providing the inoculum for primary infections, while the subsequent stages (secondary infections) are more attributed to the inoculum generated by asexual reproduction through the differentiation of sporangia (1, 3).

Although there are many testing methods to investigate the oospore germination process and oospore infection efficiency (3, 5, 8–12), to the best of our knowledge no studies have been conducted to evaluate the infection potential associated with the sporangia inoculum in vineyards. To date, testing methodologies on sporangia germination are limited because they can provide only a qualitative description of the infection process, and it is not possible to obtain a precise estimation of the percentage of sporangia able to positively infect grapevine plants in the population tested (13, 14). The only exception to this statement is represented by a few methods developed for the quantification of sporangia germination, which are based on visual observation under the microscope or at the spectrophotometer of zoospores' release (14–19). However, the reliability of this type of data are quite limited, as it only evaluates the release and mobility of the zoospores in aqueous suspension without considering the outcome of the infection process on grapevines' tissues. For these reasons, the data obtainable by investigating the primary and secondary infection cycles are not homogeneous and create a gap in the available information.

Fluorescence-activated cell sorting (FACS) is a technique to purify specific cell populations based on phenotypes or fluorescence detected by flow cytometry (FCM), which can represent an interesting opportunity to improve information on the sporangia infection process (20–22). Briefly, FCM is a technology able to provide rapid multiparametric analysis of single cells in suspension using lasers as light sources to produce both scattered and fluorescent light signals that are read by detectors such as photodiodes or photomultiplier tubes (23). These signals are converted into electronic signals which are analyzed by a computer. FACS implementation provides a method for separating a heterogeneous mixture of cells into two or more containers, one cell at a time, based upon the specific light scattering and fluorescent characteristics of each cell (24). Considering the continuous advancement of these technologies, the use of FCM rapid protocols to quantify single cells, such as fungal spores, can be set up. Indeed, FCM allows the researcher to monitor different parameters to distinguish between living and dead cells, such as membrane permeability, efflux pumps, or enzymatic activity and loss of membrane potential (25).

Implementation of FCM technologies in fungal plant pathogens investigations could be a useful and innovative approach, which in the case of *P. viticola*, could permit us to bridge the gap of information obtainable by studying the infection process in the different life stages of pathogens as mentioned above. This could represent a big step forward in the study of grapevine downy mildew, allowing the study of the secondary infection cycles of the pathogen with greater completeness and providing quantitative data. To date, no reports of applications of FMC on infection efficiency screening in plant pathogens are available. To the best of our knowledge, the only

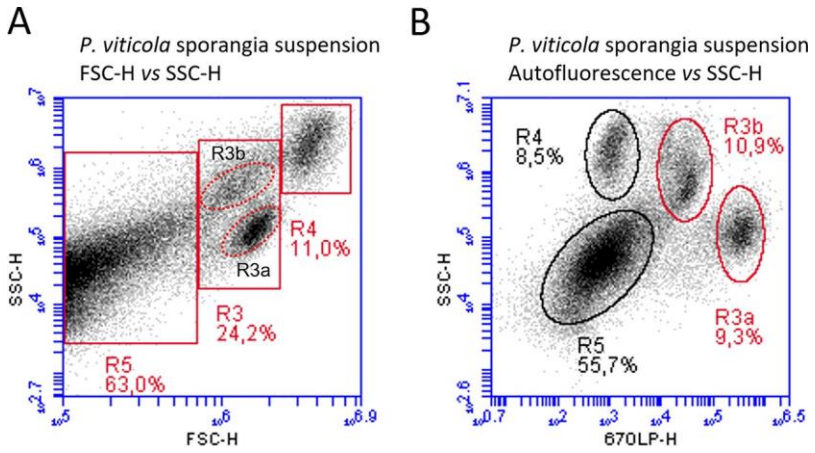

FIG 1 (A) FSC-H (particle size) versus SSC-H (granularity) density plot of a *P. viticola* sporangia suspension. (B) SSC-H (granularity) versus red fluorescence (670LP-H) density plot: four distinct subpopulations are visible (R3a, R3b, R4, and R5).

implementations of FCM have been carried out on the related oomycete species *Phytophthora infestans* (Mont.) de Bary (kingdom Chromista, phylum Oomycota, class Oomycetes, order Peronosporales, family Peronosporaceae) (26, 27). In particular, Day and collaborators used FCM to discriminate P. infestans sporangia from other airborne biological particles by using light scatter parameters and fluorescent staining. A single study was performed on *P. viticola*, to determine the sporangia viability exposed to chlorine dioxide using fluorescent dyes (28).

The aim of the present work was to characterize the sporangia suspension composition of *P. viticola* and to evaluate its infection efficiency and dynamics. This was accomplished by developing a FACS-mediated single-sporangia infection assay.

RESULTS

The molecular characterization confirmed that the ITS sequence of the isolate used in this study (OP326699) belongs to *P. viticola* species (98.1% identity with *P. viticola* internal transcribed spacer 1, 5.8S rRNA gene, and internal transcribed spacer 2, GenBank id DQ665668.1).

FCM and light microscopy discriminate the different components of *P. viticola* inoculum. The sporangia suspension of *P. viticola* obtained from infected grapevine leaves was analyzed by FCM. First, the analysis was carried out considering FSC-H and SSC-H parameters related to the ability of a particle to scatter the light. In detail, FSC-H and SSC-H are proportional to particle size and granularity, respectively (29). Results were represented in a two-dimensional plot (Fig. 1A). Both parameters have been shown to correlate with cell size and particle composition/complexity (30) and were represented with logarithmic scale. Based on FSC-H, we identified three populations (gates R3, R4, and R5) with different dimensions (R5, R3, R4). Indeed, the higher the FSC-H, the larger the particle. Interestingly, population R3 was composed by two subpopulations (R3a and R3b), differing in the SSC-H parameter. Particularly, R3a was characterized by a lower SSC-H value compared with R3b. Based on these data, SSC-H signal resulted the most discriminating parameter (rather than FSC-H) for highlighting the morphological heterogeneity of a complex suspension.

It is known that certain biological particles exhibit “autofluorescence.” Indeed, in *Blumeria graminis* DC Speer (kingdom Fungi, phylum Ascomycota, class Leotiomycetes, order Erysiphales, family Erysiphaceae) and *P. infestans* nonviable conidia and killed sporangia, respectively, exhibited red autofluorescence (27). Based on these findings, we analyzed *P. viticola* sporangia suspension by correlating light scattering (SSC-H) and intrinsic fluorescence parameters collected in the FL3 channel (Fig. 1B). It clearly appeared that some of the particles exhibited various levels of red fluorescence. Red

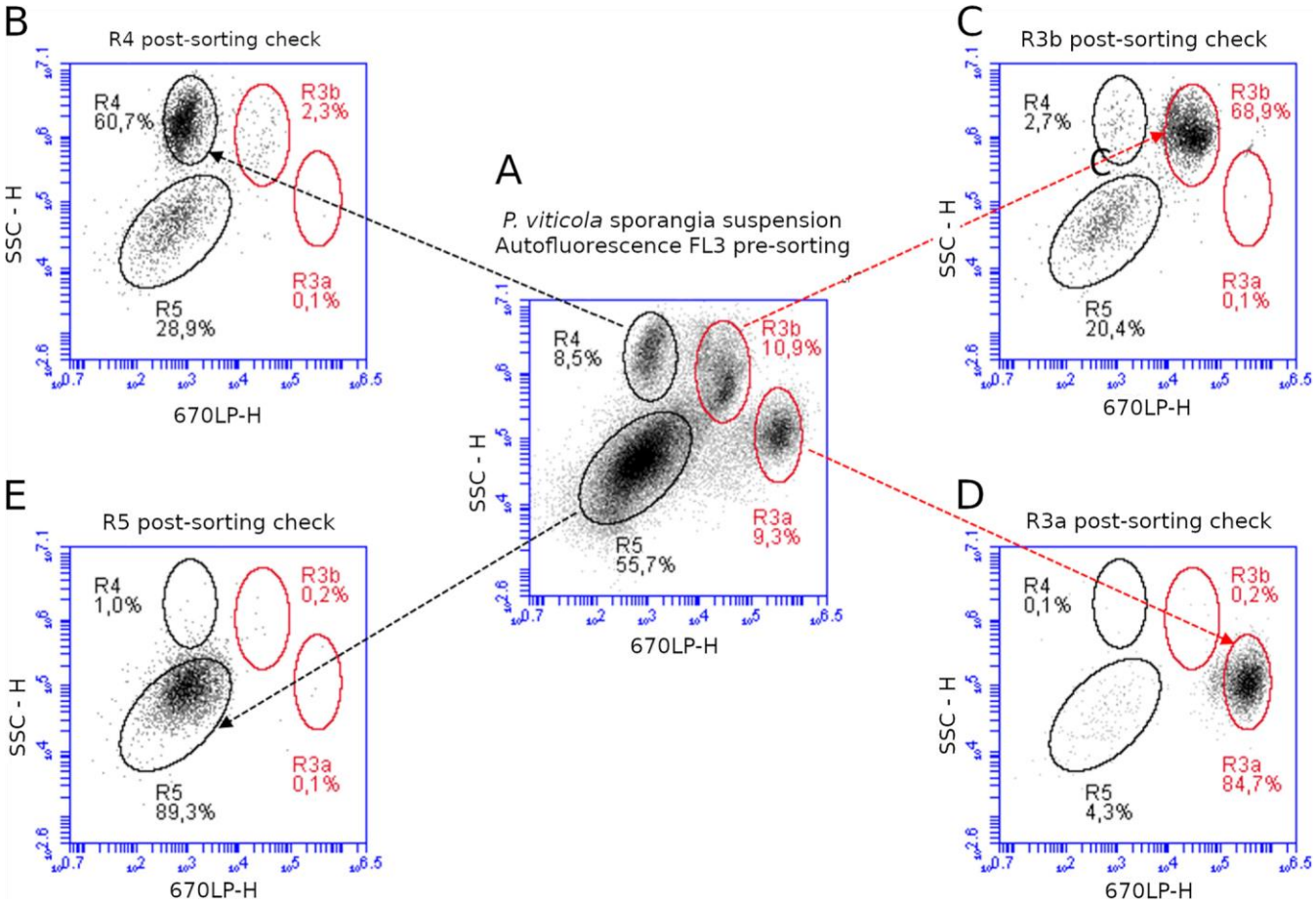

FIG 2 SSC-H (granularity) versus Red-fluorescence (670LP-H) density plots of the *P. viticola* four subpopulations before (A) and after FACS sorting (B to E). Subpopulation sorting is visible in B (R4), C (R3b), D (R3a), and E (R5) plots.

fluorescence values were comparable between R4 and R5 populations (1,071 6 53 RFU and 1,247 6 62 RFU, respectively). Conversely, R3a and R3b populations (those derived from R3 based on FSC-H and SSC-H) exhibited higher levels of fluorescence (382,138 6 19,106 RFU and 27500 6 1375 RFU, respectively).

Our results showed that SSC-H and red autofluorescence were the most useful parameters to differentiate particles of the sporangia suspension.

After FCM detection of four different subpopulations based on SSC-H and red autofluorescence (Fig. 1B), *P. viticola* sporangia suspension was used in a FACS analysis to characterize the particles present in each subpopulation. Populations R3a and R3b, R4, and R5 were sorted based on their red autofluorescence and separately collected in sterile tubes. A postsorting analysis was carried out by FCM to assess the purity of each subpopulation (Fig. 2).

Subsequently, each subpopulation was analyzed under the microscope to associate a specific morphology (Fig. 3). Specifically, the population R5 (low SSC-H and low red autofluorescence) encompassed debris (small particles) (Fig. 3D), encysted zoospores (Fig. 3E), and biflagellate swimming zoospores (Fig. 3F). Conversely, subpopulations R3a (low SSC-H, high red autofluorescence) and R3b (high SSC-H, middle red autofluorescence) corresponded to damaged sporangia. In particular, we observed that emptying sporangia with broken cell wall and intracellular content loss were present in the subpopulation R3a (Fig. 3C). Sporangia with open operculum (Fig. 3B) and vacuolated cytoplasm characterized the subpopulation R3b. Intact *P. viticola* sporangia were encompassed in subpopulation R4 (high SSC-H, low red autofluorescence) (Fig. 3A).

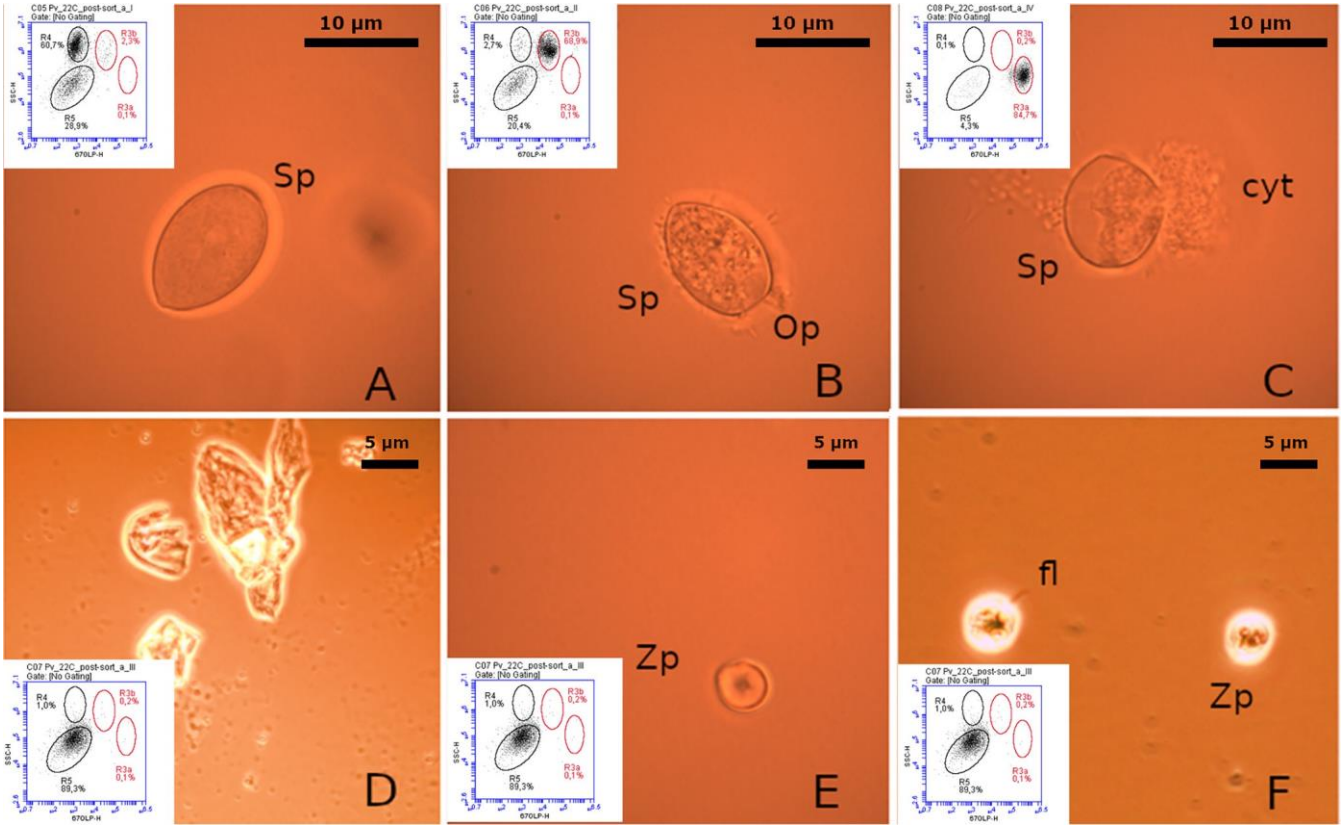

FIG 3 Microscopy pictures taken after FACS sorting of the different subpopulations. Intact *P. viticola* sporangia isolated from subpopulation R4 (A). Sporangia with open operculum and granular cytoplasm from subpopulation R3b (B). Emptying sporangia from subpopulation R3a, with broken cell wall and cytoplasm loss (C). Undefined debris isolated from population R5 (D). *P. viticola* encysted zoospore (E) and biflagellate swimming zoospores (F) isolated in population R5. Op, operculum; Sp, sporangia; Zp, zoospore; fl, flagella; cyt, cytoplasm loss.

P. viticola infection efficiency is determined by FACS-sorting individual sporangia. The isolate proved to be highly virulent, as demonstrated by the average 75.1 6 6.2% (standard deviation) disease severity assessed by inoculating the overall sporangia suspension on grapevine leaves. Subpopulation R4 (containing intact *P. viticola* sporangia) was selected to be sorted in the 24-well microtiter plates containing grapevine leaf discs. Indeed, as the aim of this experiment was the evaluation of sporangia infection efficiency, it would not have been productive to inoculate emptying sporangia with broken cell wall, debris, or biflagellate zoospores. Although the latter are theoretically capable of generating infections on their own and can be sporadically found inside the emptying sporangia or debris, the reproductive structure within which they form (the sporangium) produces numerous zoospores with the same genetic heritage, considerably increasing the chances of positive infection if inoculated. Moreover, the zoospores are cell wall-lacking structures with a short life (hours), whereas sporangia can survive for at least 1 day (2). Therefore, it was reasonably chosen to investigate the subpopulation R4 for the infection assay.

Results obtained in the four biological replicates are reported in Table 1. The cumulative number of single sporangia able to infect the leaf discs within 14 days after inoculation (DAI) into the 24-well microtiter plates, ranged from a minimum of zero in plate number 4.2 to a maximum of four, obtained in plates numbered 3.1, 3.2, and 4.4 (Table 1). The average value of infection efficiency (IE) (%) for the four biological replicates was 8.3%.

In general, no sporulated leaf discs were identified before 5 DAI, and the peak of infection was reached between 7 (biological replicate no. 1) and 8 (biological replicates no. 2, 3, and 4) DAI (Table 1). No new sporulated leaf discs were detected afterwards. The proportions of infected grapevine leaf discs calculated on the total for each population were close together and ranged from 6.3% (replicates 1 and 2) to 10.4% (remaining replicates).

TABLE1 Cumulative daily number of infected leaf discs and infection efficiency (IE %) defined as the percentage of infected leaf discs over the total, for each of the 24-microtiter plates of the four experimental replicates.

	Days after inoculation											
Exptl repetition and plate	4	5	6	7	8	9	10	11	12	13	14	IE %
Repetition 1												
Plate 1.1	0	0	0	1	1	1	1	1	1	1	1	4.2
Plate 1.2	0	0	1	1	1	1	1	1	1	1	1	4.2
Plate 1.3	0	0	1	2	2	2	2	2	2	2	2	8.3
Plate 1.4	0	0	2	2	2	2	2	2	2	2	2	8.3
Repetition 2												
Plate 2.1	0	0	0	0	1	1	1	1	1	1	1	4.2
Plate 2.2	0	0	0	1	1	1	1	1	1	1	1	4.2
Plate 2.3	0	0	2	2	2	2	2	2	2	2	2	8.3
Plate 2.4	0	0	1	2	2	2	2	2	2	2	2	8.3
Repetition 3												
Plate 3.1	0	1	1	4	4	4	4	4	4	4	4	16.7
Plate 3.2	0	1	1	3	4	4	4	4	4	4	4	16.7
Plate 3.3	0	0	0	1	1	1	1	1	1	1	1	4.2
Plate 3.4	0	0	1	1	1	1	1	1	1	1	1	4.2
Repetition 4												
Plate 4.1	0	1	1	1	3	3	3	3	3	3	3	12.5
Plate 4.2	0	0	0	0	0	0	0	0	0	0	0	0.0
Plate 4.3	0	0	2	3	3	3	3	3	3	3	3	12.5
Plate 4.4	0	0	1	4	4	4	4	4	4	4	4	16.7

TABLE2 Wald's x^2 test (type II solution) for GLMM fixed parameters

Parameter	x_2	DF	$p(>x^2)$
b_{ti} (time effect in days after inoculation)	2778.6480	1	0.001
b_j (expt, with j = {Experiment1, Experiment2, Experiment3, Experiment4}	1.8803	3	0.598

The study of infection dynamics reveals the median sporangia infection timing. The generalized linear mixed model (GLMM) fitted well, describing the infection dynamics (ID) reproduced by the single-sporangia assay (pseudo-R^2 = 0.9911) (Fig. 4A). Indeed, all the simulated IE (%) values obtained at any DAI were included within the 95% confidence limits computed for the overall observed percentage of positively infecting sporangia, regardless the experiment. Overall, the type II solution for the GLMM parameters (Table 2) showed a highly significant effect of time (DAI) on the response variable ($p(.x^2)$, 0.001), whereas the experiment's effect did not appear to significantly affect the ID ($p(.x^2)$, 0.598). On the other hand, glancing at Fig. 4B, one can observe that t_{50} bootstrap empirical distribution approaches the normal density distribution. The bootstrap t_{50} computed value was 9.795 DAI, its 95% lower confidence limit (LCL) was 9.632 DAI, and its upper confidence limit (UCL) was 9.977 DAI. The GLMM t_{50} value was 9.797; thus, it was included within the bootstrap t_{50} 95% confidence limit. Noteworthy, the difference between GLMM t_{50} and bootstrap t_{50} was 0.002 DAI, i.e. 2 min and 53 s.

DISCUSSION

The combination of FCM, FACS, and microscopy analyses allowed us for the first time to thoroughly characterize the complexity of a *P. viticola* sporangia suspension, highlighting the presence of different particles with specific morphology and sporangia with different levels of integrity.

Indeed, FCM allowed us to detect morphological heterogeneity within a population (not only based on SSC-H or FSC-H, but more interestingly based on the intrinsic fluorescence).

The sporangia suspended in aqueous solutions at room temperature naturally tend to open their operculum and release the zoospores, so that they can move in the fluid by the movement of flagella to generate new infections (2). Considering the information on *P.*

viticola macrosporangia ultrastructure (7) and similar studies performed on related oomycete species belonging to *Phytophthora* spp., such as *P. infestans* (31) and *Phytophthora parasitica* Dastur (kingdom Chromista, phylum Oomycota, class Oomycetes, order Peronosporales, family Peronosporaceae) (32), mature sporangia possess a more complex cytoplasm compared with immature spores. Indeed, the mature sporangia are characterized by the presence of structures related to the zoosporogenesis process like flagella, basal bodies, and cleavage vacuoles. The increase in cytoplasm complexity associated with indirect germination matched with microscope observations performed on the subpopulation R3a (Fig. 3B) and could explain the increase in red autofluorescence observed in subpopulations R3a and R3b, compared to subpopulation R4. Usually, the increase in autofluorescence is reported in eukaryotic cells subjected to an increase in respiratory activity in unfavorable conditions (33).

Furthermore, the presence in the cell suspension of sporangia in different physiological phases can be easily attributed to the asynchronous nature of the sporulation process on the host tissues (34). Finally, despite the preliminary filtration of the suspension, the presence of debris and other foreign particles of no relevant interest composing the subpopulation R5 is a common problem also reported by Day et al. (27) when handling material directly obtained from the host tissues. In the last years, some attempts to account for *P. viticola* secondary inoculum viability and infectivity at field scale have been described (35, 36). However, no information on the real number of sporangia able to infect grapevine and on their infection dynamics over time are available. Our study revealed the possibility to induce the infection by sorting intact sporangia belonging to the subpopulation R4 onto grapevine leaf discs. The average yield in infected leaf discs was 8% and statistical analysis showed no differences in the infection dynamics between biological replicates, making the results quite sound. Therefore, to the best of our knowledge, because we cannot make any other comparison, we cannot conclude if the achieved IE value is high, average, or low until a massive investigation on different strains will be performed. To better evaluate the sporangia infection efficiency, further experiments are necessary. Indeed, the use of fresh field suspensions (not propagated) which possess a greater infection capacity (18), extending the analysis to different plant and pathogen genotypes and investigating the pathogen infection by means of aniline blue staining, could contribute to better defining the infection efficiency of *P. viticola* sporangia. Thanks to the protocol developed within the frame of this study, it would also be possible to assess if sporangia produce different numbers of zoospores and, if so, whether the number of produced zoospores influences the disease intensity. Furthermore, the developed method could be used for isolating, in a fast and precise way, the strains that are present on single leaves or on single oilspots, and characterize them for different features (virulence, genetic profile, fungicide resistance, etc.) that nowadays are poorly investigated at this level.

GLMM models represent a well-established statistical approach in plant pathology to model disease incidence (37, 38). The GLMM employed in this study describes well the percentage of positively infected leaf discs (IE) and its dynamics over time (ID). One of the crucial parameters used in plant disease epidemiology to describe disease progress is t_{50} (time to reach 50% of disease) (39). Therefore, for the first time and with incomparable precision (single-sporangia scale), the GLMM t_{50} estimated in this study can be assumed as an appropriate index to summarize the median sporangia infection time (ca. 9.8 DAI). Moreover, considering that the difference between GLMM t_{50} and bootstrap t_{50} was very short, we can assume that the single experiment does not affect both the infection efficiency and the ID, providing useful information on *P. viticola* secondary inoculum epidemiology.

Conclusion. Overall, the single-sporangia infection assay developed in this study can represent an accurate technique for single sporangia isolation and infection efficiency evaluation, which allows a big step forward to study the secondary infection cycles of the pathogen and to provide quantitative data. In conclusion, the method proposed here opens new perspectives in different fields of study. On one hand, the isolation of single sporangia could allow better investigation of *P. viticola* biology with unmatched resolution (e.g., enzyme production, gene expression assays, or "omics" approaches). On the other hand, the developed infection assay can help to shed light on the plant-pathogen interactions (resistant and susceptible varieties), to develop predictive infection models, or for use in pathogen

population studies, for example, to quantify resistant individuals in fungicide resistance management.

MATERIALS AND METHODS

P. viticola material. The *P. viticola* monosporangial isolate n. 10, belonging to cluster 1 of Italian *P. viticola* population (40) and available at the collection of the Department of Agricultural and Environmental Sciences (DiSAA, University of Milan, Italy), was used in this study. This *P. viticola* strain, designated CAS, was isolated in 2016 as a part of an Italian downy mildew genetic study (40, 41) from a field population in north-eastern Italy (Casarsa della Delizia, province of Pordenone). The characteristics of the isolate geographic origin, cluster, and microsatellite profile are available on Dryad repository (https://datadryad.org/stash/dataset/doi:10.5061% 2Fdryad.kh189328s). From its isolation to the beginning of the experimental activity, the isolate has been maintained through weekly propagation on detached grapevine leaves (cv Pinot noir) (42). Large numbers of sporangia for experiments were obtained by massively propagating the strain on 100 leaves.

The sporangia suspension was obtained by collecting the sporangia present on grapevine leaves 7 DAI in phosphate buffered saline (PBS pH 7.4, Merck, Darmstadt, Germany). Before use, PBS was filtered through a 0.2-mm pore size polyvinylidene fluoride (PVDF) membrane filter and sterilized in an autoclave (121°C, 20 min). Sporulating lesions of each of the leaves were placed one by one in a 50-mL glass beaker and rinsed with 5 mL of PBS by using a glass pipette to detach sporangia from the infected material. Sporangia concentration was determined by using Kova chambers (Kova International, Garden Grove, CA, USA) under a microscope (Zeiss Primo Vert, Carl Zeiss Microscopy, NY, USA) and adjusted to a final concentration of 1 10^7 sporangia/mL. The sporangia suspension was filtered through a 30 mmpore size strainer (Sysmex, Gorlitz, Germany) immediately before the FCM and FACS analyses. All the material used in these activities was previously sterilized in autoclave (121°C, 20 min).

Species identity. The species identity of the strain was confirmed by sequencing the ITS region with the ITS6 (GAAGGTGAAGTCGTAACAAGG) and ITS7 (AGCGTTCTTCATCGATGTGC) primers (43). To this purpose, *P. viticola* sporangia were collected in sterile distilled water (as described in the previous section). Water was removed after centrifuging the suspension (10 min at 13,200 rpm) and the DNA extracted from the sporangia (44) was resuspended in 40 mL of TE (Tris-EDTA) buffer at 65°C for 2 min and checked for its purity and concentration (Nanodrop ND1000; Thermo Fisher Scientific, Rodano, Milan, Italy). PCR was performed in an Eppendorf Mastercycler (Eppendorf, Milano) thermal cycler using Phusion Plus PCR Master Mix (Thermo Fisher Scientific, USA), according manufacturer's instruction. The PCR contained 1 Phusion plus PCR master mix, 0.5 mM each primer, and 50 ng of DNA. Thermal cycling conditions were: 98°C for 30 s followed by 35 cycles of 98°C for 10 s, 61.5°C for 10 s, and 72°C for 15 s, and a final extension of 72°C for 5 m. The amplicon length (312 bp) was verified by agarose (2%) gel electrophoresis and the PCR product was purified and Sanger-sequenced by Eurofins Genomics Italy using ITS6 and ITS7 primers. The consensus sequence (GenBank accession number OP326699) was compared with those present in NCBI database by using BLASTn software tool.

Flow cytometry analyses, fluorescence-activated cell sorting, and microscopy. FCM analyses were performed on the Accuri C6 Plus (BD Biosciences, Franklin Lakes, NJ, USA) flow cytometer equipped with a blue (488 nm, 20 mW) laser. Forward scatter (FSC), side scatter (SSC), and red fluorescence (.670 nm in FL3 channel equipped with 670LP filter) signals were collected by acquiring 9,000 events. All parameters were collected as logarithmic signals, and data were analyzed with the BD Accuri C6 Plus software (version 1.0.23.1).

To characterize the composition of *P. viticola* sporangia suspension, individual subpopulations detected by FCM analysis (Fig. S1A) were isolated by FACS by means of the FACSJazz (BD Biosciences, Franklin Lakes, NJ, USA) cell sorter equipped with a blue laser (488 nm, 80 mW). In detail, a fresh and unstained sporangia suspension was 2.5-fold diluted with PBS buffer and subjected for sorting. The instrument was triggered on forward scatter (FSC-H), and the sorting gate was set first on forward scatter (FSC-H) versus side scatter (SSC-H) of 0.5- to 7-mm diameter uniform microspheres (Fluoresbrite YG Microspheres 0.50 mm [Polysciences, Hirschberg an der Bergstrasse, Germany, Cat. No. 17152-10], Sphero Rainbow Calibration Particles 3.0 to 3.4 mm [BD Biosciences, Cat. No. 559123], CountBright Absolute Counting Beads 7 mm [Thermo Fisher Scientific Life Technologies; Eugene, OR, USA, Cat. No. C36950]) and further on side scatter (SSC-H) versus red fluorescence (FL3-H). The drop delay was calculated with AccuDrop beads (BD Biosciences) using BD FACS Sortware v1.2. The fixed sheath pressure used was 27 lb/in^2. The sample differential was set at 0.5 lb/in^2, and kept constant for the duration of the experiment. The drop drive frequency was 39.20 kHz.

Once sorting parameters were established, the subpopulations (SSC-H versus FL3-H) detected inside the sporangia suspensions were sorted using either the sort mode "1.0 drop Pure" into sterile 15-mL centrifuge tubes, subsequently observing an aliquot in a bright field under a light microscope (AX10 Axio Lab A1, Zeiss, Carl Zeiss Microscopy, NY, USA) at 100 magnification with immersion oil to assess the identity of the sorted structures or the sort mode "1.0 drop Single" in case of sorting on grapevine leaf discs for infection efficiency experiments, as reported below.

Infection efficiency assay. To assess the infection efficiency of the *P. viticola* asexual inoculum, a single-sporangia infection assay, where single sporangia were isolated and sorted through FACS on healthy grapevine leaf discs placed inside a 24-well microtiter plate, was designed. The experimental scheme of the assay is reported in Fig. S1. In detail, four sporangia suspensions (biological replicates) were derived from four different sets of 100 leaves inoculated as previously described. For each biological replicates, 96 grapevine leaf discs (technical replicates) were prepared. To this purpose, four 24-well microtiter plates (Falcon multiwell 24, Biosigma, Cona, Italy) were filled in with 1 mL of wateragar (0.5% wt/vol Agar Bacto BD Difco; Becton Dickinson Italia, Milan, Italy) per well. Grapevine (*Vitis vinifera* L. cv Pinot noir, kingdom Plantae, phylum Spermatophyta, subphylum Angiospermae, Class Dicotyledonae, order Rhamnales, family Vitaceae) leaf discs (15 mm diameter) were excised with a cork borer and placed, with their abaxial surface upwards, into separate wells of a multiwell plate 24 h before the inoculation. Immediately before the inoculation, the leaf discs were sprayed with sterile distilled water to reach 100% relative humidity inside the plate. Each leaf disc was inoculated by FACS-sorting with an individual droplet (about 6 nL volume) containing a single sporangium. An additional plate (not inoculated) was prepared for each replicate as a negative control. The infectivity (virulence) of the isolate was determined by spray-inoculating 1 mL of the overall the sporangia suspension on three healthy grapevine leaves (cv. Pinot noir) placed with their abaxial surface up, in a Petri dish with

moistened filter paper underneath, and calculating disease severity at 9 dpi (45). Inoculated plates were incubated for 14 days in a climate chamber (22°C, 10 mmol/m^2 s, 12/12 h light/darkness period, 70% relative humidity). Leaf discs were scored daily under a stereomicroscope (Leica Wild M10; Leica Microsystems, Wetzlar, Germany) at 40 x magnification from 4 to 14 DAI to check for the presence of sporulation, as confirmation of successful outcome of the infection process. In this context, infection efficiency (IE) was defined as the percentage of infected leaf discs over the total inoculated leaf discs.

Sporangia infection dynamics. Because the single-sporangia assay reproduces the ID imputable to *P. viticola* secondary inoculum along the experimental time frame of investigation of 14 d (i.e., time function) in laboratory conditions, such phenomenon can be investigated by fitting a GLMM defined as follows:

$$g(y_{tij}) = n_{tij} = \beta_0 + \beta_{ti}t + \beta_j + e_{ij}$$

where y_{tij} is the number of infected leaf discs out of the total number n_i of inoculated leaf discs (i.e., the proportion of infecting sporangia) at time t for the i-th plate with i = {plate1, plate2, plate3 ... plate16} and at the j-th experiment (biological replicate) with j = {Experiment1, Experiment2, Experiment3, Experiment4}; h_{tij} is the linear predictor expressed according to the Probit link function g() = φ(); $\beta_0 = b_0\, 1\, u_{0i}$ is the intercept, where b_0 is the intercept's fixed term and u_{0i} is the intercept's random component, which represents the plate-dependent effect arising from the random inclusion of any i-th plate in the j-th experiment; $b_{ti} = b_t\, 1\, t_i$ is the slope for the time effect on the i-th plate's ID, where b_t is the fixed slope's component representing the sporangia infection general trend in time and t_i is the random plate-dependent slope's component accounting for the plate's effect on ID; t is the time expressed as DAI, which is the same for any i-th plate and j-th experiment, as all of the plates were inoculated and incubated on the same day; b_j is the fixed experiment's effect and «$_{ij}$ is the error term. The variance heterogeneity is managed by setting n_i as weights during the GLMM fitting procedure. This GLMM parameterization allows one to compute both a general $t_{50} = -b_0/b_t$ (named here as the GLMM t_{50}) and a plate-specific $t_{50}^i = -b_0/b_t$ at one time, according to the equation suggested by Faraway and coworkers (46). Such index is useful to summarize the spore germination dynamics, such as in the case of *P. viticola* oospores (5). Thus, assuming that all of the sporangia used in this trial were collected from the same population, and the GLMM described above is really representative of the ID, i.e., the GLMM's fitted data values approach the observed ones according to the pseudo-R^2 computed via observed versus simulated simple linear regression after (47), the single-sporangia assay proposed here can be considered reliable if: (i) the experiment fixed effect b_j is not significantly different from 0 for a= 0.05, and the simulated data do not fall out of the 95% Probit confidence limits (48) computed for the overall observed infecting sporangia at the time t; and (ii) the t_{50}^i expected value is not significantly different from general t_{50} for a = 0.05. The former condition is readily assessed by computing the Wald's x^2 test (type II solution) for the GLMM parameters (49) and by comparing simulated data to 95% Probit confidence limits cited above; the latter condition is assessed by comparing the general t_{50} value (i.e., the GLMM t_{50}) to the bootstrap t_{50} and its 95% confidence limits. The bootstrap t_{50} is computed by resampling 10^4 times by bootstrap method (50) from the set of t_{50}^i and then obtaining its expected value as a mean of the values arising from 10^4 simulations. The bootstrap t_{50} 95% is directly computed by extracting the 2.5th and the 97.5th quantile from the bootstrap distribution.

GLMM model, as described above, was fitted by glmer() function implemented in lme4 R 3.4.3. statistical packages, whereas its type II solution was computed by Anova() function implemented in car R 3.4.3. statistical packages. The 95% Probit confidence limits (48) computed for the overall observed ID were computed by binom.probit() function implemented in binom R 3.4.3. statistical packages, while the bootstrap simulations and bootstrap 95% confidence limits were obtained by bootstrap() function implemented in bootstrap R 3.4.3. statistical packages and quantile() function implemented in stats R 3.4.3. statistical packages.

Data availability. The sequence used for confirming the species identity of our *P. viticola* isolate is available on GenBank (accession number OP326699). Information on the geographic cluster of origin and microsatellite profile of the strain is available on Dryad (10.5061/dryad.kh189328s).

SUPPLEMENTAL MATERIAL

Supplemental material is available online only. SUPPLEMENTAL FILE 1, PDF file, 0.3 MB.

ACKNOWLEDGMENTS

We wish to thank Stefania Prati and Andrea Giupponi for the plant management in the glasshouse and Davide Sordi of Vivai Cooperativi Rauscedo for providing Pinot noir plants. This research was funded by the University of Milan - Department of Agricultural and Environmental Sciences (DiSAA), Research Support Plan Line 2, 2018 within the project entitled "From phenotyping to genome editing: strategies to limit the damage ca by downy mildew and bois noir in grapevine (ResVite)".

REFERENCES

1. Lafon R, Clerjeau M. 1988. Downy mildew, p 11–13. In Pearson RC, Goheen AC (ed), Compendium of grape diseases. APS Press, St. Paul, MN, USA.
2. Gessler C, Pertot I, Perazzolli M. 2011. *Plasmopara viticola*: a review of knowledge on downy mildew of grapevine and effective disease management. Phytopathol Mediterr 50:3–44.
3. Vercesi A, Vavassori A, Faoro F, Bisiach M. 2002. Effect of azoxystrobin onthe oospores of *Plasmopara viticola*, p 195–199. In Spencer-Phillips PTN, Gisi U, Lebeda A (ed), Advances in downy mildew research. Springer, Dordrecht, the Netherlands.
4. Rossi V, Caffi T. 2007. Effect of water on germination of *Plasmopara viticola* oospores. Plant Pathol 56:957–966. https://doi.org/10.1111/j.1365-3059.2007 .01685.x.
5. Maddalena G, Russo G, Toffolatti SL. 2021. The study of the germinationdynamics of *Plasmopara viticola* oospores highlights the presence of phenotypic synchrony with the host. Front Microbiol 12:698586. https://doi .org/10.3389/fmicb.2021.698586.
6. Hill GK. 1998. Studies on the germination of *Plasmopara viticola* oospores with a floating disc test. Bull OILB I SRO 21:1–2.
7. Vercesi A, Tornaghi R, Sant S, Burruano S, Faoro F. 1999. A cytological andultrastructural study on the maturation and germination of oospores of *Plasmopara viticola* from overwintering vine leaves. Mycol Res 103: 193–202. https://doi.org/10.1017/S095375629800700X.
8. Lehoczky J. 1956. Observations on oospore production by *Plasmopara viticola* in floating leaf discs in artificial culture. Vitis 5:17–19.
9. Si Ammour M, Bove F, Toffolatti SL, Rossi V. 2020. A Real-Time PCR Assayfor the Quantification of *Plasmopara viticola* Oospores in Grapevine Leaves. Front Plant Sci 11:1202. https://doi.org/10.3389/fpls.2020.01202.
10. Toffolatti SL, Prandato M, Vercesi A. 2007. Germination dynamics and viability of *Plasmopara viticola* oospores, p 47–51. In Lebeda A, Spencer-Phillips PTN (ed), Advances in downy mildew research, volume 3, Proceedings of the 2nd International Downy Mildews Symposium. Palacky University and Jola, Olomuc and Kostelec na Hané, Czech Republic.
11. Toffolatti SL, Russo G, Campia P, Bianco PA, Borsa P, Coatti M, Torriani SFF,Sierotzki H. 2018. A time-course investigation of resistance to the carboxylic acid amide mandipropamid in field populations of *Plasmopara viticola* treated with anti-resistance strategies. Pest Manag Sci 74:2822–2834. https:// doi.org/10.1002/ps.5072.
12. Vercesi A, Toffolatti SL, Zocchi G, Guglielmann R, Ironi L. 2010. A newapproach to modelling the dynamics of oospore germination in *Plasmopara viticola*. Eur J Plant Pathol 128:113–126. https://doi.org/10.1007/s10658-010 -9635-8.
13. Corio-Costet M-F. 2015. Monitoring resistance in obligate pathogensby bioassays relating to field use: grapevine powdery and downy mildews, p 251–279. In Ishii I, Hollomon DW (eds), Fungicide resistance in plant pathogens. Springer, Japan.
14. Massi F, Torriani SFF, Borghi L, Toffolatti SL. 2021. Fungicide resistance evolution and detection in plant pathogens: *Plasmopara viticola* as a case study. Microorganisms 9:119. https://doi.org/10.3390/microorganisms9010119.
15. Andrieu N, Jaworska G, Genet JL, Bompeix G. 2001. Biological mode ofaction of famoxadone on *Plasmopara viticola* and Phytophthora infestans. Crop Prot 20:253–260. https://doi.org/10.1016/S0261-2194(00)00156-3.
16. Blum M, Boehler M, Randall E, Young V, Csukai M, Kraus S, Moulin F,Scalliet G, Avrova AO, Whisson SC, Fonne-Pfister R. 2010. Mandipropamid targets the cellulose synthase-like PiCesA3 to inhibit cell wall biosynthesis in the oomycete plant pathogen, Phytophthora infestans. Mol Plant Pathol 11:227–243. https://doi.org/10.1111/j.1364-3703.2009.00604.x.
17. Genet JL, Vincent O. 1999. Sensitivity to famoxate [famoxadone] of European *Plasmopara viticola* populations. Agris 64:559–564.
18. Kennelly MM, Gadoury DM, Wilcox WF, Magarey PA, Seem RC. 2007. Primary infection, lesion productivity, and survival of sporangia in the grapevine downy mildew pathogen *Plasmopara viticola*. Phytopathology 97: 512–522. https://doi.org/10.1094/PHYTO-97-4-0512.
19. Hong CF, Scherm H. 2020. A spectrophotometric approach for determining sporangium and zoospore viability of *Plasmopara viticola*. J Phytopathol 168:297–302. https://doi.org/10.1111/jph.12892.
20. Shapiro HM. 2005. Practical flow cytometry. John Wiley & Sons, Vorhees, NJ, USA.
21. Ishii S, Tago K, Senoo K. 2010. Single-cell analysis and isolation for microbiology and biotechnology: methods and applications. Appl Microbiol Biotechnol 86:1281–1292. https://doi.org/10.1007/s00253-010-2524-4.
22. D'Hondt L, Höfte M, Van Bockstaele E, Leus L. 2011. Applications of flow cytometry in plant pathology for genome size determination, detection and physiological status. Mol Plant Pathol 12:815–828. https://doi.org/10 .1111/j.1364-3703.2011.00711.x.
23. Winson MK, Davey HM. 2000. Flow cytometric analysis of microorganisms.Methods 21:231–240. https://doi.org/10.1006/meth.2000.1003.
24. Czechowska K, Johnson DR, van der Meer JR. 2008. Use of flow cytometric methods for single-cell analysis in environmental microbiology. Curr Opin Microbiol 11:205–212. https://doi.org/10.1016/j.mib.2008.04.006.
25. Joux F, Lebaron P. 2000. Use of fluorescent probes to assess physiological functions of bacteria at single-cell level. Microbes Infect 2:1523–1535. https://doi.org/10.1016/s1286-4579(00)01307-1.
26. Catal M, King L, Tumbalam P, Wiriyajitsomboon P, Kirk WW, Adams GC.2010. Heterokaryotic nuclear conditions and a heterogeneous nuclear population are observed by flow cytometry in Phytophthora infestans. Cytometry A 77:769–775. https://doi.org/10.1002/cyto.a.20888.
27. Day JP, Kell DB, Griffith GW. 2002. Differentiation of Phytophthora infestans sporangia from other airborne biological particles by flow cytometry. Appl Environ Microbiol 68:37–45. https://doi.org/10.1128/AEM.68.1.37-45 .2002.
28. Sergeeva V, Nair N, Legendre L, Darley E, Spooner-Hart R. 2002. The use offluorochromes to determine the effect of chlorine dioxide on survival of *Plasmopara viticola* on grapevine. Austral Plant Pathol 31:295–297. https:// doi.org/10.1071/AP02018.
29. Zand E, Froehling A, Schoenher C, Zunabovic-Pichler M, Schlueter O,Jaeger H. 2021. Potential of flow cytometric approaches for rapid microbial detection and characterization in the food industry-a review. Foods 10:3112. https://doi.org/10.3390/foods10123112.
30. Bleichrodt R-J, Read ND. 2019. Flow cytometry and FACS applied to filamentous fungi. Fungal Biol Rev 33:1–15. https://doi.org/10.1016/j.fbr.2018 .06.001.
31. Elsner PR, VanderMolen GE, Horton JC, Bowen CC. 1970. Fine structure ofPhytophthora infestans during sporangial differentiation and germination. Phytopathology 60:1765–1772. https://doi.org/10.1094/Phyto-60-1765.
32. Hohl HR, Hamamoto ST. 1967. Ultrastructural changes during zoosporeformation in Phytophthora parasitica. Am J Bot 54:1131–1139. https://doi .org/10.1002/j.1537-2197.1967.tb10743.x.
33. Surre J, Saint-Ruf C, Collin V, Orenga S, Ramjeet M, Matic I. 2018. Strongincrease in the autofluorescence of cells signals struggle for survival. Sci Rep 8:12088. https://doi.org/10.1038/s41598-018-30623-2.
34. Caffi T, Gilardi G, Monchiero M, Rossi V. 2013. Production and release of asexual sporangia in *Plasmopara viticola*. Phytopathology 103:64–73. https://doi.org/10.1094/PHYTO-04-12-0082-R.
35. Brischetto C, Bove F, Fedele G, Rossi V. 2021. A weather-driven model forpredicting infections of grapevines by sporangia of *Plasmopara viticola*. Front Plant Sci 12. https://doi.org/10.3389/fpls.2021.636607.
36. Brischetto C, Bove F, Languasco L, Rossi V. 2020. Can spore sampler databe used to predict *Plasmopara viticola* infection in vineyards? Front Plant Sci 11:1–12.
37. Madden LV, Turechek WW, Nita M. 2002. Evaluation of generalized linearmixed models for analyzing disease incidence data obtained in designed experiments. Plant Dis 86:316–325. https://doi.org/10.1094/PDIS.2002.86 .3.316.
38. Garrett KA, Madden LV, Hughes G, Pfender WF. 2004. New applications ofstatistical tools in plant pathology. Phytopathology 94:999–1003. https:// doi.org/10.1094/PHYTO.2004.94.9.999.

39. Berger RD. 1988. The analysis of effects of control measures on the development of epidemics, p. 137–151. In Kranz J, Rotem J (eds), Experimental Techniques in Plant Disease Epidemiology. Springer Berlin Heidelberg, Berlin, Heidelberg.
40. Maddalena G, Delmotte F, Bianco PAPA, De Lorenzis G, Toffolatti SL. 2020. Genetic structure of Italian population of the grapevine downy mildew agent, *Plasmopara viticola*. Ann Appl Biol 176:257–267. https://doi.org/10 .1111/aab.12567.
41. Sargolzaei M, Maddalena G, Bitsadze N, Maghradze D, Bianco PA, Failla O,Toffolatti SL, De Lorenzis G. 2020. Rpv29, Rpv30 and Rpv31: three novel genomic loci associated with resistance to *Plasmopara viticola* in Vitis vinifera. Front Plant Sci 11:562432. https://doi.org/10.3389/fpls.2020.562432.
42. Toffolatti SL, De Lorenzis G, Costa A, Maddalena G, Passera A, Bonza MC,Pindo M, Stefani E, Cestaro A, Casati P, Failla O, Bianco PA, Maghradze D, Quaglino F. 2018. Unique resistance traits against downy mildew from the center of origin of grapevine (Vitis vinifera). Sci Rep 8:12523. https://doi.org/10.1038/s41598-018-30413-w.
43. Cooke DEL, Drenth A, Duncan JM, Wagels G, Brasier CM. 2000. A molecular phylogeny of Phytophthora and related oomycetes. Fungal Genet Biol 30:17–32. https://doi.org/10.1006/fgbi.2000.1202.
44. Toffolatti SL, Venturini G, Maffi D, Vercesi A. 2012. Phenotypic and histochemical traits of the interaction between *Plasmopara viticola* and resistant or susceptible grapevine varieties. BMC Plant Biol 12:124. https://doi .org/10.1186/1471-2229-12-124.
45. Ricciardi V, Marcianò D, Sargolzaei M, Maddalena G, Maghradze D, TirelliA, Casati P, Bianco PA, Failla O, Fracassetti D, Toffolatti SL, De Lorenzis G. 2021. From plant resistance response to the discovery of antimicrobial compounds: the role of volatile organic compounds (VOCs) in grapevine downy mildew infection. Plant Physiol Biochem 160:294–305. https://doi .org/10.1016/j.plaphy.2021.01.035.
46. Faraway JJ. 2016. Extending the linear model with R: generalized linear,mixed effects and nonparametric regression models. CRC Press, Boca Raton, FL, USA.
47. Piñeiro G, Perelman S, Guerschman JP, Paruelo JM. 2008. How to evaluatemodels: observed vs. predicted or predicted vs. observed? Ecol Modell 216:316–322. https://doi.org/10.1016/j.ecolmodel.2008.05.006.
48. Dorai-Raj S. 2014. Binomial confidence intervals for several parameterizations, R package version 1.0–6.
49. Fox J. 2015. Applied regression analysis and generalized linear models.Sage Publications, Thousand Oaks, CA, USA.
50. Efron B, Tibshirani R. 1994. An introduction to the bootstrap. Chapmanand Hall/CRC, New York, NY, USA.

Paper II

Introduction to paper II

Supervised machine learning (SML) is a well-established subcategory of machine learning which represents a valuable tool to overcome limitations of traditional statistical methods. In essence, SML algorithms utilize a labelled training dataset to predict outcomes, aiming to establish a mapping function between input and output variables. These algorithms are frequently applied in image analysis and computer vision applications such as image classification, segmentation, and object recognition. To date, plant pathologists commonly rely on visual estimation as the traditional method for quantifying disease severity. However, this approach is prone to subjectivity, and inconsistency, and is time-consuming. Although the potential advantages in terms of reproducibility and repeatability compared with traditional methods, computer vision tools for disease severity estimation are poorly employed by researchers. This fact is often associated with limitations in accessibility and support to user needs that characterize existing tools. In the following section, we introduce the second research article included in this thesis work, named paper II. Here we present the results related to the design and validation of a platform devoted to disease severity estimation at the laboratory level based on SML algorithms and computer vision. The idea is to provide plant pathologists with an open-source and user-friendly tool specifically tailored to plant pathologists needs.

From the horse's mouth: an open-source platform to meet plant pathologists with computer vision and machine learning algorithms for efficient plant disease assessment

Authors: Demetrio Marcianò[1], Beatrice Lecchi[1], Giuliana Maddalena[1], Silvia Laura Toffolatti[1]

[1]Dipartimento di Scienze Agrarie ed Ambientali, Università degli Studi di Milano, Milan, Italy

Abstract

Phytopathometry, defined as the practice of quantifying and analyzing plant diseases, is a key task in plant pathology for several purposes. Traditional methods of disease severity estimation rely on visual assessments performed using either qualitative or quantitative scales. However, in the case of poor training and standardization, these methods can be inaccurate and unreliable, thereby negatively influencing plant pathology experiments. In this context, automated disease severity estimation using RGB images captured by widely available digital cameras has emerged as a valuable alternative to visual estimation. In this framework, the use of Supervised Machine Learning (SML), enables high reproducibility and repeatability with a cost-effective and accessible approach. However, algorithm training and application may require time-consuming preprocessing steps and are mostly implemented using command-line tools. In this study, a Python-based, open-source pipeline to carry out image pre-processing, SML training and automated disease severity assessment was developed and evaluated on three different pathosystems: *Phytophthora capsici* – tobacco, *Phytophthora infestans* – tomato and *Plasmopara viticola* - grapevine. The pipeline effectively detected and isolated plant samples, accurately recognized disease symptoms, and provided consistent severity measurements, with a good agreement level compared to the gold standard methodology. The pipeline offers an automated and accessible solution for disease severity estimation, and it can be integrated with existing tools as standalone software for manual segmentation and training dataset generation. Further implementations in terms of algorithm selection and the extension to multispectral imaging will enhance the range of applications. Active participation of the community is encouraged to further improve and adapt the pipeline to the evolving needs in the field of phytopathometry, placing plant pathologists at the core of the decision-making process.

Introduction

Phytopathometry can be defined as the field of study that involves the measurement, quantification, and analysis of plant diseases [1]. Quantifying plant diseases has various practical applications, such as monitoring disease progression to estimate crop losses, establishing decision-making thresholds, and enhancing our understanding of disease epidemiology and plant-pathogen interaction. Another crucial aspect is assessing the efficacy of different crop protection product

treatments, at both field and laboratory levels [1, 2]. In phytopathometry, disease severity is defined as the proportion of the plant unit exhibiting visible disease symptoms. Traditionally, to determine disease severity, plant pathologists score disease symptoms using qualitative or quantitative scales, which can be converted into a disease severity index (DSI), usually expressed as a percentage [3, 4, 5].

The introduction of digital imaging in the 1990s led to the use of visible spectrum imaging for the assessment of plant diseases. Indeed, researchers have developed image analysis softwares to assess manually disease severity on leaves, plants, and small plots [6]. In recent years, a growing interest in sensor technologies like multispectral imaging and artificial intelligence for phytopathometry has been observed. However, the high cost and time-consuming setup procedures associated with these technologies pose challenges to their widespread adoption [2, 6]. In this context, the use of RGB images captured by readily available digital cameras, including mobile devices, represents a valuable resource for computer vision applications in phytopathometry. In fact, RGB images offer a cost-effective and widely accessible solution for potential users [2, 7].

Several studies over the last 30 years have demonstrated that visual estimates can be inaccurate and unreliable, especially in situations where the operators are not well-trained and lack Standard Area Diagrams [8]. In contrast, the assessment based on visible spectrum image analysis has the potential to be accurate, repeatable, and reproducible, but image pre-processing and manual segmentation are time-consuming tasks that need to be automated [2].

Assessing disease severity from an image is essentially a classification problem, in which individual observations (e.g. pixel intensities) are related to an explanatory variable. Traditionally, this task has been accomplished using a classifier described in terms of a linear or a generalized linear model (glm) [9]. Another popular tool to achieve classification is machine learning, and in particular, supervised machine learning (SML). SML algorithms define a function that maps an input to an output based on example input-output pairs provided by the training dataset [10]. Over other classifiers, SML-based has the advantage to have *a priori* exact idea about the classes in the training data, which is useful in classification problems regarding the prediction of numerical target values from given data and labels. Furthermore, SML algorithms can be easily integrated with various imaging technologies, including visible light photography, multispectral and hyperspectral imaging, thus enhancing disease detection and characterization. However, their training and classification may require extended computations, especially for large datasets [11, 12]. Moreover, manual annotation of a large dataset for SML training is a time-consuming task and it may require specific software or extensions under commercial licenses [13, 14].

The tremendous acceleration and availability of open-source tools for image processing and ML applications can mitigate these challenges and facilitate the successful application of SML in phytopathometry. In this context, the Python programming language has emerged with some popular computer vision and image processing libraries such as OpenCV [15] and Scikit-image (Skimage) [16], which provide a comprehensive set of functions and algorithms for image manipulation that integrate well with other scientific computing libraries and are widely used for computer vision tasks in various fields. Another valuable library is Scikit-learn (Sklearn), which provides a comprehensive set of tools and functions for ML applications in Python [17]. Its user-friendly interface, the availability of extensive documentation, and strong community support make it a valuable resource for researchers working on diverse ML tasks [18]. Notably, Sklearn offers various algorithms that can be used for binary or multiclass classification problems (Table 1).

Table 1: summary of common SML algorithms employed in classification. The algorithms are briefly described along with their respective reference to the original papers or works that introduced or popularized them.

Classifier	*Description*	*Reference*
K-Nearest Neighbors (KNN)	Non-parametric classification method that assigns a label to a data point based on the labels of its nearest neighbors in the training set. It calculates the distance between the data point and its neighbors and determines the class label by majority voting among the k-nearest neighbors.	[19]
Decision Tree (DTC)	The algorithm builds a tree-like model by recursively partitioning the data based on feature values. Each internal node represents a feature, and the branches represent possible feature values, leading to leaf nodes that correspond to class labels or predictions.	[20]
Random Forests (RFC)	An ensemble learning method that combines multiple decision trees to make predictions. It constructs a forest of decision trees, where each tree is built using a random subset of features and a random subset of the training data.	[21]
Multi-layer Perceptron (MLPC)	The MLP Classifier, belongs to the Neural Net algorithm family. The neural network is a powerful ML algorithm inspired by the structure and function of the human brain. It consists of interconnected nodes (neurons) organized in layers, where each neuron applies a non-linear activation function to its inputs. The activation function enables the network to capture intricate patterns and relationships within the data.	[22]
Adaptive Boosting (ABC)	Ensemble learning algorithm that combines multiple weak classifiers to create a strong classifier. The algorithm iteratively adjusts the weights of misclassified samples to give them higher importance, forcing subsequent weak learners to focus on difficult examples.	[23]
Naive Bayes (NBC)	Probabilistic classifier based on Bayes' theorem with a naive assumption of feature independence. It calculates the probability of a data point belonging to a particular class based on the probabilities of its features given each class.	[24]
Quadratic Discriminant Analysis (QDA)	Classification algorithm that assumes each class follows a multivariate Gaussian distribution and uses quadratic decision boundaries to separate the classes. QDA estimates the parameters of the Gaussian distributions and assigns a class label.	[25]

Notably, in recent years, two main attempts have been made to implement open-source and automated disease severity on RGB images using open-source software. The first is PlantCV, an open-source library designed to address plant phenotyping challenges through a command-line interface. The library provides robust support for creating pipelines with image processing tools, including an NBC, accompanied by extensive documentation [26]. To generate the training dataset for NBC, the authors recommend using the “Pixel Inspection Tool” in ImageJ [27] to collect

samples of RGB pixel intensities from the desired image. Despite the success of this library in plant phenotyping studies, to the best of our knowledge, no peer-reviewed articles have been published utilizing the NBC classifier in this framework. The pliman R package developed by Olivoto and collaborators [14] offers a collection of functions designed to conduct plant image analysis, including plant disease severity assessment. This package enables users to discriminate the object of interest (e.g the leaf) from the background and to predict pixel classes associated with disease symptoms using RGB images. The pliman software utilizes sample images provided by the user (including healthy, diseased, and background samples) and employs a glm (binomial family) to classify the pixels accordingly. Both libraries represent valuable tools, but the choice of command-line interface has certain drawbacks, such as a steeper learning curve and potential accessibility challenges. Moreover, to achieve classification, both approaches require image pre-processing which relies on third-party software, which may not be handy in processing large datasets. Furthermore, the choice for classifiers is limited to NBC and binomial glms, which may have assumptions incompatible with the data provided (e.g., independence among features).

Considering that the successful application of statistical classifiers in phytopathometry relies on the availability of well-annotated training datasets and the careful selection of appropriate algorithms and features, some points need to be addressed. Plant diseases can manifest in diverse ways due to genetic diversity at the plant (e.g. different cultivars) or pathogen (e.g. different strains) levels or due to environmental factors, leading to variations in disease symptoms appearance and plant tissue responses. This variability poses challenges for pre-determined classifiers, as their learned patterns may not adequately capture the diversity of new instances, resulting in reduced accuracy and reliability [28]. To overcome this limitation, one potential solution is to adopt a data-driven approach, wherein algorithms are trained on a dataset that reflects the specific experimental conditions thus incorporating experiment-specific variations. However, a drawback of this approach is that it requires training the algorithm with experiment-specific datasets, making it less efficient and time-consuming than pre-determined classifiers that can be readily applied across different scenarios. For this reason, the development of a unified pipeline involving data pre-processing, dataset annotation, machine learning training, and utilization, tailored for large datasets through the optimization of repetitive tasks, would enhance the utilization and reliability of SML in phytopathometry datasets.

Biotrophic and hemibiotrophic pathogens represent a diverse group of organisms that establish intimate relationships with their host plants [29, 30]. For this reason, accurate phenotypic characterization of their interaction with the host is essential for a comprehensive understanding of their biology and for testing effective control strategies. *Phytophthora* and *Plasmopara* spp. genera encompass prominent plant pathogens belonging to the oomycetes clade. These pathogens are responsible for devastating diseases in plants and are characterized by hemibiotrophic and

biotrophic lifestyles, respectively. The impact of these organisms on agricultural production is significant, and they continue to pose a constant threat to global food security, resulting in substantial yield losses, especially in regions with favorable environmental conditions for disease development, such as high humidity and rainfall. Some well-known examples of challenging pathogens are: (i) *Phytophthora infestans* Mont. (de Bary), which causes late blight in potatoes and tomatoes. (ii) *Phytophthora capsici* Leonian, which is responsible for diseases in a wide range of hosts, including Solanaceae, legumes, cucurbit crops; and (iii) the grapevine downy midew agent *Plasmopara viticola* (Berk. et Curtis) Berl. & De Toni [31].

In the present study, we present a Python-based pipeline suitable for inexpert users that integrates RGB image preprocessing and SML training for the implementation of plant disease severity estimation at the laboratory level. Three different pathosystems were employed for pipeline validations: (i) *P. capsici* - tobacco leaves, (ii) *P. infestans* - tomato leaf discs, and (iii) *P. viticola* -grapevine leaf discs. Pipeline performance was compared with measurements performed by plant pathology experts used as the gold standard to determine the accuracy and reliability of disease severity measurements obtained through SML algorithms.

Materials and methods

Experimental inoculations

P. capisci strain Hd11 [32] mycelial plugs (5 mm diameter) obtained from the edge of actively growing cultures on PDA (Potato Dextrose Agar; Liofilchem, Italy) were inoculated on *Nicotiana benthamiana* leaves placed in a Petri dish with filter paper underneath [33]. After 16 hours post inoculation (hpi), mycelial plugs were removed.

A *P. infestans* isolate (n. 111344; CBS; Baarn, The Netherlands) was routinely propagated on rye-sucrose agar medium to achieve a sporangia suspension ($1x10^4$ sporangia/mL) [34]. Sporangia were resuspended in modified Petri's solution [35] and stored at 4°C for 3 h to induce zoospore release. Tomato (cv. Marmande) leaf discs (1.5 cm diameter) were placed lower surface upwards in a Petri dish containing moistened filter paper and inoculated with a 10 µl drop of sporangia suspension in the disc center.

A *P. viticola* sporangia suspension ($5x10^4$ sporangia/mL) was obtained by mixing field populations with different geographical origins as previously described [36, 37] and inoculated on grapevine (cv. Pinot noir) leaf discs placed in Petri dishes as described for tomato. Inoculation was carried out with five drops (5 µL) of the *P. viticola* sporangia suspension on each disc. After 24 hpi, drops were gently absorbed using filter paper [37, 38]. After the inoculations, all the Petri dishes were maintained in a growth chamber at 22°± 1°C with a 16:8 (light:dark) photoperiod until image acquisition.

Image acquisition and disease severity measurements

Image acquisition was performed after 3-, 5- and 7-days post inoculation (dpi) for *P. capisci*, P. *infestans* and *P. viticola,* respectively. RGB images of infected plant tissues were captured with a digital camera (Fujifilm Digital camera A160) with a resolution of 10.2 Mpx (3664 × 2748 pixels) and merged to form three distinct datasets (Table 2). To standardize the acquisition conditions, the Petri dishes were placed under artificial illumination with a 10 inches ring light (Meromore, China) at a height of 10 cm. The diseased area (DA) of each plant unit (i.e., entire leaf or leaf disc) was determined by manual segmentation of pixels [37, 39] corresponding to visible symptoms using the GIMP 2.10 software (https://docs.gimp.org/2.10/en/, accessed on 5 July 2023).

Table 2: dataset composition for each pathosystem involved in the study.

	No. of pictures	*No. of plant units (leaf discs or leaves)*
Dataset 1: P. capsici - tobacco	90	90
Dataset 2: P. infestans - tomato	32	292
Dataset 3: P. viticola - grapevine	23	211

Pipeline description

Scripts were developed and executed using Spyder3 IDE [40] with Python version 3.8 [41]. The code was run on a computer equipped with an Intel Core i5-6300 processor and 8 GB RAM on Linux Mint 20 operating system. The specific versions of the libraries employed were: Matplotlib 3.4.3, NumPy 1.21.1, OpenCV 4.5.3, Pandas 1.3.1, PlantCV 3.9.0, Scikit-image 0.18.3, and Scikit-learn 0.24.2. The Python scripts utilized in this study can be accessed on GitHub (https://github.com/demar2/Plant-pathology-computer-vision).

Figure 1. The pipeline proposed in this study aims to automate plant disease severity estimation using RGB images as input. **(A) Pre-processing**: the RGB images undergo pre-processing to remove the background that is different from the plant. Additionally, if multiple plant units (e.g., leaf discs) are detected in an image, the same is split into several pictures, each containing a single plant unit. **(B) User input segmentation**: a user-interface-based approach is implemented for image labeling. The user can either perform manual segmentation using the HSV colorspace or using a flood-fill algorithm similar to those included in common graphic software tools (e.g., magic wand tool). **(C) Supervised Machine Learning Training**: the user can easily train SML models using the Sklearn utility by combining the labeled images obtained in step (B) with their original images. **(D) Disease severity assessment**: the trained SML algorithm is then applied to new, unseen images to generate a label picture representing both the diseased and healthy areas. Additionally, a disease severity report file is generated, providing quantitative information on the diseased area in both absolute (in pixels) and relative terms (as a percentage of the whole area).

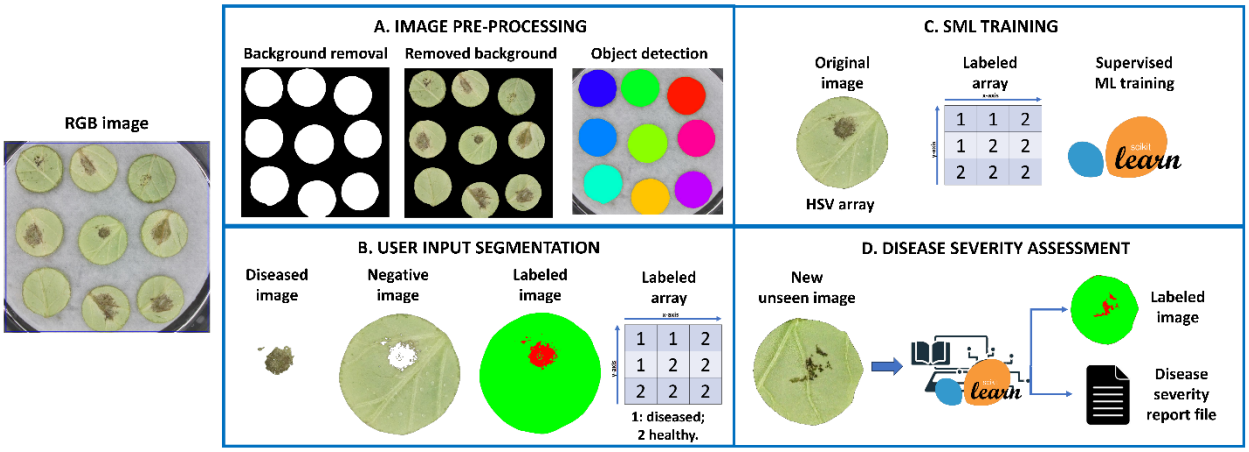

1. Image pre-processing

All the functions employed in this step use functions from PlantCV library. To isolate the plant unit from the background in the RGB input image, the image was converted to the LAB color space [42], and the brightness (B) channel was selected for further processing. To reduce noise, a Gaussian blur was applied, and thresholding via Otsu's method [43] was employed to isolate plant units of interest. The binary image obtained (i.e., the plant unit was represented by white pixels and the background by black pixels), was processed to fill any holes within the plant region, creating a continuous mask. To refine the borders of the plant unit, erosion was applied using the *pcv.erode* function, with user defined parameters. Once the background was effectively removed, object detection was performed by finding contours within the masked image, using the method described by Gehan et al. [26] (Figure 1A). Finally, the identified objects, corresponding to individual plant units, were split into new images, and used for further analysis.

2. User input segmentation

Two user-interface-based approaches were implemented for image labeling. Both the segmentation tools generated a segmented image, and its corresponding negative image highlighting the areas that do not meet the threshold conditions (Figure 1B).

(i) HSV segmentation approach: a trackbar-based thresholding function allow the users to interactively set threshold values for different HSV channels. The user interface (UI) displays the original RGB image, and sliders representing the intensity of the HSV channels are provided. By adjusting these sliders, users can set real-time thresholds on the regions of interest (ROIs), which can represent either healthy or diseased areas.

(ii) Flood-fill segmentation approach: it also employs a UI that displays the original RGB image. This technique is based on the flood-fill algorithm implemented in OpenCV, which identifies, and segments connected regions within an image. The flood-fill segmentation is performed based on the user's mouse interaction, allowing to define ROIs by selecting specific areas. The program offers flexibility in segmentation by supporting modifier keys to add or subtract the existing segmented regions. A tolerance value can be adjusted using a trackbar, enabling users to control the flood-fill behavior and fine-tune the segmentation results.

Segmented and negative images are then employed to generate label images and arrays, where pixel values equal to 1 indicate the diseased area (in red), and 2 the healthy area (in green). Simultaneously, a report file is generated to summarize the analysis outcomes allowing for a quantitative assessment of the disease severity. This report file includes essential information such as the pixel counts for diseased and healthy areas, and the disease severity index (DSI - Eq. 1).

$$\mathrm{DSI} = \frac{n°pixel[diseased]}{(n°pixel[healthy] + n°pixel[diseased])} \quad (1)$$

3-4. SML training and application

Seven ML models were trained using the Sklearn library in Python using custom parameters (table 3). Approximately 2% of plant units for each dataset were selected and labeled for model training. Original images were converted to the HSV colorspace, and pixel intensity values extracted from each channel as features. Simultaneously, the annotation was carried out based on the information provided in the labeled arrays. Next, features and annotations were stacked as 1D array, resulting in the training dataset (Figure 1C). To assess the performance of the trained models on unseen data, a 10% validation set was randomly selected from the training set. Accuracy scores and confusion matrices were utilized to evaluate the models' predictions on the validation data. To enhance the user's understanding of the training results, labeled images were generated. In these images, diseased pixels were highlighted in red, while healthy pixels were shown in green. This visualization aided in interpreting the classification output and evaluating the quality of the classification.

Using the same approach of data pre-processing, trained classifiers were applied to unseen RGB images, employing the same feature stack procedure from the HSV channels used during training. Resulting labeled images and report file were also provided to the user as previously described in sections 3 and 2 respectively (Figure 1D).

Table 3: resume of SML algorithms trained with details on function used for the implementation and their parameters (in brackets).

Classifier	*Sklearn function*
K-Nearest Neighbors (KNN)	KNeighborsClassifier(25)
Decision Tree (DTC)	DecisionTreeClassifier(max_depth=5)
Random Forests (RFC)	RandomForestClassifier(max_depth=5, random_state=0)
Multi-layer Perceptron (MLPC)	MLPClassifier(hidden_layer_sizes = (5,2), max_iter = 200,activation = 'relu', solver = 'adam')
Adaptive Boosting (ABC)	AdaBoostClassifier()
Naive Bayes (NBC)	GaussianNB()
Quadratic Discriminant Analysis (QDA)	QuadraticDiscriminantAnalysis()

Statistical analyses

To assess the agreement between different SML algorithms and the gold standard method based on expert's measurement of the continuous outcome provided by the DA, Lin's concordance correlation coefficient (CCC) was employed [44]. The CCC quantifies the level of agreement between a new test or measurement and a gold standard test or measurement of the same variable. According to Altman, the CCC should be interpreted like other correlation coefficients, such as Pearson's, where values below 0.2 indicate poor agreement and values above 0.8 indicate excellent agreement [45]. CCC values were calculated using the *CCC()* function from the DescTools package in R [46]. To visualize the agreement between the experts and SML algorithm measurements, we utilized the Bland-Altman (BA) plot. The BA plot is a scatter plot that shows the difference between paired measurements (A-B) on the Y-axis and the average of these measurements ((A+B)/2) on the X-axis for each observation. Additionally, the plot includes lines representing the mean difference and limits of agreement, as introduced by Bland and Altman (BA) [47]. BA plots were generated using the *blandr* package in R [48]. To account for the assumptions of normality and heteroscedasticity in the data, all DA measurements expressed as mm^2 underwent transformation using either square-root or cube-root transformations. All the analyses were conducted in R, using R Studio 9.1 [49].

Results

The pathogens were able to successfully infect plant tissues, leading to visible symptoms or pathogen manifestations, which were quantified as necrosis for *P. infestans* and *P. capsici*, and as sporulation for *P. viticola* (Figure 2A). The visual inspection of the pictures generated by the pipeline proved to be a valuable tool for quickly assessing the quality of object detection and disease severity evaluation performed by the different SML algorithms. Notably, both whole leaves (tobacco) and leaf discs (grapevine and tomato) were effectively detected and successfully isolated from the background (Figure 2B). Additionally, the algorithms demonstrated an overall good recognition of the symptoms they were trained on, with minor deviations observed across all three tested pathosystems (Figure 2C; Figure 3).

Figure 2: A. Examples of observed visible symptoms or pathogen manifestations for each pathosystem on different plant tissues. B. Visual inspection of pictures generated by the pipeline showing effective detection and isolation of both leaves (tobacco) and discs (grapevine and tomato) from the background. C. Performance evaluation of the SML algorithm (DTC) across the investigated images (healthy plant tissues in green, diseased areas in in red).

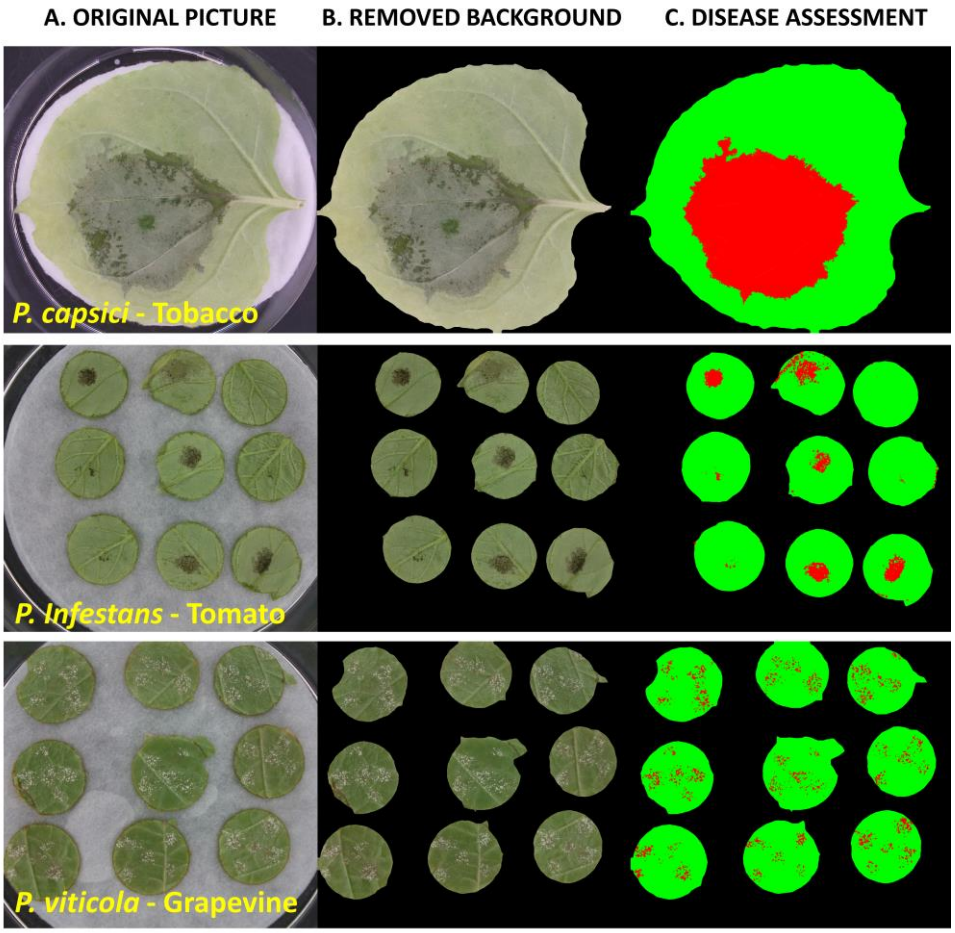

Figure 3: Examples of disease severity assessment among the three pathosystems. The figure showcases original pictures, along with corresponding labels provided by both the experts and the seven different SML algorithms. This visual representation shows healthy plant tissues as green, while diseased areas are labeled in red.

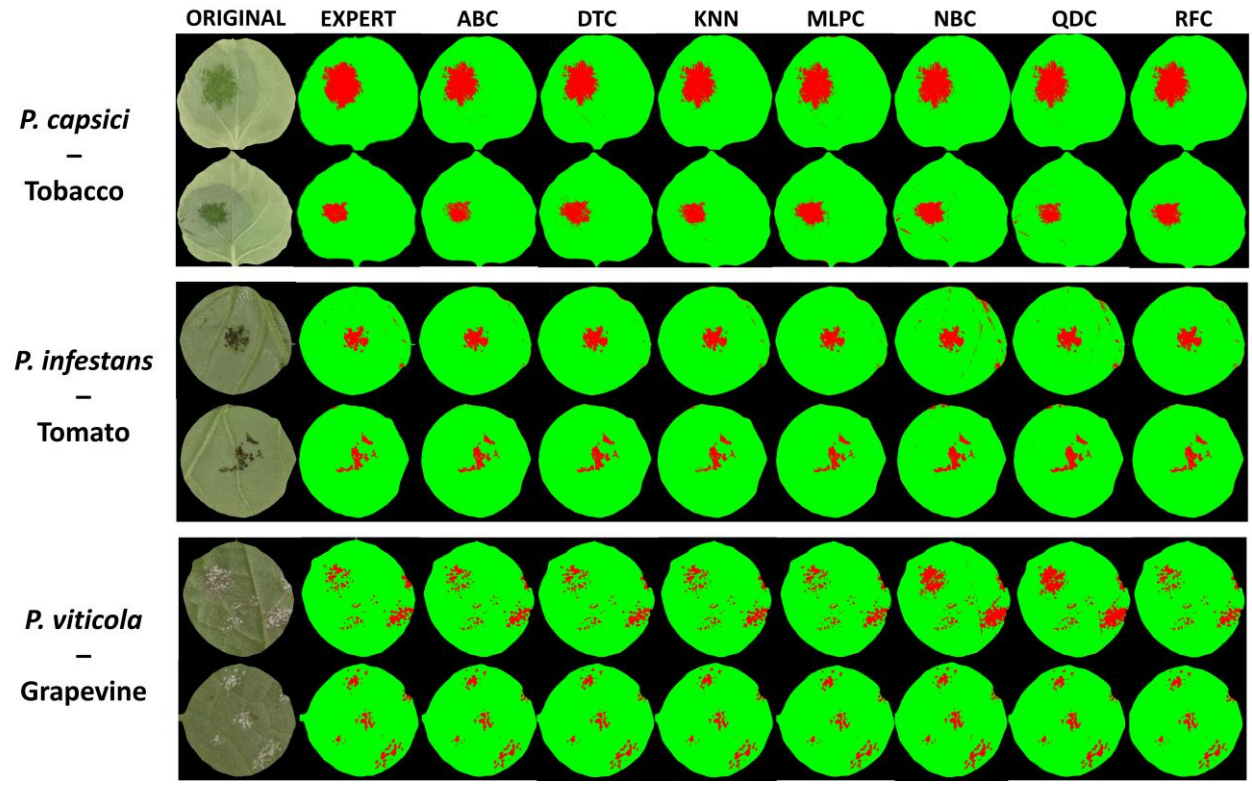

Furthermore, when analyzing the recorded disease severity values expressed in mm^2, it is noteworthy that all the employed methods exhibited comparable overall values for DA across all three pathosystems (Table 4).

Table 4: Disease severity values and standard deviations (expressed as mm^2) recorded for each pathosystem using different methods. The values measured by the experts are reported in bold.

	Mean (mm^2) ± SD		
	***P. capsici* - Tobacco**	***P. infestans* - Tomato**	***P. viticola* - Grapevine**
ABC	130.72 ± 86.88	9.95 ± 6.99	6.05 ± 5.44
DTC	153.06 ± 95.15	12.04 ± 8.56	5.73 ± 5.41
Experts	**145.71 ± 129.48**	**10.69 ± 9.21**	**6.75 ± 7.16**
KNN	137.66 ± 87.39	10.82 ± 7.19	5.81 ± 5.42
MLPC	152.2 ± 96.49	10.16 ± 6.81	6.65 ± 5.61
NBC	115.02 ± 87.61	14.05 ± 8.02	8.03 ± 7
QDC	103.89 ± 82.17	12.96 ± 7.97	7.46 ± 7.23
RFC	139.79 ± 89.19	11.01 ± 7.36	5.65 ± 5.4

To provide a comprehensive overview of the agreement between experts measurements and the SML algorithms, Lin's CCC was employed. Overall, the results demonstrate varying degrees of agreement between experts measurements and SML algorithms across the different pathosystems

(Table 5). As regards the *P. infestans* - tomato pathosystem, the CCC values ranged from 0.73 to 0.89. Notably, ABC and RFC demonstrated the highest CCC values, indicating a strong agreement, while NBC exhibited comparatively lower concordance. On the other hand, in the *P. viticola* - grapevine pathosystem, CCC values varied from 0.77 for NBC to 0.9 for KNN. Moving to the *P. capsici* - tobacco pathosystem, all SML algorithms performed slightly less effectively compared to the previous pathosystems, with CCC values ranging from 0.72 for QDC to 0.89 for both ABC and RFC. Notably, ABC and RFC consistently showed the highest agreement in the *P. infestans* - tomato and *P. capsici* - tobacco pathosystems, while KNN and RFC exhibited the highest agreement in the *P. viticola* - grapevine pathosystem.

Table 5: Lin's concordance correlation coefficients (CCC) between experts measurements and each SML algorithm for the three different pathosystems. The values in brackets represent the 95% confidence intervals.

	ABC	***DTC***	***KNN***	***MLPC***	***NBC***	***QDC***	***RFC***
P. capsici – tobacco	0.89 (0.84-0.92)	0.86 (0.8-0.9)	0.89 (0.84-0.92)	0.85 (0.79-0.9)	0.73 (0.62-0.81)	0.72 (0.62-0.8)	0.89 (0.84-0.92)
P. infestans – tomato	0.89 (0.87-0.91)	0.83 (0.79-0.86)	0.87 (0.85-0.9)	0.87 (0.85-0.9)	0.73 (0.68-0.77)	0.81 (0.77-0.84)	0.89 (0.86-0.91)
P. viticola – grapevine	0.84 (0.81-0.87)	0.88 (0.85-0.9)	0.9 (0.87-0.92)	0.78 (0.73-0.82)	0.77 (0.71-0.81)	0.79 (0.74-0.83)	0.89 (0.87-0.91)

The Bland-Altman plot (Figure 4) effectively displayed the agreement between the experts's measurements and those obtained from SML algorithms. Across all three pathosystems, the mean line closely approximated 0, indicating minimal systematic bias between the methods. Moreover, the limits of agreement (LOA) were observed to lay mostly within the range -1 - +1, corresponding to a deviation of ± 1 mm^2 in the back-transformed scale (i.e., $|1|^x = 1$; with x = 2 or 3). This suggests that approximately 95% of the differences between the methods fell within this range. Only a small portion of each dataset exhibited values outside the 95% interval, specifically, n = 11 out of 292 samples for *P. infestans* when using RFC, n = 11 out of 211 discs for *P. viticola*, and n = 1 out of 90 leaves for *P. capsici* when using KNN.

Figure 4: Bland-Altman (A) plots illustrating the comparison between DA measured by the experts and each SML algorithm [(A) ABC, (B) DTC, (C) KNN, (D) MLPC, (E) NBC, (F) QDC, and (G) RFC] represented individually in their respective subplots. Points are expressed in transformed scale (square-root for *P. infestans* and cube-root transformed for *P. capsici*, respectively). Dashed lines represent upper and lower limits of agreement (LOA), while solid line the mean difference between observed measures. Light colored ribbons display 95% confidence interval.

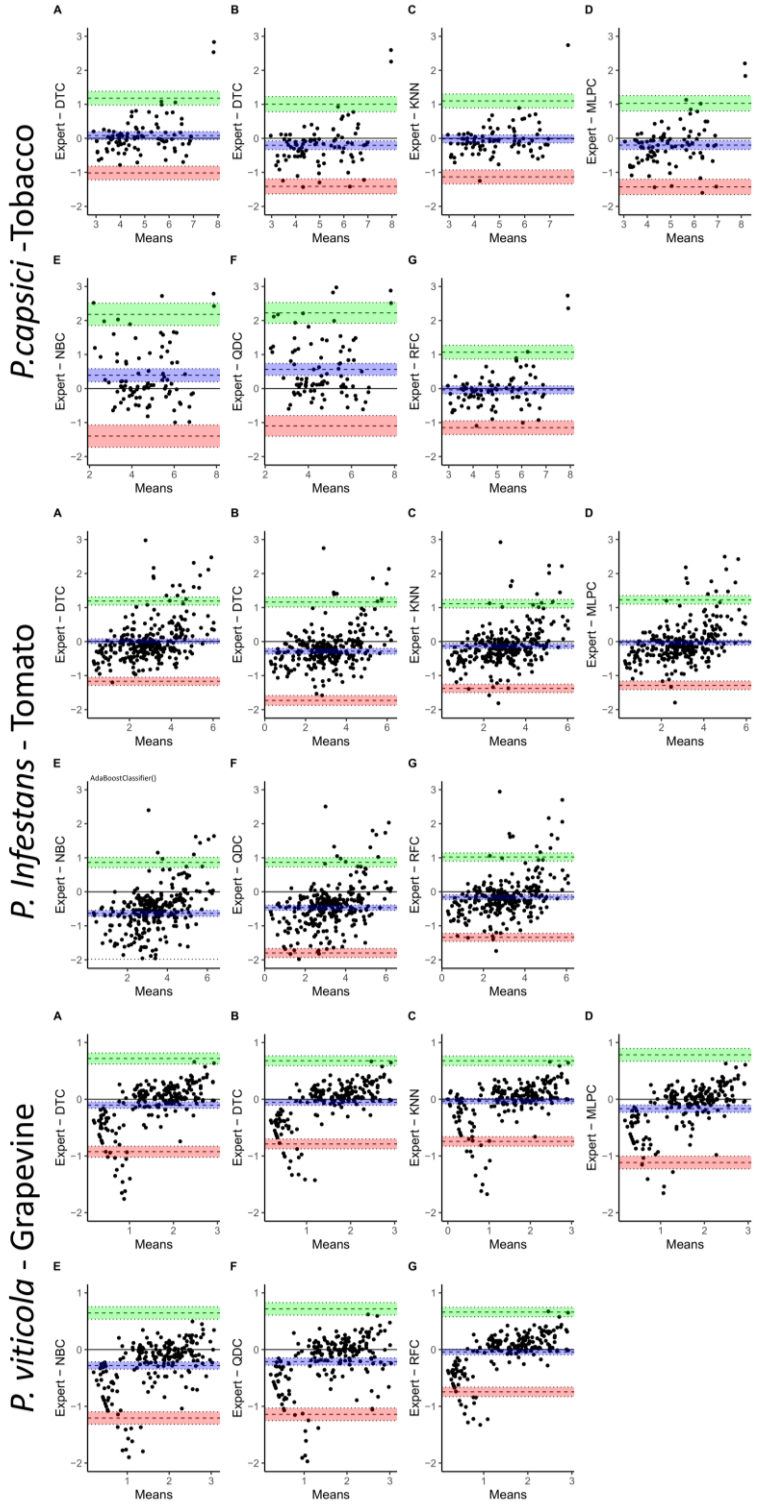

Discussion

Previous studies focused their attention on the assessment and quantification of disease severity at laboratory level in *P. viticola* – grapevine pathosystem, using different techniques and algorithms, ranging from traditional image thresholding (e.g. Otsu) coupled with fuzzy-logic to deep-learning approaches [50, 51, 52]. However, in many case the developed platforms are not accessible to potential users or are restricted to command-line interface. On the other hand, although the large number of studies published involving image analysis in plants affected by *Phytophthora* spp. [53, 54, 55], to the best of our knowledge, no specific tools focused on disease severity assessment at laboratory level have been specifically designed. On the contrary, many studies employ common image manipulation softwares (e.g. ImageJ) to quantify lesions caused by these pathogens [33, 56, 57, 58].

In this study, a novel pipeline for plant disease severity assessment at the laboratory level was developed and evaluated. The pipeline employed computer vision algorithms based on Python and SML algorithms provided within its library Sklearn. Three different pathosystems were used for validation: *P. infestans* – tomato leaf discs, *P. viticola* – grapevine leaf discs, and *P. capsici* – tobacco leaves. The pipeline well performed in image pre-processing leading to excellent background removal and object detection. Moreover, the disease severity assessment performed by the SML algorithms well recognized the specific symptoms associated with each pathosystem, exhibiting consistent and reliable performances. Indeed, the results highlighted a minimal systematic bias between the different SML algorithms and the gold standard method, indicating a good level of agreement.

The primary objective of the presented pipeline is to address the specific needs in disease severity assessment while prioritizing the role of plant pathologists in driving the decision-making process. In this framework, the pipeline aims to provide broader access to advanced computer vision and ML techniques for the plant pathology community, offering a versatile tool. During the implementation, our goal was to minimize the number of user-input parameters required, ensuring a user-friendly and straightforward experience to a broader audience, with varying levels of technical expertise.

The pipeline comprises four main modules that can be executed independently, offering enhanced flexibility and seamless integration with existing tools. Specifically, the pre-processing and segmentation utilities serve as alternatives to conventional image processing software like ImageJ and Assess [59] within a unified environment. Notably, the software design is optimized for efficiently handling multiple images in directory-based operations, thereby accelerating processes, particularly when dealing with large datasets. Furthermore, the training approach employed in the pipeline offers remarkable flexibility in selecting and fine-tuning SML algorithms. Indeed, users can effortlessly train different models provided by Sklearn by simply modifying a single parameter. Moreover, plant pathologists have the freedom to determine the optimal

number of images to be used for effective training, drawing on their expertise and experience. Furthermore, the segmentation utilities offer an alternative to SML-based disease severity assessment, presenting a valuable tool for comparing manual measurements with the model's accuracy. In future implementations, we aim to introduce multiclass classifiers that will enable discrete segmentation of multiple symptoms on the same plant unit, providing a more comprehensive and detailed analysis of complex disease scenarios. Moreover, with the increasing availability of GPU-based hardware, we plan to incorporate unsupervised and deep learning models into the pipeline. This addition will significantly expand the tool's capabilities, allowing for advanced tasks such as semantic segmentation and image classification. These advancements will enhance the pipeline's versatility, making it suitable for a broader range of symptoms and plant pathosystems. To improve the system, the active involvement of the community in the continuous development and improvement of the pipeline is strongly encouraged. We believe that through collaborative efforts, we can collectively enhance phytopathometry tools to meet the requirements of the plant pathology field, with user-friendly solutions.

References

1. Fang Y, Ramasamy RP. 2015. Current and prospective methods for plant disease detection. Biosensors 5:537–561.
2. Bock CH, Barbedo JG, Del Ponte EM, Bohnenkamp D, Mahlein A-K. 2020. From visual estimates to fully automated sensor-based measurements of plant disease severity: status and challenges for improving accuracy. Phytopathology Research 2:1–30.
3. Chester KS. 1950. Plant disease losses: their appraisal and interpretation. Plant disease losses: their appraisal and interpretation.
4. Nutter Jr F, Teng P, Shokes F. 1991. Disease assessment terms and concepts. Plant disease.
5. Madden LV, Hughes G, Van Den Bosch F. 2007. The study of plant disease epidemics.
6. Bock C, Poole G, Parker P, Gottwald T. 2010. Plant disease severity estimated visually, by digital photography and image analysis, and by hyperspectral imaging. Critical reviews in plant sciences 29:59–107.
7. Mahlein A-K. 2016. Plant disease detection by imaging sensors–parallels and specific demands for precision agriculture and plant phenotyping. Plant disease 100:241–251.
8. Bock C, El Jarroudi M, Kouadio L, Mackels C, Chiang K-S, Delfosse P. 2015. Disease severity estimates—Effects of rater accuracy and assessment methods for comparing treatments. Plant Disease 99:1104–1112.
9. Knoblauch K, Maloney LT. 2008. Estimating classification images with generalized linear and additive models. Journal of Vision 8:10–10.
10. Kotsiantis SB, Zaharakis I, Pintelas P. 2007. Supervised machine learning: A review of classification techniques. Emerging artificial intelligence applications in computer engineering 160:3–24.
11. Singh AK, Ganapathysubramanian B, Sarkar S, Singh A. 2018. Deep learning for plant stress phenotyping: trends and future perspectives. Trends in plant science 23:883–898.
12. Pugliese R, Regondi S, Marini R. 2021. Machine learning-based approach: Global trends, research directions, and regulatory standpoints. Data Science and Management 4:19–29.
13. Del Ponte EM, Pethybridge SJ, Bock CH, Michereff SJ, Machado FJ, Spolti P. 2017. Standard area diagrams for aiding severity estimation: scientometrics, pathosystems, and methodological trends in the last 25 years. Phytopathology 107:1161–1174.
14. Olivoto T, Andrade SM, M. Del Ponte E. 2022. Measuring plant disease severity in r: introducing and evaluating the pliman package. Tropical Plant Pathology 47:95–104.
15. Bradski G. 2000. The openCV library. Dr Dobb's Journal: Software Tools for the Professional Programmer 25:120–123.
16. Van der Walt S, Schönberger JL, Nunez-Iglesias J, Boulogne F, Warner JD, Yager N, Gouillart E, Yu T. 2014. scikit-image: image processing in Python. PeerJ 2:e453.
17. Pedregosa F, Varoquaux G, Gramfort A, Michel V, Thirion B, Grisel O, Blondel M, Prettenhofer P, Weiss R, Dubourg V. 2011. Scikit-learn: Machine learning in Python. the Journal of machine Learning research 12:2825–2830.
18. Müller AC, Guido S. 2016. Introduction to machine learning with Python: a guide for data scientists. O'Reilly Media, Inc.
19. Fix E, Hodges JL. 1989. Discriminatory analysis. Nonparametric discrimination: Consistency properties. International Statistical Review/Revue Internationale de Statistique 57:238–247.
20. Quinlan JR. 1986. Induction of decision trees. Machine learning 1:81–106.
21. Breiman L. 2001. Random forests. Machine learning 45:5–32.
22. McCulloch WS, Pitts W. 1943. A logical calculus of the ideas immanent in nervous activity. The bulletin of mathematical biophysics 5:115–133.
23. Freund Y, Schapire RE. 1997. A decision-theoretic generalization of on-line learning and an application to boosting. Journal of computer and system sciences 55:119–139.
24. Friedman N, Geiger D, Goldszmidt M. 1997. Bayesian network classifiers. Machine learning 29:131–163.
25. Friedman JH. 1989. Regularized discriminant analysis. Journal of the American statistical association 84:165–175.
26. Gehan MA, Fahlgren N, Abbasi A, Berry JC, Callen ST, Chavez L, Doust AN, Feldman MJ, Gilbert KB, Hodge JG. 2017. PlantCV v2: Image analysis software for high-throughput plant phenotyping. PeerJ 5:e4088.
27. Schneider CA, Rasband WS, Eliceiri KW. 2012. NIH Image to ImageJ: 25 years of image analysis. Nature methods 9:671–675.
28. Mohanty SP, Hughes DP, Salathé M. 2016. Using deep learning for image-based plant disease detection. Frontiers in plant science 7:1419.
29. O'Connell RJ, Panstruga R. 2006. Tête à tête inside a plant cell: establishing compatibility between plants and biotrophic fungi and oomycetes. New Phytologist 171:699–718.
30. Koeck M, Hardham AR, Dodds PN. 2011. The role of effectors of biotrophic and hemibiotrophic fungi in infection. Cellular microbiology 13:1849–1857.

31. Kamoun S, Furzer O, Jones JD, Judelson HS, Ali GS, Dalio RJ, Roy SG, Schena L, Zambounis A, Panabières F. 2015. The Top 10 oomycete pathogens in molecular plant pathology. Molecular plant pathology 16:413–434.
32. Pang Z, Shao J, Chen L, Lu X, Hu J, Qin Z, Liu X. 2013. Resistance to the novel fungicide pyrimorph in Phytophthora capsici: risk assessment and detection of point mutations in CesA3 that confer resistance. PLoS One 8:e56513.
33. Yang K, Dong X, Li J, Wang Y, Cheng Y, Zhai Y, Li X, Wei L, Jing M, Dou D. 2021. Type 2 Nep1-like proteins from the biocontrol oomycete Pythium oligandrum suppress Phytophthora capsici infection in solanaceous plants. Journal of Fungi 7:496.
34. Marcianò D, Toffolatti SL. 2023. Methods for Fungicide Efficacy Screenings: Multiwell Testing Procedures for the Oomycetes Phytophthora infestans and Pythium ultimum. Microorganisms 11:350.
35. Judelson HS, Blanco FA. 2005. The spores of Phytophthora: weapons of the plant destroyer. Nature Reviews Microbiology 3:47–58.
36. Marcianò D, Ricciardi V, Marone Fassolo E, Passera A, Bianco PA, Failla O, Casati P, Maddalena G, De Lorenzis G, Toffolatti SL. 2021. RNAi of a putative grapevine susceptibility gene as a possible downy mildew control strategy. Frontiers in Plant Science 12:667319.
37. Marcianò D, Ricciardi V, Maddalena G, Massafra A, Marone Fassolo E, Masiero S, Bianco PA, Failla O, De Lorenzis G, Toffolatti SL. 2023. Influence of Nitrogen on Grapevine Susceptibility to Downy Mildew. Plants 12:263.
38. Colombo M, Masiero S, Rosa S, Caporali E, Toffolatti SL, Mizzotti C, Tadini L, Rossi F, Pellegrino S, Musetti R. 2020. NoPv1: a synthetic antimicrobial peptide aptamer targeting the causal agents of grapevine downy mildew and potato late blight. Scientific reports 10:17574.
39. Mattos A do P, Tolentino Júnior JB, Itako AT. 2020. Determination of the severity of Septoria leaf spot in tomato by using digital images. Australasian Plant Pathology 49:329–356.
40. Raybaut P. 2009. Spyder-documentation. Available online at: pythonhosted org.
41. Van Rossum G, Drake F. 2009. Python 3 Reference Manual. Scotts Valley, CA: CreateSpace.
42. Tkalcic M, Tasic JF. 2003. Colour spaces: perceptual, historical and applicational background. IEEE.
43. Otsu N. 1979. A threshold selection method from gray-level histograms. IEEE transactions on systems, man, and cybernetics 9:62–66.
44. Lawrence I, Lin K. 1989. A concordance correlation coefficient to evaluate reproducibility. Biometrics 255–268.
45. Altman DG. 1990. Practical statistics for medical research. CRC press.
46. Andri S, Ken A, Andreas A, Nanina A, Tomas A, Chandima A, Antti A, Adrian B, Kamil B, Ben B. 2021. DescTools: Tools for descriptive statistics. R package version 099 43.
47. Bland JM, Altman DG. 1999. Measuring agreement in method comparison studies. Statistical methods in medical research 8:135–160.
48. Datta D. 2017. blandr: A Bland-Altman Method Comparison Package for R. Zenodo. doi: 10.5281/zenodo. 824514.
49. Team Rs. 2021. RStudio: integrated development for R. RStudio, PBC, Boston, MA. 2020.
50. Hernández I, Gutiérrez S, Ceballos S, Iñíguez R, Barrio I, Tardaguila J. 2021. Artificial intelligence and novel sensing technologies for assessing downy mildew in grapevine. Horticulturae 7:103.
51. Divilov K, Wiesner-Hanks T, Barba P, Cadle-Davidson L, Reisch BI. 2017. Computer vision for high-throughput quantitative phenotyping: a case study of grapevine downy mildew sporulation and leaf trichomes. Phytopathology 107:1549–1555.
52. Zendler D, Malagol N, Schwandner A, Töpfer R, Hausmann L, Zyprian E. 2021. High-throughput phenotyping of leaf discs infected with grapevine downy mildew using shallow convolutional neural networks. Agronomy 11:1768.
53. Appeltans S, Pieters J, Mouazen A. 2022. Potential of laboratory hyperspectral data for in-field detection of Phytophthora infestans on potato. Precision Agriculture 23:876–893.
54. Ozyilmaz U. 2020. Evaluation of the effectiveness of antagonistic bacteria against Phytophthora blight disease in pepper with artificial intelligence. Biological Control 151:104379.
55. Chakraborty KK, Mukherjee R, Chakroborty C, Bora K. 2022. Automated recognition of optical image based potato leaf blight diseases using deep learning. Physiological and Molecular Plant Pathology 117:101781.
56. Liang X, Bao Y, Zhang M, Du D, Rao S, Li Y, Wang X, Xu G, Zhou Z, Shen D. 2021. A Phytophthora capsici RXLR effector targets and inhibits the central immune kinases to suppress plant immunity. New Phytologist 232:264–278.
57. De Vrieze M, Germanier F, Vuille N, Weisskopf L. 2018. Combining different potato-associated Pseudomonas strains for improved biocontrol of Phytophthora infestans. Frontiers in microbiology 9:2573.
58. Karki HS, Halterman DA. 2021. Phytophthora infestans (late blight) infection assay in a detached leaf of potato. Bio-protocol 11:e3926–e3926.
59. Lamari L. 2008. Assess 2.0 [recurso electrónico]: image analysis software for plant disease quantification. APS Press.

Paper III

Introduction to paper III

Antimicrobial peptides (AMPs) are a class of small peptides which attracted attention for their potential as next-generation antibiotics. AMPs have a wide range of inhibitory effects against several organisms, including plant pathogenic bacteria, fungi, and oomycetes. For this reason, AMPs have been proposed as a potential game-changing alternative for crop protection. In particular, peptide aptamers (PA), combinatorial aminoacid sequences that specifically bind target proteins with high specificity and a strong affinity, look promising for this purpose. An ideal fungicide displays high specificity towards target species and reduced negative environmental impact. In this context, the cell wall metabolism of phytopathogens represents an ideal target for fungicide discovery since its proven relevance to infection processes and pathogen survival. During my PhD I was involved in the NoPest project (https://www.h2020nopest.org/). The project aims to explore new solutions to counteract oomycete infections in crops. The idea is to develop new-generation fungicides with high specificity and lower environmental impact compared to products currently employed. This was achieved through the identification of PAs with anti-oomycete activity derived from genetically encoded peptide libraries. In the following section, we introduce the results regarding the two leading peptides arising from the project and presented in the third research article included this thesis work, named paper III.

CP20 and CP32: two novel antimicrobial peptide aptamers exhibiting strong anti-oomycete activity

Authors: Demetrio Marcianò[1#], Stefano Rosa[2#], Monica Colombo[2], Vaibhav Srivastava[3], Lucia Feni[4], Sara Pellegrino[4], Silvia Laura Toffolatti[1], Paolo Pesaresi[2], Simona Masiero[2]

[1] Department of Agricultural and Environmental Sciences, University of Milan, 20133 Milan, Italy

[2] Department of Biosciences, University of Milan, 20133 Milan, Italy

[3] Division of Glycoscience, Department of Chemistry, School of Engineering Sciences in Chemistry, Biotechnology and Health, KTH Royal Institute of Technology, AlbaNova University Center, 106 91 Stockholm, Sweden

[4] DISFARM-Department of Pharmaceutical Sciences, University of Milan, 20133 Milan, Italy

# Demetrio Marcianò and Stefano Rosa contributed equally to this article.

Abstract

Phytopathogenic oomycetes, are fungal-like eukaryotes that pose significant threats to agriculture. These pathogens are often controlled using fungicides but increasing limitations in their use and the rapid development of resistance challenge effective disease management. The inhibition of cell wall biosynthesis in oomycetes could represent a crucial target for disease control, but traditional fungicide discovery is costly and time-consuming. Recently, the use of Peptide aptamers (PAs) (i.e short amino acid chains specifically binding to target proteins), have emerged as promising molecular tools for disease control. In this study, PAs interacting with proteins involved in oomycete cell wall biosynthesis were screened for their antimicrobial activity. Out of 77 PAs, two aptamers exhibiting strong antimicrobial activity towards *Phytophthora infestans, Phytophthora capsici, Pythium ultimum* and *Plasmopara viticola* were identified. The PAs resulted in strong inhibition *in vitro* at concentrations higher than 50 μM, and successfully inhibited infection development on plant tissues. The results obtained from microscopy data demonstrate that CP20 and CP32 can efficiently interfere with *P. infestans* development causing structural and ultra-structural aberrations. Moreover, both PAs interact efficiently with *P. infestans* membranes and accumulate in hyphal tips, where cellulose synthase enzymes mainly localize. Further experiments are ongoing to shed light on the mode of action associated with the anti-oomycete activity of the two molecules.

Introduction

Oomycetes are fungal-like eukaryotes belonging to the TSAR supergroup [1], which includes many species that represent a threat to forestry, agriculture and aquaculture [2]. Phytopathogenic oomycetes have significant relevance in crop production and food security due to their ability to cause devastating plant diseases. Indeed, if not adequately controlled, oomycete borne diseases can result in substantial crop losses, impacting the economy, food availability, and access to staple crops [3].

Phytophthora infestans Mont. (de Bary) is a highly destructive and extensively studied species among plant-pathogenic oomycetes. This organism is responsible for causing late blight in tomatoes and potatoes, resulting in annual economic losses estimated in billions of dollars [4]. The main mode of infection by this hemibiotrophic pathogen involves both asexual spores (zoospores produced in sporangia) spreading on aerial organs and mycelium in infected tubers [4, 5]. *Phytophthora capsici* Leonian., is a plant pathogen responsible for important losses to vegetable production worldwide, in several crops including Solanaceae, legumes and cucurbits. *P. capsici* survives in soil for extended periods as thick-walled oospores, which gave rise to infections. Under optimal conditions, sporangia are produced from infected plant tissues thus further spreading the disease [6]. *Plasmopara viticola* (Berk. et Curtis) Berl. & De Toni, is the oomycete causing grapevine downy mildew, a major threat to grapevine production worldwide. Indeed, severe disease epidemics caused by this pathogen are often associated with consistent quantitative and qualitative yield losses [7]. Infections are carried out by zoospores, either developed from oospores (primary infections) or sporangia (secondary infections). Also in this case, disease control is often carried out using fungicides [8, 9]. Another significant phytopathogenic oomycete is *Pythium ultimum* Trow var. *ultimum*, which is the most extensively studied species in its genus. It is a widely distributed necrotrophic pathogen, causing damping off and root rot in over 300 different hosts, including staple crops like corn and wheat [3]. In this case, infections are mainly carried out by sporangia-like hyphal swellings [10]. However, chemical control through soil treatments is not always practical due to economic and ecological considerations [11]. The tremendous evolutionary potential demonstrated by these organisms [12] and their rapid development of resistance to fungicides represent a constant threat to effective disease management. Indeed, while chemical control remains a widespread approach, the progressive reduction in the number of active substances available [2], and the increase of resistant strains in pathogens' field populations are challenging its exploitation [9].

The cell wall of oomycetes mainly consists of polysaccharides (mostly 1,4- and 1,3-β-linked glucans) and plays a crucial role in their life cycle [13]. For instance, the inhibition of cellulose synthesis in *P. infestans* either through chemical treatment or gene silencing has been proved to cause a complete loss of pathogenicity [14]. Another example is represented by the Carboxylic

Acid Amide (CAA) fungicides class, which is currently employed for controlling oomycete-borne diseases in various crops and interferes with cell wall deposition and cellulose biosynthesis [15]. For this reason, targeting enzymes involved in the biosynthesis of cell wall components, could be an effective approach for controlling oomycete diseases. However, our understanding of the biochemical properties of these enzymes is limited, making it challenging to develop specific inhibitors that can effectively hinder the growth of pathogenic oomycetes [16]. Traditional fungicide discovery is a lengthy and costly process. In fact, the overall costs for discovering and developing a new crop protection product reached $286 million in 2014, and it typically takes an average of 11.3 years from the initial synthesis to market availability [17]. Due to these challenges, researchers are exploring alternative approaches alongside traditional methods. Biotechnology-based and target-oriented approaches such as small RNAs and peptide aptamers (PAs) are attracting the interest of the scientific community [18, 19, 20]. In particular, PAs emerged as novel molecular tools for disease control. PAs are short chains of amino acids selected for their ability to specifically bind, and inhibit a given target molecule. These molecules are often selected from combinatorial libraries based on their affinity and specificity to a given target protein, taking advantage of multiple *in vivo* and *in vitro* selection procedures. One common *in vivo* procedure is represented by the yeast two hybrid (Y2H) approach. Indeed, the Y2H allows researchers to identify and validate protein-peptide interactions under physiological conditions [21]. For this reason, some authors suggested the potential role of PAs in the development of antimicrobial compounds characterized by a better environmental fate, lower off-target effects and possibly a low-risk alternative to conventional pesticides [18]. In the present study PAs selected from a combinatorial library through Y2H, putative interacting with target proteins involved in cell wall biosynthesis and remodeling were screened against selected oomycetes species to determine their antimicrobial activity. Furthermore, the activity of two best-performing PAs was deeply characterized through a combination of radiometric and microscopy assays to get insights on their mode of action.

Materials and methods

Peptide Library Construction, Yeast Two-Hybrid Assay and Peptide synthesis

A combinatorial library encompassing 8 amino acids cyclic peptides was constructed following the protocol described in Rosa et al. [22]. Linear peptides were selected using the library described by Colombo and collaborators [18]. In both cases, the combinatorial peptide-encoding sequences were fused with the GAL4-AD domain and introduced into the AH109 yeast strain. The GAL4-BD domain fused with bait sequences from oomycete enzymes of interest were expressed as bait using the pGBKT7 vector and individually transformed into the Y187 yeast strain. Co-cultivation step resulted in the generation of diploid yeast cells containing both the plasmid encoding the GAL4-BD bait fusion and the library plasmid expressing a cyclic peptide (CP) fused to GAL4-AD. Positive yeast clones capable of interacting with the bait were selected based on their ability to grow on selective media. The DNA of the plasmid within the positive clones was then amplified by PCR and sequenced, allowing the determination of the primary structure of PAs [18, 22]. Cyclic and linear peptides were synthesized, using solid-phase peptide synthesis (SPPS) with Fmoc/tBu strategy, automated and microwave-assisted as described previously [18, 23]. Once ready, the peptides were purified through precipitation, followed by RP-HPLC, and stored at -15°C until use. Alternatively, PAs were purchased as lyophilized powder from Caslo ApS (Denmark). All PAs stock solutions and corresponding mocks were prepared using the same solvent, either distilled water or 20% v/v DMSO, according to the overall solubility.

Screening of PAs for their antimicrobial activity against selected oomycete species

Preliminary screenings of the synthesized PAs were conducted to evaluate their antimicrobial activity against four selected oomycete species. The fungal materials used in the experiments were as follows: the *P. infestans* isolate n. 111344 (CBS; Baarn, The Netherlands) grown on pea agar medium (PAM, 12.5% w/v frozen peas in distilled water and 1.2% w/v bacteriological agar). *P. capisci* strain Hd11 [24] and *P. ultimum* isolate (n. 724.94; CBS; Baarn, The Netherlands) cultured on PDA (Potato Dextrose Agar) plates (Liofilchem, Italy); and finally, the *P. viticola* monosporangial isolate n. 10 maintained on detached grapevine leaves [25].

For preliminary screenings, all the PAs were tested at a final concentration of 200 µM, and every assay included a negative control amended with sterile distilled water in place of the PA, and a positive control amended with a commercial fungicide, either Pergado SC (containing 250 g/L mandipropamid) or Ridomil Gold SL (465 g/L metalaxyl-M) (Syngenta, Milan, Italy). *In vitro* antimicrobial activity against *P. infestans* was evaluated using either the liquid medium (Pea broth) assay in 96-wells plates inoculated with asexual spores (sporangia), or the agar medium (PAM) assay in 24-wells plates inoculated with mycelial plugs. The activity against *P. capsici* was evaluated using the liquid medium (PDB, Potato Dextrose Broth) assay with 96-wells inoculated

with sporangia, while the activity against *P. ultimum* was assessed using the agar medium (PDA) assay inoculated with mycelium (Table 1) [26]. Mycelial growth was assessed after 3 days post inoculation (dpi).

The ability to prevent *P. infestans* and *P. viticola* infections on plant tissues was assessed through co-inoculation assays, on tomato and grapevine leaf discs respectively (Table 1). For this purpose, PAs were directly added to the spore suspension at the desired concentration immediately before inoculation of plant tissues. Leaf discs with a diameter of 1.5 cm were obtained from tomato leaves (*Solanum lycopersicum*, cv. Marmande) using a cork borer. Nine discs were placed (lower surface upwards) in a Petri dish containing moistened filter paper. A *P. infestans* sporangia suspension ($1x10^4$ sporangia/mL) was obtained from 7 days old cultures as previously described [26], and resuspended in modified Petri's solution (0.25 mM $CaCl_2$; 1 mM $MgSO_4$; 1 mM KH_2PO_4; 0.8 mM KCl). The pathogen was inoculated with a 10 µL drop in the disc center and plates stored at 4°C for 3 h to induce zoospore release. The activity against *P. viticola* was evaluated using the co-inoculation assay described by Colombo et al. [18]. After inoculation, plates were stored in a growth chamber at 22 ± 1 °C with a photoperiod of 16 hours light and 8 hours dark. After the incubation period (5 days post inoculation for *P. infestans* and 7 days for *P. viticola*). The disease severity was evaluated by assigning a class to each leaf disc based on the percentage of leaf disc surface covered with symptoms [27].

Table 1: Comprehensive resume of *in vitro* and *ex vivo* assays performed on selected Oomycete species [18, 26].

Name of the test	***Species of interest***	***Substrate***	***Inoculum source***	***Response variable***	***Efficacy index***
Multiwell culture assay (24 wells) with mycelial plugs on solid medium	*P. infestans*	PAM (pea agar medium)	Mycelial plugs	Colony diameter (cm)	PGI_S
Multiwell culture assay (96 wells) with mycelium on liquid medium	*P. ultimum*	PDB (Potato Dextrose Broth)	Mycelial suspension	Absorbance (OD620)	PGI_L
Multiwell culture assay (96 wells) with sporangia suspension on liquid medium	*P. capsici* *P. infestans*	PDB; PB (Pea Broth)	Sporangia suspension	Absorbance (OD620)	PGI_L
Experimental inoculation of a P. infestans sporangia suspension on tomato leaf discs	*P. infestans*	Tomato leaf discs	Sporangia suspension	Disease severity index	PPI
Experimental inoculation of a *P. viticola* sporangia suspension on grapevine leaf discs	*P. viticola*	Grapevine leaf discs	Sporangia suspension	Disease severity index	PPI

According to the test, a percentage efficacy index was calculated (Table 2), based on the reduction in the pathogen growth (or in disease symptoms) compared to the untreated control. The use of these indexes was chosen to guarantee an immediate comparison in the efficacy of the PAs across different experiments and experimental conditions. PAs exhibiting an efficacy higher than 70% were selected for further validation.

Table 2: General formulas of percentage efficacy indexes derived from the experimental procedures.

Efficacy index	*Formula*	*Input variables*
Percentage Protection Index (Leaf discs) - PPI	$PPI = 100 - \frac{(DSI_1 \times 100)}{DSI_2}$	DSI_1: Disease Severity Index (DSI) of treated leaf discs. DSI_2: mean DSI of untreated leaf discs.
Growth inhibition percentage (solid medium) - GIP_S	$GIP_S = 100 - \frac{(D_1 \times 100)}{D_2}$	D_1: diameter (in cm or mm) measured for the treated colonies. D_2: mean diameter (in cm or mm) of untreated colonies.
Growth inhibition percentage (liquid medium) - GIP_L	$GIP_L = 100 \times \frac{[(At_{fNT} - At_{0NT}) - (At_{fT} - At_{0T})]}{[(At_{fNT} - At_{0NT})]}$	At_f: absorbance measured at final time point; At_0: absorbance measured at initial time point; NT: not-treated with fungicide/aptamer; T: treated with fungicide/aptamer.

Statistical analyses were always performed to assess the presence of significant differences among the efficacies of different PAs tested and the fungicide used as positive control in the assays. On this purpose, since percentage indexes can be assumed to be a sample from beta distribution, a beta regression model (BRM) was employed. Pairwise comparisons among different treatments, were performed on estimated marginal means (EMMs) retrieved from the fitted model as previously described [26]. All the analysis were conducted in R, using R Studio 9.1 [28].

Deep characterization of best performing PAs

Dose response analysis

Considering the high sequence homology of orthologous genes encoding the target proteins among *Phytophthora* species and other *Peronosporales* [29], the promising PAs emerged from the preliminary screenings were tested against other oomycete species using the same procedures described for the screenings (Table 1). Furthermore, to determine effective concentrations (ECx - i.e. the active molecule dose that inhibits growth by "x%" compared to a non-amended control) [30], a dose-response analysis (DRA) was conducted on *P. infestans* sporangia using decreasing PA concentrations (0.02; 0.2; 2; 20 and 200 µM). The ECx concentrations were determined by interpolation from a non-linear regression curve of percentage growth inhibition data (GIP_L), following well-established procedures [26, 31]. To fine-tune the DRA results, the resazurin (RZ) reduction test was employed. RZ is a nontoxic dye used to estimate cell viability via the spectrophotometric determination of the dye properties. More into details, cell metabolism induces the RZ reduction from dark blue to a fluorescent (pink) form [32]. On this purpose, the

liquid medium assay was modified to account for the reduction of resazurin (final concentration = 40 µM) in PA amended media at different concentrations (200, 100, 50, 25, 12.5, 6.25, 3.12, 1.56, 0.78 µM). The OD_{600} of each well was measured for three consecutive days and ECx values were determined as previously described using absorbance values recorded at 3 dpi as response variable.

In vitro radiometric assays on P. infestans *cellulose synthases (CesA)*

To investigate the effect of PAs on the activity of *P. infestans* cellulose synthases (PiCesA), a radiometric assay was employed. The assay aimed to measure the incorporation of glucose (Glc) into glucans produced by PiCesA proteins, using radioactive labelled UDP-Glc. Two protein sources from *P. infestans* mycelium were employed in the assay: microsomal fractions (MF) and their detergent extracts (DE). MF were retrieved as previously described and the whole procedure was carried out at 4°C [29, 33, 34, 35, 36]. More into details, 5-day-old *P. infestans* cultures grown in pea broth medium (PB) were rinsed in an extraction buffer (EB: Tris-HCl 10 mM pH 7.4) supplemented with a protease inhibitor cocktail (Roche cOmplete™), homogenized in a Waring blender, and centrifuged at 8,000 rcf for 10 minutes. The resulting supernatant was filtered through Miracloth (20 µm mesh) to remove floating debris and lipids, and then centrifuged at 100,000 rcf for 1 hour using a Beckman-Coulter Optima L-100 XP ultracentrifuge. The pelleted membranes (MF) were resuspended in 100 µl of EB containing 10% glycerol and the protein content in determined using the Bradford assay, and the concentration adjusted to 4 mg/mL. Detergent extraction was performed using 0.5% w/v CHAPS (3-[(3-cholamidopropyl)dimethylammonio]-1-propanesulfonate) with gentle continuous stirring for 30 minutes [35, 37]. The detergent-treated MF were then centrifuged at 100,000 rcf for 1 hour, the resulting supernatant (DE) collected and proteins quantified as above. The enzymatic reaction mixture consisted of 150 µg of proteins (from either MF or DE), 7.5 mM Pipes/Tris pH 6.0, 1.25 mM DTT, 1 µM UDP-[14C-U]glucose (302 mCi/mmol; Perkin Elmer, Boston, USA), 1 mM UDP-glucose, and 10 mM $MgCl_2$ in a total volume of 200 µl. After 1 hour of incubation, the reactions were stopped and processed according to the protocol described by Brown et al. [35]. The radioactivity incorporated into insoluble and soluble fractions was measured using a scintillation counter (MicroBeta2® Microplate Counter, PerkinElmer), using Ultima Gold F or Ultima Gold scintillation cocktail in a final volume of 4 mL.
Once the method was established, a new set of reactions was conducted using DE as the protein source. Selected PAs were directly added to the reaction mixtures to reach a final concentration of 100 µM. The glucan synthase inhibitor flupoxam (500 µM) was used as positive control [38]. Three reactions per treatment were carried out, and the experiment was repeated twice. Cpm (count per minutes) values obtained from scintillation counting were then converted to nmol of [$_{14}$C]glucose incorporated according to equation 1 and related to mg of protein employed in the reaction.

$$Sugar\ incorporated\ [nmol] = \left(\frac{cpm\ sample - cpm\ blank}{cpm\ total} * 10\right) * sugar\ concentration\ \left[\frac{nmol}{\mu l}\right] * 200\ \mu l\ sample\ volume \quad (1)$$

In order to determine if there were variations in the amount of [$_{14}$C]glucose incorporated among the different treatments, a one-way ANOVA was conducted using the aov() function in R. *Post-hoc* comparisons were performed using the REGW method implemented through dedicated function in the R package *agricolae* [39] in R Studio 9.1 [28]. To characterize products formed in glucan synthase assays, Thin Layer Chromatography (TLC) was carried out on reaction products devoid of radiolabeled glucose. Before TLC, freeze dried reaction products (soluble fractions) were resuspended in a 1:1 chloroform:water partition and purified from protein residues. Finally, 1 µL purified reaction product was spotted on silica gel-60 plates (Merck), as well as control standards including glucose, UDP-glucose, cellobiose and cellotriose (0.1 mg/mL). Plates were developed using a 2:1:1 butan-1-ol/acetic acid/water solution until the full height of the plates (20 cm). Upon completion of the run, plates were successively dried, dipped into 8% H_2SO_4 ethanol solution and heated with a heat gun until spots became visible [37].

Zoospore release assay

The asexual multinucleated sporangia of *P. infestans* can germinate directly through a germ tube or indirectly by releasing zoospores [40]. To determine the specific effects of PAs on zoospore release, 200 µl of a *P. infestans* sporangia suspension (2 x 10^4 sporangia/mL) prepared in ice-cold modified Petri's solution was treated with selected PAs at their respective EC_{50}, EC_{75}, and EC_{90} concentrations. In addition, a negative (Petri's buffer only), and a positive control, including the known cellulose synthase inhibitor DCB (40 µM) (2,6-Dichlorobenzonitrile; Sigma Aldrich, Milan, Italy) were also included [14]. Three biological replicas were prepared, and the experiment carried out twice. Sporangia were incubated at 4°C for 4 hours to release zoospores. Zoospore encystment was induced through mechanical agitation by vortexing at maximum speed for 60 seconds. Samples were fixed using 2.5% glutaraldehyde in 1x PBS and stored at 4°C until count. The total number of sporangia and the number of indirectly germinated sporangia (empty sporangia with open operculum) and encysted zoospores were counted in KOVA slides following manufacturer's instructions (KOVA Inc., USA) under a light microscope (Primo Vert, Zeiss). The rate of indirect germination was calculated, and a BRM with pairwise comparisons among EMMs, as described for antimicrobial activity screenings, was employed to investigate whether the treatment with selected PAs had any significant effects on zoospore release.

Structural alteration in sporangia treated cultures via *optical microscopy*

To investigate the effects of PAs on *P. infestans* sporangia growth, sporangia were incubated in PB medium amended with selected PAs (100 µM) for 3 days. Moreover, a negative control with PB

alone was also included in the assay. Samples were directly stained on a microscope slide using 10 mg/l Trypan blue (Sigma Aldrich, Milan, Italy) [41] to highlight glucans composing cell wall and observed under a Zeiss Axiophot D1 fluorescent microscope equipped with differential interface contrast (DIC) optics. Images were recorded with an Axiocam MRc5 camera (Zeiss) using the Axiovision program (version 4.1).

Ultrastructural observation of P. infestans *mycelium* via *Transmission Electron Microscopy (TEM)*

To assess the ultrastructural alterations induced by PAs on mycelial growth, a 5 mm mycelial plug of *P. infestans* was inoculated in 6 cm diameter Petri dishes containing PB medium amended with antibiotics (100 µg/mL ampicillin, 50 µg/mL vancomycin and 1 unit/mL nystatin). After 36 hours post inoculation (hpi), the liquid phase was removed by gently pipetting, and 5 mL of fresh media was amended with a sublethal dose (EC_{50}) of selected PA. Three plates per treatment were prepared, including a negative (unamended medium) and a positive control (DCB, 40 µM) following the protocol developed by [14]. At 72 hpi, the medium was removed, cultures rinsed twice in PBS 0.5 M, pH 7.4, fixed in 2.5% glutheraldeyde, processed as previously described [14, 42, 43]. More into details, samples were post-fixed in 1 % osmium tetroxide in distilled water for 4 h, and then dehydrated in ethanol. After Epon embedding, thick sections (0-5 µm) for light microscopy were cut and stained with 1 % toluidine blue in a 1 % sodium tetraborate solution. Thin sections for TEM (800 Å) were stained using uranyl acetate and lead citrate. Observations were performed using a using a Talos L120C transmission electron microscope (Thermo Fisher Scientific) equipped with a 4 K digital camera Ceta CMOS (Thermo Fisher Scientific).

Co-localization of selected PAs with P. infestans *membranes*

To address whether selected PAs can preferentially interact with *P. infestans* membranes, where their putative target enzymes are localized, FM 4-64 dye (ThermoFisher Scientific) was used to label the phospholipid bilayer and FITC labelled peptides (Caslo ApS, Denmark) have been used to track their cyclic peptides translocation. *P. infestans* sporangia grown overnight in PB medium were stored 10 minutes in ice and centrifuged at 700 rcf for 5 minutes. Supernatant was then removed, and the oomycete structures were resuspended in an equal volume of fresh PB. Samples were maintained in ice until microscope observations. FM 4-64 dye was added at 2.5 mM while FITC labelled peptides were added at their EC_{50} concentration. The samples were then spotted on glass slides for confocal microscopy observation (ECLIPSE Ni-E with A1 Confocal and PicoQuant FLIM, Nikon). FM 4-64 dye and FITC labelled peptides have been both excited at 488 nm, while collection was performed between 620-660 nm for the former dye and 510-530 nm for the latter. At least 3-4 structures have been observed for each sample.

Results

Screening of PAs for their antimicrobial activity against selected oomycete species

A total of 77 PAs identified through yeast two-hybrid (Y2H) screening were synthesized and assessed for their efficacy against four distinct oomycete species. The summarized outcomes of these tests are presented in Table 3. Among the 77 PAs evaluated, 45 targeted *P. infestans*, whereas 17 *P. capsici*, 8 *P. ultimum*, and 7 *P. viticola* enzymes. Noteworthy, no peptide sequences related to NoPEST (https://www.h2020nopest.org/) project are reported in this PhD thesis work as they are considered confidential information or would be object of patenting.

Table 3: key details of the peptide aptamers (PAs), including the target proteins for each species, the number of target proteins involved in the screenings, and PAs form (cyclic or linear). The number of PAs that exhibited growth inhibition percentage GIP or PPI values higher than 70% is reported in brackets.

Target	*Number*	*Species*	*Cyclic/Linear*
Cellulose synthase A3 (CesA3)	4 (2)	*P. capsici*	Cyclic
Cellulose synthase A1 (CesA1)	3	*P. capsici*	Cyclic
RxLR, PME, EPIC effectors	11	*P. infestans*	Linear
Chitin synthase (CHS)	12	*P. infestans*	Cyclic
Cellulose synthase A2 (CesA2)	6 (1)	*P. infestans*	Cyclic
Cellulose synthase A3 (CesA3)	6 (1)	*P. infestans*	Cyclic
Glycosyl hydrolase (GH)	2	*P. infestans*	Cyclic
B 1,3-glucanosyltransferase (GT)	2	*P. infestans*	Cyclic
Cellulose synthase A1 (CesA1)	6	*P. ultimum*	Cyclic
Glycoside Hydrolase Family 72 (GH 72)	2	*P. ultimum*	Cyclic
Cellulose synthase A1 (CesA1)	12 (6)	*P. viticola*	Linear
Cellulose synthase A2 (CesA2)	5	*P. viticola*	Linear

Out of this pool, 2 PAs exhibited a significant GIP exceeding 70% inhibition for *P. infestans*, 2 for *P. capsici*, and 6 for *P. viticola*, prompting further investigation into their cross-species activity. Among these, only 2 candidates, CP20 and CP32, targeting *P. infestans* CesA3 and CesA2, respectively, displayed good cross-activity against other species (Table 3). These were selected for further analyses.

In vitro and *ex vivo* atimicrobial activity towards *P. infestans*

CP20 and CP32 caused a strong inhibition of the oomycete when tested at 200 µM (Table 4). On one hand, the *in vitro* assay against mycelium (Figure 1; Table 4), displayed an inhibitory effect of 87.5% and 85.29% for CP20 and CP32 respectively. On the other hand, the *in vitro* assay performed against sporangia, exhibited inhibition values higher than 90% for both the PAs, and no differences with the positive control (mandipropamid) were identified by the statistical analyses (Table 4). In the *ex vivo* leaf disc assay, CP20 and CP32 showed 87.92% and 92.31% inhibition, respectively (Table 4; Figure 2). These results suggest that both CP20 and CP32 have significant antifungal activity in all three assay conditions tested, with CP32 generally displaying higher inhibitory effects compared to CP20.

Table 4: Results obtained from the *P. infestans* activity tests on each single PA against the mycelium on solid medium, the sporangia on liquid medium and the ex vivo assay on tomato leaf discs. Values represent the GIP/PPI index ± standard deviation. Letters indicate significant differences based on statistical analyses (pairwise contrasts among EMMs derived from BRM).

	GIP_S (vs. mycelium)	***GIP_L (vs. sporangia)***	***PPI - Leaf disc assay***
CP20	87.5 ± 9.45 a	95.4 ± 6.5 a	87.92 ± 3.07 a
CP32	85.29 ± 5.65 a	98.86 ± 0.52 a	92.31 ± 2.95 b
Fungicide	100 ± 0 b	100 ± 0 a	100 ± 0 c
BRM output	F = 13.06; df = 2; p-value < 0.001; RMSE = 0.06	F = 2.6; df = 2; p-value = 0.08; RMSE = 0.03	F = 61; df = 2; p-value < 0.001; RMSE = 0.03

Figure 1: Pictures of Petri multiwell dishes inoculated with 5 mm diameter mycelium plugs of *P. infestans* on culture medium treated as indicated in the figure. A: Untreated control; B: CP20 at 200 µM concentration; C: CP32 at 200 µM concentration; D: mandipropamid (10 mg/l).

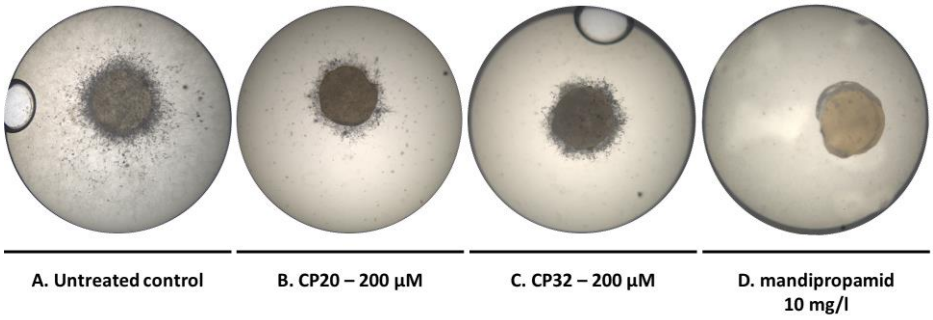

Figure 2: tomato leaf discs (cv. Marmande) inoculated with *P. infestans* sporangia and grapevine leaf discs (cv. Pinot noir) subjected to various treatments as indicated in the figure. A: Untreated control; B: CP20 at 200 µM concentration; C: CP32 at 200 µM concentration; D: mandipropamid (10 mg/l).

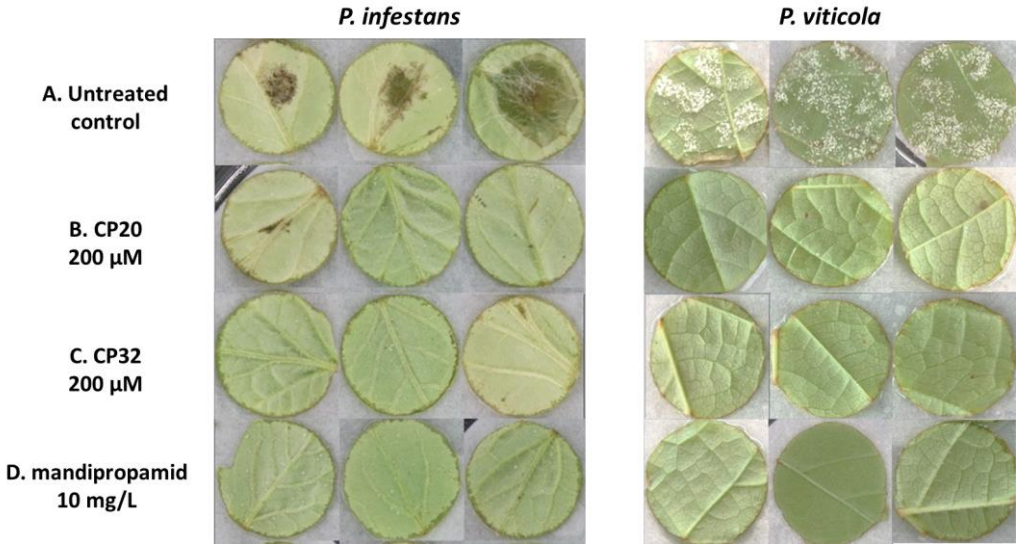

Spectrum of action

CP20 and CP32 exhibited remarkable antifungal activity also against *P. capsici*, *P. ultimum*, and *P. viticola*, with GIPs/PPIs ranging from 80 to 100% (Table 3; Fig. 2).

Table 4: results obtained from the cross-activity tests of CP20 and CP32 against *P. capsici*, *P. viticola* and *P. ultimum*. Values represent the GIP/PPI index ± standard deviation. Letters indicate significant differences based on statistical analyses (Pairwise contrasts among EMMs derived from BRM).

	***P. capsici* - GIP_L**	***P. viticola* - PPI**	***P. ultimum* - GIP_S**
CP20	100 ± 0 b	89.93 ± 11.69 a	79.19 ± 6.18 a
CP32	84.26 ± 6.59 a	94.92 ± 6.45 a	85.43 ± 7.28 a
FUNGICIDE*	100 ± 0 b	100 ± 0 a	100 ± 0 b
BRM output	F = 51.42 ; df = 2 ; p-value < 0.001; RMSE = 0.04	F = 1.8 ; df = 2 ; p-value = 0.16; RMSE = 0.07	F = 45.15 ; df = 2 ; p-value < 0.01; RMSE = 0.05

* mandipropamid (*P. capsici* e *P. viticola*); metalaxyl-M (*P. ultimum*)

Deep characterization of best performing PAs

Dose response analysis

Dose-response analyses (DRA) revealed the strong bioactivity of CP20 and CP32 against *P. infestans* sporangia at concentrations higher than 50 µM (Figure 3 A-B), as also confirmed by the colorimetric cell viability assay with RZ (Figure 3 C). Both the GIP_L and RZ-based assays yielded similar results, with the RZ assay providing more precise estimates due to its shorter confidence intervals (Table 5). Specifically, in the RZ-based assay, CP20 displayed an EC_{50} value of approximately 22 µM while its EC_{99} value was around 60 µM. CP32 exhibited a comparable response, with an EC_{50} value around 19 µM and an EC_{99} value close to 50 µM.

Table 5: ECx values obtained from dose-response curves using both the Growth Inhibition Percentage liquid (GIP_L) and the Resazurin (RZ) based methods. The values are expressed as µM, and the numbers in brackets represent the 95% confidence interval for each estimate.

Ecx	*CP20*		*CP32*	
	GIP_L assay	**RZ assay**	**GIP_L assay**	**RZ assay**
50	23.75 (17.44-30.05)	22.27 (21.49-23.04)	16.34 (11.55-21.14)	18.98 (18.1-19.86)
75	34.42 (23.76-45.07)	28.27 (26.98-29.57)	25.87 (18.73-33.01)	23.87 (22.67-25.08)
90	45.08 (29.5-60.67)	35.9 (32.94-38.87)	35.39 (25.23-45.56)	30.03 (27.9-32.15)
99	68.37 (41.54-95.2)	60.48 (49.94-71.01)	56.18 (38.8-73.56)	49.53 (42.95-56.11)

Figure 3: Dose response analysis (DRA) performed through the RZ-based assay for CP20 (A) and CP32 (B). Points represent mean OD_{600} values registered at 3 days post inoculation (dpi); error bars represent standard deviations and light grey ribbons display 95% confidence interval for the non-linear regression model (4 parameters log-logistic curve) C. Results of the cell viability assay using resazurin (RZ), a metabolic indicator of living cells. Shift from blue to pink/colorless signals resazurin reduction and indicates the presence of metabolically active spores after 72 h.

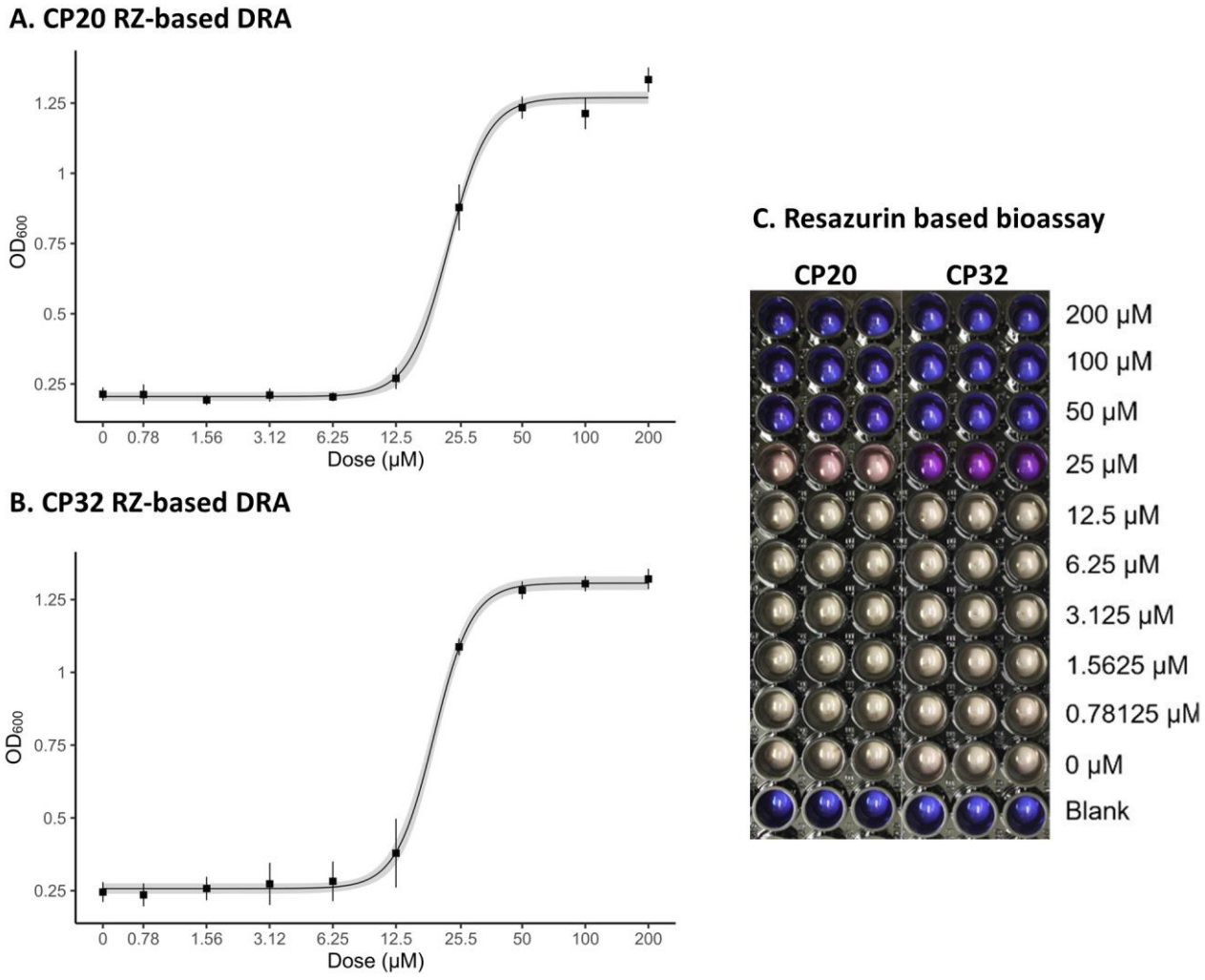

In vitro *radiometric assays of* P. infestans *cellulose synthases*

The extraction of protein sources from *P. infestans* and the subsequent radiometric assays allowed to determine the glucan synthase activity with respect to cellulose. The highest enzymatic activity was observed using DE (0.5% CHAPS) as the enzyme source and collecting the soluble fraction. Conversely, negligible activity was observed under all other tested conditions (Figure 4 A). Therefore, all subsequent assays, including the testing of putative and known inhibitors, were conducted using these specific conditions.

Figure 4: A. comparison of [$_{14}$C]glucose incorporation (nmol/mg protein) between microsomal fractions (MF) and 0.5% CHAPS extract in soluble and insoluble glucans fractions. B. comparison of [$_{14}$C]glucose incorporation (nmol/mg protein) in the soluble glucans fraction for various treatments, including putative (CP20 and CP32, 100 µM) and known (flupoxam, 500 µM) inhibitors. Letters indicate significant differences based on statistical analyses (One-way ANOVA with REGW post-hoc). Error bars represent standard deviations.

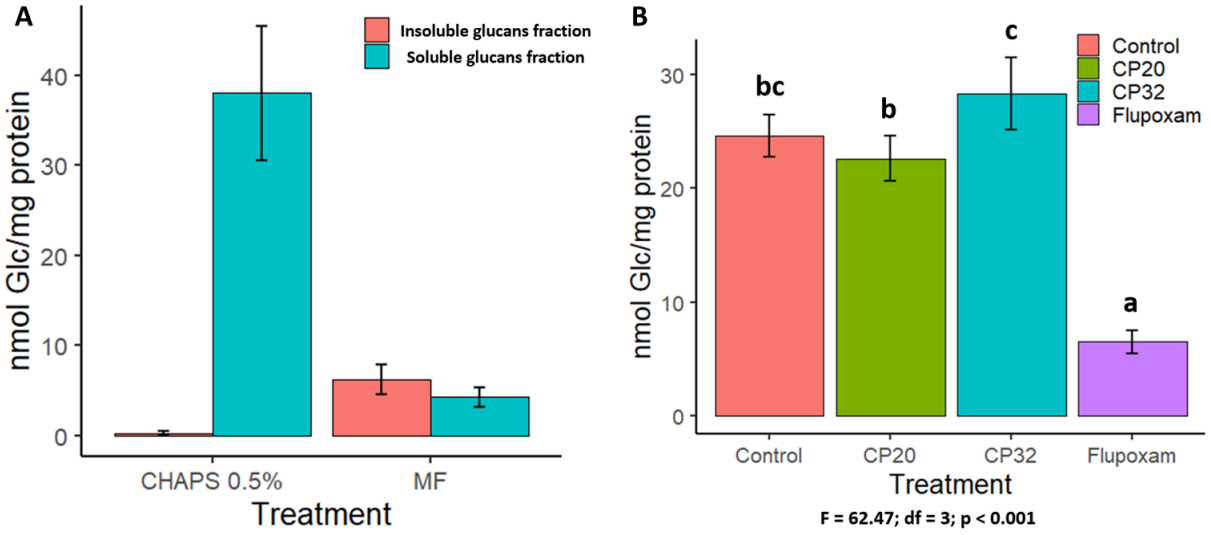

The inclusion of CP20 and CP32 in the reaction mixture did not lead to a significant reduction in the incorporation of labeled glucose compared to the unamended control. However, it is worth noting that the addition of 500 µM flupoxam resulted in the inhibition of glucan synthase activity (Figure 4 B) as previously observed in the fish pathogen *Saprolegnia parasitica* [38]. Furthermore, the TLC analysis reveals that the primary product synthesized during the reaction is cellobiose, which is a dimer composed of glucose molecules linked by 1,4 ß-bonds. Additionally, the TLC results demonstrate that all the UDP-glucose introduced into the reaction mixture was utilized (Figure 5).

Figure 5: Thin Layer Chromatography (TLC) analysis of glucans produced by *P. infestans* cellulose synthases. The TLC plate shows the separation of glucans synthesized by *P. infestans* in the presence of different inhibitors (CP20, CP32) and the untreated control. Moreover, reference standards (glucose, cellobiose, cellotriose and UDP glucose) are also present for direct comparison.

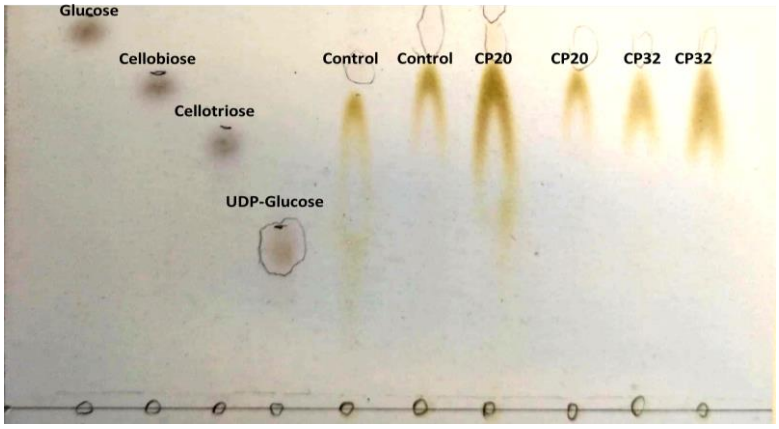

Zoospore release assay

Indirect germination of sporangia was achieved successfully in the experimental conditions, thus allowing to calculate sporangia germination percentage. Sporangia in the untreated control showed a germination percentage of 53.25%, while all the treatments resulted in a significant reduction of sporangia indirect germination, with the positive control (DCB) exhibiting a percentage of 22.16%. At their EC_{50} concentrations, CP20 reduced germination to 26.52%, while CP32 resulted in a germination percentage of 23.8%, notably at this doses no significant differences with DCB were identified by the statistical analyses. As the dose increased to EC_{75} and EC_{99} concentrations, the inhibitory effects of both PAs became more pronounced, with CP20 showing 7.31% and 0.57% germination, and CP32 showing 12.01% and 8.56% germination rate, respectively (Table 6). These findings indicate that both CP20 and CP32 have the potential to significantly reduce zoospore release in *P. infestans*.

Table 6: Values represent the percentage of sporangia germinated indirectly ± standard deviation. Letters indicate significant differences based on statistical analyses (Pairwise contrasts among EMMs derived from BRM).

Treatment	*ECx concentration*	*Sporangia germination (%)*
CP20	50	26.52 ± 1.84 c
	75	7.31 ± 1.84 b
	99	0.57 ± 1 a
CP32	50	23.8 ± 5.99 c
	75	12.01 ± 1.18 b
	99	8.56 ± 1.74 b
Untreated control	-	53.25 ± 6.43 d
DCB	40 µM	22.16 ± 5.51 c

F = 106.98; df = 7; p- value < 0.001; RMSE = 0.03

Structural alteration in sporangia treated cultures via optical microscopy

After 3 days of incubation on the untreated control medium, sporangia (arrows) gave rise to an expanded network of hyphae (Figure 6 A-B). However, when treated with CP20 and CP32 at a concentration of 100 µM, the growth of mycelia was either completely inhibited (Figure 6 C-D) or stunted (Figure 6 E-F), indicating the effectiveness of the treatment in preventing mycelial growth. Ungerminated sporangia appeared broken with consistent cytoplasm loss (Figure 6 C). Moreover, both PAs treated hyphae were characterized by the irregular shape (Figure 6 E-F) and the presence of periodic constrictions, particularly on CP20 treated samples (Figure 7A; arrows) which were absent in untreated hyphae (Figure 7B)

Figure 6. optical microscopy observation of *P. infestans* structures after 3 days post inoculation. A-B: untreated controls. C-E: CP20 treated cultures (100 µM). F: CP32 treated cultures (100 µM). Red fluorescent structures were stained using trypan blue to highlight glucans deposition. Size bar represents 50 µm.

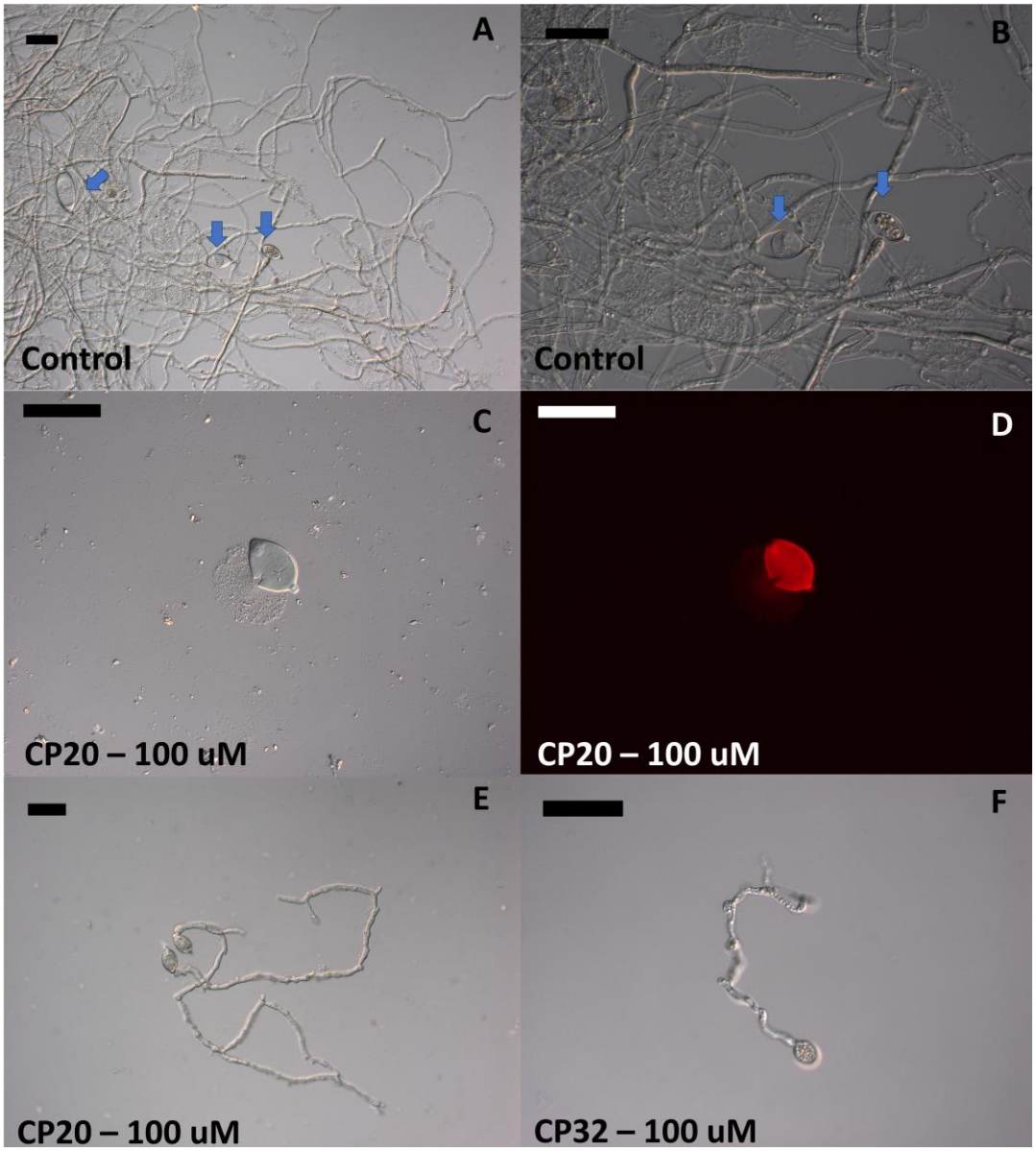

Figure 7. enlarged images of *P. infestans* structures after 3 days post inoculation. A: CP20 treated cultures (100 μM); B: untreated control. Size bar represents 50 μm.

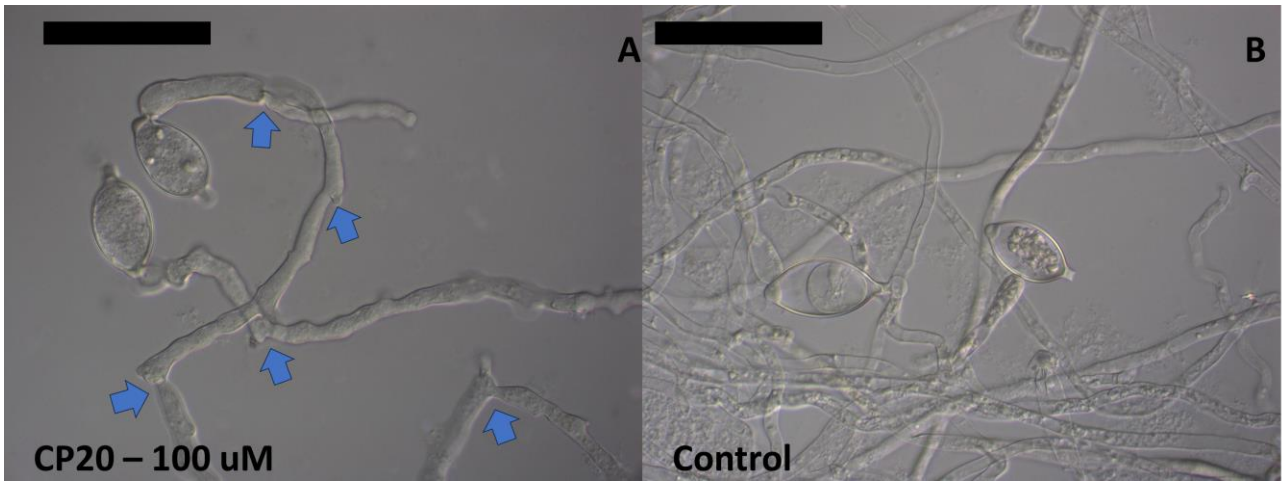

Ultrastructural observation of P. infestans *mycelium via Transmission Electron Microscopy (TEM)*

Cross section of *P. infestans* hyphae subjected to sublethal doses of the two PAs resulted in evident alterations, characterized by stunted growth and irregular shape. Compared to the untreated control (Figure 8A), no evidence of reduction in cell wall thickness was observed in CP20 (Figure 8B) and CP32 (Figure 8C) samples, however, irregular deposition of cell wall was observed (indicated by arrowheads). Moreover, large lipid bodies and irregular vacuolization pattern were also observed. On the contrary, DCB-treated samples exhibited a large central vacuole compartmentation (Figure 8D). Additionally, the deposition of the cell wall was significantly hampered, resulting in a thinner and less densely packed cell wall layer compared to the untreated samples.

Figure 8: TEM sections of *P. infestans* hyphae (cross-section). A: Untreated sample. B: sample treated with CP20 (EC_{50}). C: sample treated with CP32 (EC_{50}). D: Sample treated with DCB (40 µM). Scale bar = 1 µm.

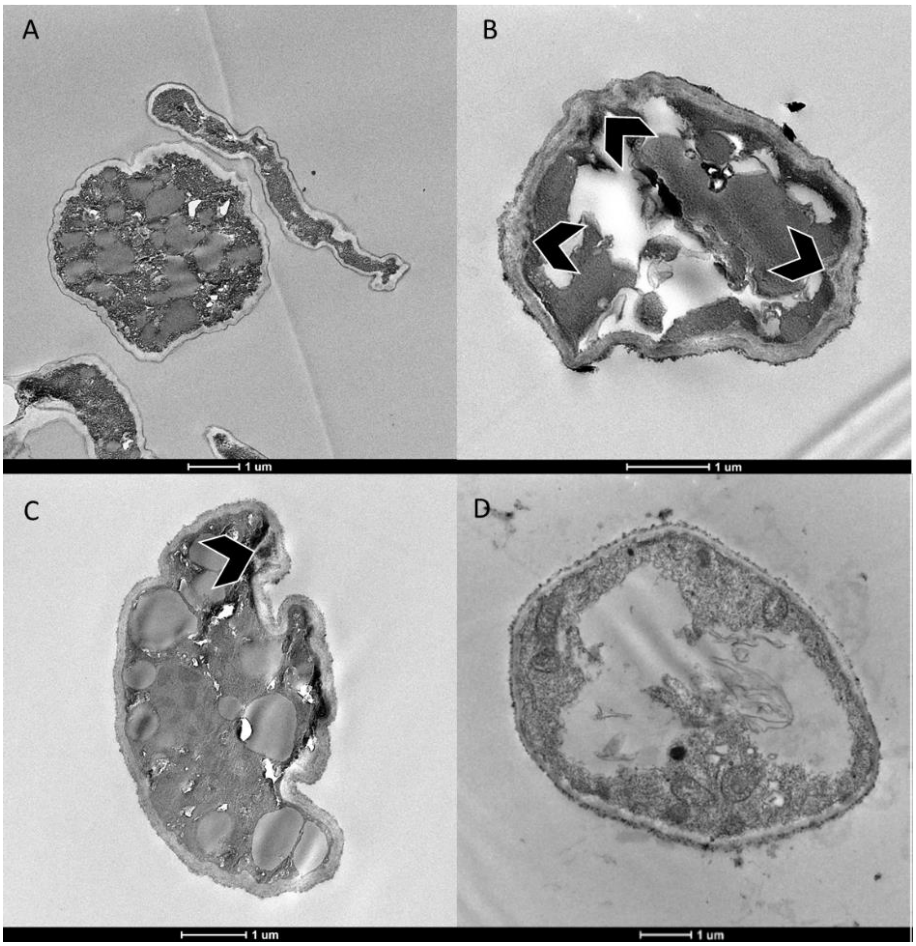

Co-localization of CP20 and CP32 with P. infestans *membranes*

After FM 4-64 labelling, FITC-CP20 or FITC-CP32 were added at their EC_{50} values and samples observed. As it can be noticed in Figure 9, no fluorescence can be detected in absence of treatment nor when single dyes were employed on non-specific channel (Figure 9A). FITC-CP20 and FITC-CP32 co-localized with FM4-64 stained membranes of *P. infestans*, especially at hyphal tips (Figure 9C for FITC-CP20; Figure 9D, Figure 10 for FITC-CP32). Merged channels allowed to appreciate where co-localization events occur for FITC-CPs and membranes. Notably, both FITC-CP20 and FITC-CP32 mainly localized at the hyphal tip, where the cellulose biosynthesis occurs [14], and on *P. infestans* membranes. We observed a faster kinetic for CP32, which promptly localizes to cell membranes and hyphal tips within 15 minutes, while CP20 takes more time (60 minutes) to accumulate on *P. infestans* cell membrane and hyphal tips to an appreciable extent, although producing lower levels of FITC fluorescence.

Figure 9. Bright field (first column), FM 4-64 (second column), FITC (third column) and merged (fourth column) images obtained at the confocal microscope after staining with FM4-64 and FITC-CPs treatment of *P. infestans* germinating sporangia. (A) untreated and unstained samples. (B) untreated samples stained with FM4-64. (C) samples treated with FITC-CP20. (D) samples treated with FITC-CP32. SP: sporangium. H: hypha.

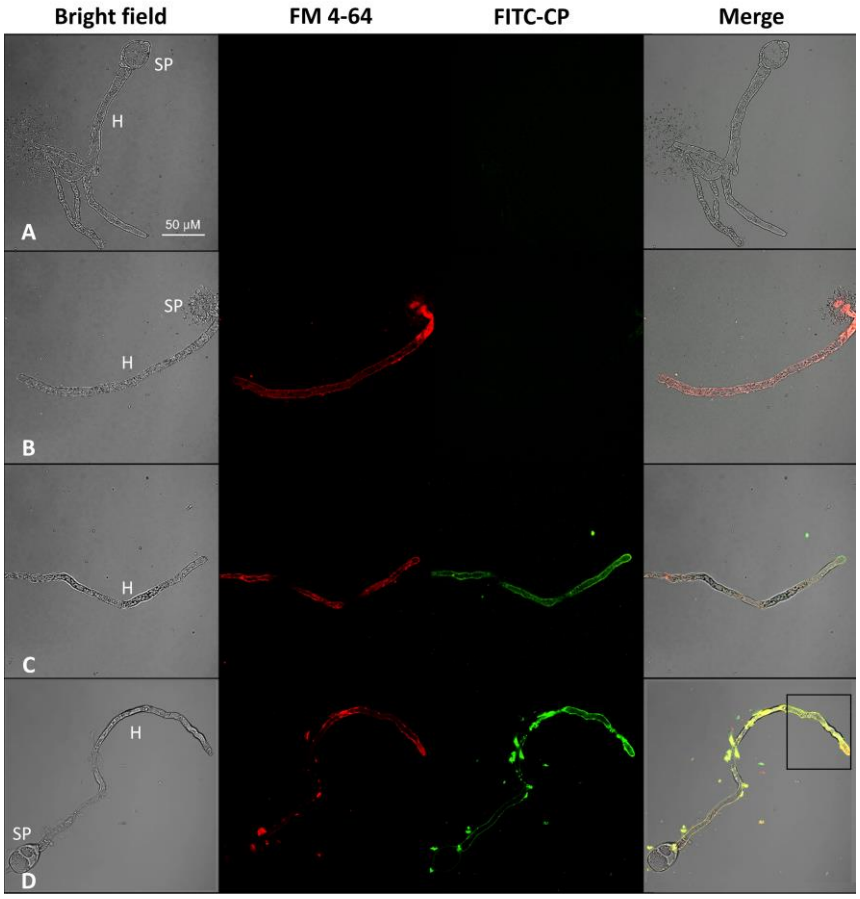

Figure 10. Enlarged images of *P. infestans* hyphal tip obtained at the confocal microscope after staining with FM4-64 and FITC-CPs. Different letters discriminate among stanings: (A) Bright field (B) FITC-CP32 (C) FM 4-64, (D) merged.

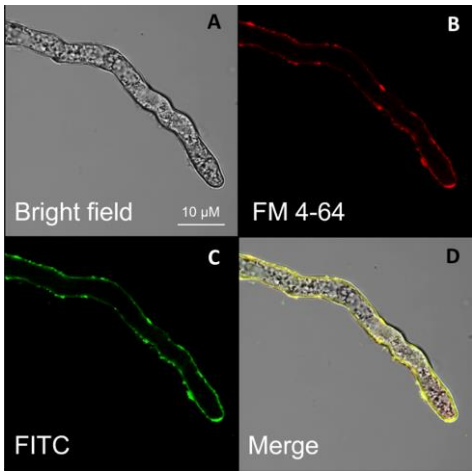

Preliminary results on ongoing experiments

The recombinant CBM3a-GFP is a fusion protein composed by the green fluorescent protein (GFP) combined with the Carbohydrate Binding Protein (also known as cellulose-binding domain family III) from *Clostridium stercorarium* (CBM3A). The intrinsic specificity towards crystalline cellulose of this dye, allows the qualitative evaluation of accessible cellulose via fluorescence microscopy [44]. Interestingly, preliminary observations carried out through confocal microscopy on *P. infestans* samples treated with sublethal concentration of the aptamer CP32, highlighted a visible reduction in fluorescence intensity of in several structures. In particular, reduction in fluorescence seems to be localized at hyphal tip region, where cellulose deposition is usually observed (Figure 11).

Figure 11. Images of *P. infestans* hyphal tip obtained at the confocal microscope after staining with CBM3a-GFP. Different letters discriminate among treatments: (A) untreated and unstained samples (B) untreated samples stained with CBM3a-GFP (C) samples treated with CP32 at EC_{75} concentration.

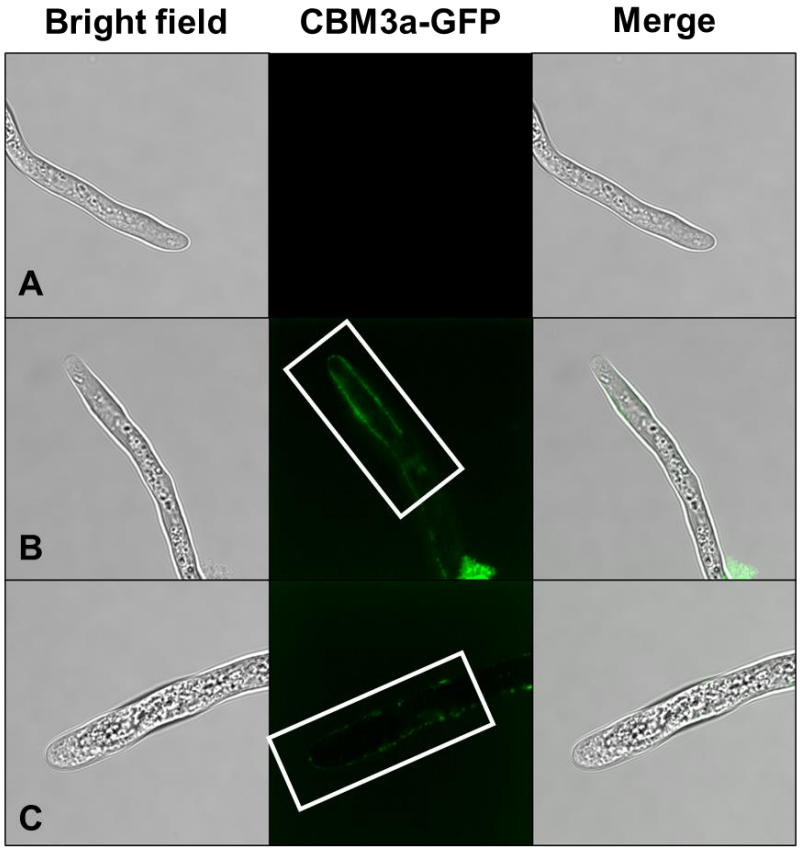

Discussion

Peptides as anti-oomycetes compounds

In recent years, there has been a significant focus on the use of functional peptides, whether purified or derived from cell-free extracts, as tools for controlling plant diseases, including those caused by oomycetes [45, 46]. Particularly, antimicrobial peptides (AMPs) isolated from plants as host defense molecules emerged because of their low toxicity against mammalian cells [47]. AMPs are generally characterized by short chains with cationic (positively charged) and amphiphilic (hydrophilic and hydrophobic) properties. Plant AMPs usually exert their antimicrobial effect on the plasma membrane or interfere with metabolic processes at extracellular and/or intracellular sites [48, 49], thus resulting in a broad-spectrum activity against bacteria, fungi, viruses and oomycetes [50]. Indeed, AMPs have demonstrated significant efficacy against oomycetes pathogens [51, 52].

Reverting the discovery paradigm, PAs recently emerged as an alternative for developing antimicrobial compounds [21]. Indeed, PAs are combinatorial molecules artificially selected for their ability to bind specific sites on their target protein with a high specificity and a strong affinity [53]. In this context, PAs targeting vital enzymes have been proposed as an innovative approach for oomycete control [18, 54]. Although limited information is available, the synthetic PAs identified in previous studies showed efficacy at very low concentration (µM range) and good specificity. More into details, Lee and collaborators [55], identified inhibitory peptides against alpha- and beta-tubulin of *P. capsici*. The best performing peptide demonstrated the inhibition of tubulin depolymerization at low-micromolar range, and high specificity towards the target enzyme. However, neither the *in vivo* effect on the pathogen nor the effectiveness on disease control was assessed. On the contrary, NoPV1, a PA targeting *P. viticola* cellulose biosynthesis, demonstrated its effectiveness in preventing germ tube formation and leaf infection at 200 µM without any side-effects on non-target organisms and human cells [18]. Moreover, the PA resulted in good activity towards *P. infestans* growth, probably due to the high similarity in cellulose synthases sequences among the two species.

Anti-oomycete activity of selected PAs

In this study, we tested a total of 77 PAs selected from Y2H, specifically interacting with baits related to cell wall biosynthesis and remodeling in four oomycete species. Among them, two PAs (CP20 and CP32) putatively interacting with cell wall biosynthesis, showed strong inhibition towards *P. infestans* mycelium and sporangia. In addition, both PAs also exhibited remarkable antifungal activity against other three oomycete species (*P. capsici*, *P. viticola*, *P. ultimum*) and

the ability to counteract plant tissue infection in *ex vivo* assays. Further dose-response analyses indicated the strong efficacy especially at concentrations higher than 50 µM. Overall, these findings highlight the strong bioactivity of CP20 and CP32 and their potential use as anti-oomycete agents for several important phytopathogenic species.

The findings presented in this study, align with a previous research [18] and suggest that the choice of PAs targeting cell wall active enzymes could represent a valuable tool for the development of effective antimicrobial substances against phytopathogenic oomycetes. Indeed, the inhibition of cell wall biosynthesis is a well-known target for traditional fungicides, including Carboxilic Acid Amides (CAAs), which target cellulose biosynthesis [15], and two peptide-based inhibitors families, the peptidyl nucleosides nikkomicins [54] that interfere with chitin synthesis and the lipopeptides echinocandins, which interfere with 1,3-ß glucan synthesis [56].
However, due to their combinatorial nature, PAs can theoretically bind numerous polymorphic protein surfaces [57], therefore their specificity of binding must be addressed. Moreover, bioactive PAs may share several features (small size, amphipathicity, and net charge) with the AMPs, therefore general killing mechanism through the physical disruption of cell membranes should also be accounted.

Insights into the mode of action

Zoospores are important infection sources for oomycetes pathogens; therefore, their inhibition can be useful in the control of the corresponding disease [58]. On the other hand, many compounds exhibiting anti-oomycete activity towards *Phytophthora* spp. and proven to cause cell membrane damages and cytoplasm leaking are usually related to indirect germination suppression [59, 60, 61, 62]. However, the effect of different putative cellulose synthase inhibitors on zoospore release is controversial. Indeed, while DCB and the CAA fungicide pyrimorph have been proven to reduce indirect germination in dose dependent manner [14, 63], other CAA fungicides (e.g. mandipropamid, dimethomorph, benthiavalicarb) did not affect zoospore release [64, 65, 66]. Interestingly, both CP20 and CP32, impaired zoospore release in a dose dependent manner, with strong inhibition when tested at EC_{99} concentrations, while at sublethal concentrations (EC_{50}), indirect germination was comparable to the inhibitor DCB, aligning with data from previous study [14].

Microscopy analyses demonstrated that CP20 and CP32 effectively inhibit *P. infestans* mycelial growth, causing either complete inhibition or stunted growth, with hyphae characterized by irregular development and the presence of periodic constrictions. More into detail, TEM observation revealed ultrastructural alterations in hyphal structures, characterized by irregular

cell wall deposition, the presence of large lipid bodies, and abnormal vacuolization patterns. This agrees with results obtained in previous studies, indeed cell wall thickening and false septation was also observed in the presence of putative cell-wall inhibitors dimethomorph and pyrimorph for several *Phytophthora* species [63; 67] as well as for mandipropamid-treated *P. viticola* hyphae [68]. Moreover, irregular cell wall deposition, with areas of thickening were also observed in *P. infestans* lines in which cellulose synthases were transiently silenced [14] and *P. capsici* mutants in which CesA1 was knocked down [69].

CesA proteins are localized in the cell membrane thanks to multiple transmembrane domains [37]. Co-localization studies performed in this study with FITC-labeled PAs, demonstrated their interaction with *P. infestans* membranes, although different translocation kinetics for the two peptides were observed. Moreover, PAs were particularly localized at the hyphal tip, where cellulose biosynthesis occurs [14, 69].

On the other hand, the PAs do not seem to reduce the *in vitro* activity of CesA extracted from the membranes, as it is for the glucan synthase inhibitor flupoxam. However, it must be pointed out that the results obtained from the radiometric assay indicate that *P. infestans* CesAs are likely incapable of adding additional glucose residues to cellobiose under the tested conditions. This could be attributed to the lack of essential interactions or favorable conditions required for optimal enzyme function. Indeed, it is important to consider the potential involvement of unidentified proteins that are crucial for polymerizing longer cellulose chains found in oomycete cell walls, which are not present in this system [37].

Potential future research

Based on these results, additional investigations are necessary to determine whether the activity of the two PAs is related to cellulose biosynthesis and CesAs activity or to an unspecific direct effect on the plasma membrane integrity. To exclude a direct effect on the membrane integrity in the presence of the PAs, further insights coming from microscope observations under nucleic acid staining using SYTOX green, a dye that permeates fungal cells when their plasma membrane integrity is compromised, should be assessed [70]. Furthermore, electrolyte leakage assays performed following well-established protocols are also required to exclude plasma membrane disruption [59, 60, 61, 62]. In addition, refined co-localization assays involving mCherry-tagged PiCesA targets, coupled with longer observations (e.g. using time lapse microscopy) could provide further insights into PAs localization on the target sites as well as shedding light on translocation dynamics in this cellular compartment.

The direct quantification of cellulose content and the effects on the target's enzymatic activities could provide further insights into PA specificity. To assess variations in cellulose content, the direct quantification of radiolabeled glucose incorporation into *P. infestans* cell wall fraction, as well as the relative change in glycosidic linkage composition from mycelium exposed at sublethal concentrations of PAs could be employed [66, 69]. Furthermore, although difficult, the heterologous expression of the target proteins in a eukaryotic system (e.g. *Saccharomyces cerevisiae* or mammal cells) could allow to perform the radiometric assays in the presence of the PAs on the purified protein [37], meanwhile providing a suitable system for the determination of the three-dimension protein structure and of its interaction with the putative inhibitors (e.g. by NMR or X-ray crystallography) [71].

References

1. Strassert JF, Jamy M, Mylnikov AP, Tikhonenkov DV, Burki F. 2019. New phylogenomic analysis of the enigmatic phylum Telonemia further resolves the eukaryote tree of life. Molecular biology and evolution 36:757–765.
2. Benavent-Celma C, López-García N, Ruba T, Ściślak ME, Street-Jones D, van West P, Woodward S, Witzell J. 2022. Current practices and emerging possibilities for reducing the spread of oomycete pathogens in terrestrial and aquatic production systems in the European Union. Fungal Biology Reviews 40:19–36.
3. Kamoun S, Furzer O, Jones JD, Judelson HS, Ali GS, Dalio RJ, Roy SG, Schena L, Zambounis A, Panabières F. 2015. The Top 10 oomycete pathogens in molecular plant pathology. Molecular plant pathology 16:413–434.
4. Judelson HS, Blanco FA. 2005. The spores of Phytophthora: weapons of the plant destroyer. Nature Reviews Microbiology 3:47–58.
5. Fry W, Birch P, Judelson H, Grünwald N, Danies G, Everts K, Gevens A, Gugino B, Johnson D, Johnson S. 2015. Five reasons to consider Phytophthora infestans a reemerging pathogen. Phytopathology 105:966–981.
6. Lamour KH, Stam R, Jupe J, Huitema E. 2012. The oomycete broad-host-range pathogen Phytophthora capsici. Molecular plant pathology 13:329–337.
7. Lafon R, Clerjeau M. 1988. Downy mildew. Compendium of grape diseases 11–13.
8. Gessler C, Pertot I, Perazzolli M. 2011. Plasmopara viticola: a review of knowledge on downy mildew of grapevine and effective disease management. Phytopathologia Mediterranea 50:3–44.
9. Massi F, Torriani SF, Borghi L, Toffolatti SL. 2021. Fungicide resistance evolution and detection in plant pathogens: Plasmopara viticola as a case study. Microorganisms 9:119.
10. Stanghellini ME. 1971. The sporangium of Pythium ultimum as a survival structure in soil. Phytopathology 61:157.
11. Salman M, Abuamsha R. 2012. Potential for integrated biological and chemical control of damping-off disease caused by Pythium ultimum in tomato. BioControl 57:711–718.
12. Derevnina L, Petre B, Kellner R, Dagdas YF, Sarowar MN, Giannakopoulou A, De la Concepcion JC, Chaparro-Garcia A, Pennington HG, Van West P. 2016. Emerging oomycete threats to plants and animals. Philosophical Transactions of the Royal Society B: Biological Sciences 371:20150459.
13. Mélida H, Sandoval-Sierra JV, Diéguez-Uribeondo J, Bulone V. 2013. Analyses of extracellular carbohydrates in oomycetes unveil the existence of three different cell wall types. Eukaryotic cell 12:194–203.
14. Grenville-Briggs LJ, Anderson VL, Fugelstad J, Avrova AO, Bouzenzana J, Williams A, Wawra S, Whisson SC, Birch PR, Bulone V. 2008. Cellulose synthesis in Phytophthora infestans is required for normal appressorium formation and successful infection of potato. The Plant Cell 20:720–738.
15. Gisi U, Lamberth C, Mehl A, Seitz T, Blum M. 2019. Carboxylic acid amide (CAA) fungicides. Modern Crop Protection Compounds 2:845–869.
16. Brown C. 2015. Characterization of specific domains of the cellulose and chitin synthases from pathogenic oomycetes.
17. McDougall P. 2016. The Cost of New Agrochemical Product Discovery, Development and Registration in 1995, 2000, 2005–8 and 2010–2014. R&D expenditure in 2014 and expectations for 2019. A Consultancy Study for CropLife International, CropLife America and the European Crop Protection Association. Agribusiness intelligence, Informa, Saughland, Pathhead, Midlothian.
18. Colombo M, Masiero S, Rosa S, Caporali E, Toffolatti SL, Mizzotti C, Tadini L, Rossi F, Pellegrino S, Musetti R. 2020. NoPv1: a synthetic antimicrobial peptide aptamer targeting the causal agents of grapevine downy mildew and potato late blight. Scientific reports 10:17574.
19. Marcianò D, Ricciardi V, Marone Fassolo E, Passera A, Bianco PA, Failla O, Casati P, Maddalena G, De Lorenzis G, Toffolatti SL. 2021. RNAi of a putative grapevine susceptibility gene as a possible downy mildew control strategy. Frontiers in Plant Science 12:667319.
20. Rosa S, Pesaresi P, Mizzotti C, Bulone V, Mezzetti B, Baraldi E, Masiero S. 2022. Game-changing alternatives to conventional fungicides: Small RNAs and short peptides. Trends in Biotechnology 40:320–337.
21. Colombo M, Mizzotti C, Masiero S, Kater MM, Pesaresi P. 2015. Peptide aptamers: The versatile role of specific protein function inhibitors in plant biotechnology. Journal of integrative plant biology 57:892–901.
22. Rosa S, Tagliani A, Bertaso C, Tadini L, Visentin C, Gourlay LJ, Pricl S, Feni L, Pellegrino S, Pesaresi P. 2023. The cyclic peptide G4CP2 enables the modulation of galactose metabolism in yeast by interfering with GAL4 transcriptional activity. Frontiers in Molecular Biosciences 10:1017757.
23. Pellegrino S, Annoni C, Contini A, Clerici F, Gelmi ML. 2012. Expedient chemical synthesis of 75mer DNA binding domain of MafA: An insight on its binding to insulin enhancer. Amino acids 43:1995–2003.

24. Pang Z, Shao J, Chen L, Lu X, Hu J, Qin Z, Liu X. 2013. Resistance to the novel fungicide pyrimorph in Phytophthora capsici: risk assessment and detection of point mutations in CesA3 that confer resistance. PLoS One 8:e56513.
25. Massi F, Marcianò D, Russo G, Stuknytė M, Arioli S, Mora D, Toffolatti SL. 2022. Evaluation of the Characteristics and Infectivity of the Secondary Inoculum Produced by Plasmopara viticola on Grapevine Leaves by Means of Flow Cytometry and Fluorescence-Activated Cell Sorting. Applied and Environmental Microbiology 88:e01010-22.
26. Marcianò D, Toffolatti SL. 2023. Methods for Fungicide Efficacy Screenings: Multiwell Testing Procedures for the Oomycetes Phytophthora infestans and Pythium ultimum. Microorganisms 11:350.
27. Toffolatti SL, Venturini G, Maffi D, Vercesi A. 2012. Phenotypic and histochemical traits of the interaction between Plasmopara viticolaand resistant or susceptible grapevine varieties. BMC Plant Biology 12:1–16.
28. RStudio RsT. 2020. Integrated development environment for R. RStudio, PBC: Boston, MA, USA.
29. Fugelstad J, Bouzenzana J, Djerbi S, Guerriero G, Ezcurra I, Teeri TT, Arvestad L, Bulone V. 2009. Identification of the cellulose synthase genes from the Oomycete Saprolegnia monoica and effect of cellulose synthesis inhibitors on gene expression and enzyme activity. Fungal Genetics and Biology 46:759–767.
30. Noel ZA, Wang J, Chilvers MI. 2018. Significant influence of EC50 estimation by model choice and EC50 type. Plant Disease 102:708-714.
31. Ritz C, Baty F, Streibig JC, Gerhard D. 2015. Dose-response analysis using R. PloS one 10:e0146021.
32. Vega B, Liberti D, Harmon PF, Dewdney MM. 2012. A rapid resazurin-based microtiter assay to evaluate QoI sensitivity for Alternaria alternata isolates and their molecular characterization. Plant disease 96:1262–1270.
33. Bulone V, Girard V, Fevre M. 1990. Separation and partial purification of 1, 3-ß-glucan and 1, 4-ß-glucan synthases from Saprolegnia. Plant physiology 94:1748–1755.
34. Guerriero G, Avino M, Zhou Q, Fugelstad J, Clergeot P-H, Bulone V. 2010. Chitin synthases from Saprolegnia are involved in tip growth and represent a potential target for anti-oomycete drugs. PLoS pathogens 6:e1001070.
35. Brown C, Leijon F, Bulone V. 2012. Radiometric and spectrophotometric in vitro assays of glycosyltransferases involved in plant cell wall carbohydrate biosynthesis. nature protocols 7:1634–1650.
36. Rzeszutek E, Díaz-Moreno SM, Bulone V. 2019. Identification and characterization of the chitin synthase genes from the fish pathogen Saprolegnia parasitica. Frontiers in Microbiology 10:2873.
37. Pang Z, McKee LS, Srivastava V, Klinter S, Díaz-Moreno SM, Orlean P, Liu X, Bulone V. 2020. Analysis of a cellulose synthase catalytic subunit from the oomycete pathogen of crops Phytophthora capsici. Cellulose 27:8551–8565.
38. Rzeszutek E. 2019. Cell wall biosynthesis in the pathogenic oomycete Saprolegnia parasitica. TRITA-CBH-FOU. Doctoral thesis, comprehensive summary. KTH Royal Institute of Technology, Stockholm.
39. de Mendiburu F, de Mendiburu M. 2019. Package 'agricolae'. R Package, Version, 1, 3.
40. Walker CA, Köppe M, Grenville-Briggs LJ, Avrova AO, Horner NR, McKinnon AD, Whisson SC, Birch PR, Van West P. 2008. A putative DEAD-box RNA-helicase is required for normal zoospore development in the late blight pathogen Phytophthora infestans. Fungal Genetics and Biology 45:954–962.
41. Liesche J, Marek M, Günther-Pomorski T. 2015. Cell wall staining with Trypan blue enables quantitative analysis of morphological changes in yeast cells. Frontiers in Microbiology 6:107.
42. Wastling J, Mackenzie K, Chappell L. 1992. Effects of cyclosporin A on the morphology and tegumentary ultrastructure of Hymenolepis microstoma in vivo. Parasitology 104:531–538.
43. Bishop ET, Bell GT, Bloor S, Broom I, Hendry NF, Wheatley DN. 1999. An in vitro model of angiogenesis: basic features. Angiogenesis 3:335–344.
44. Nguyen M H, Ojima Y, Sakka M, Sakka K, Taya M (2014). Probing of exopolysaccharides with green fluorescence protein-labeled carbohydrate-binding module in Escherichia coli biofilms and flocs induced by bcsB overexpression. Journal of bioscience and bioengineering, 118(4): 400-405.
45. Rogozhin EA, Vasilchenko AS, Barashkova AS, Smirnov AN, Zavriev SK, Demushkin VP. 2020. Peptide extracts from seven medicinal plants discovered to inhibit oomycete phytophthora infestans, a causative agent of potato late blight disease. Plants 9:1294.
46. Montesinos E. 2023. Functional Peptides for Plant Disease Control. Annual Review of Phytopathology 61.
47. López-García B, Pérez-Payá E, Marcos JF. 2002. Identification of novel hexapeptides bioactive against phytopathogenic fungi through screening of a synthetic peptide combinatorial library. Applied and Environmental Microbiology 68:2453–2460.
48. Nawrot R, Barylski J, Nowicki G, Broniarczyk J, Buchwald W, Goździcka-Józefiak A. 2014. Plant antimicrobial peptides. Folia microbiologica 59:181–196.
49. Tam JP, Wang S, Wong KH, Tan WL. 2015. Antimicrobial peptides from plants. Pharmaceuticals 8:711–757.

50. Lei J, Sun L, Huang S, Zhu C, Li P, He J, Mackey V, Coy DH, He Q. 2019. The antimicrobial peptides and their potential clinical applications. American journal of translational research 11:3919.
51. López-García B, San Segundo B, Coca M. 2012. Antimicrobial peptides as a promising alternative for plant disease protection. Small wonders: peptides for disease control 263–294.
52. Stotz H, Waller F, Wang K. 2012. Innate immunity in plants: the role of antimicrobial peptides. Antimicrobial peptides and innate immunity 29–51.
53. Reverdatto S, Burz DS, Shekhtman A. 2015. Peptide aptamers: development and applications. Current topics in medicinal chemistry 15:1082.
54. Lee S-C, Kim S-H, Hoffmeister RA, Yoon M-Y, Kim S-K. 2019. Novel peptide-based inhibitors for microtubule polymerization in Phytophthora capsici. International Journal of Molecular Sciences 20:2641.
55. Matejuk A, Leng Q, Begum M, Woodle M, Scaria P, Chou S, Mixson AJ. 2010. Peptide-based antifungal therapies against emerging infections. Drugs of the Future 35:197.
56. Sucher AJ, Chahine EB, Balcer HE. 2009. Echinocandins: the newest class of antifungals. Annals of Pharmacotherapy 43:1647–1657.
57. Baines IC, Colas P. 2006. Peptide aptamers as guides for small-molecule drug discovery. Drug discovery today 11:334–341.
58. Matheron M, Porchas M. 2000. Impact of azoxystrobin, dimethomorph, fluazinam, fosetyl-Al, and metalaxyl on growth, sporulation, and zoospore cyst germination of three Phytophthora spp. Plant Disease 84:454–458.
59. Liang C, Gao W, Ge T, Tan X, Wang J, Liu H, Wang Y, Han C, Xu Q, Wang Q. 2021. Lauric acid is a potent biological control agent that damages the cell membrane of Phytophthora sojae. Frontiers in Microbiology 12:666761.
60. Wang Y, Zhang C, Liang J, Wu L, Gao W, Jiang J. 2020. Iturin A extracted from Bacillus subtilis WL-2 affects Phytophthora infestans via cell structure disruption, oxidative stress, and energy supply dysfunction. Frontiers in Microbiology 11:536083.
61. Wang B, Li P, Xu S, Liu L, Xu Y, Feng X, Zhao X, Chen Y. 2021. Inhibitory effects of the natural product esculetin on Phytophthora capsici and its possible mechanism. Plant Disease 105:1814–1822.
62. Wang B, Liu F, Li Q, Xu S, Zhao X, Xue P, Feng X. 2019. Antifungal activity of zedoary turmeric oil against Phytophthora capsici through damaging cell membrane. Pesticide biochemistry and physiology 159:59–67.
63. Yan X, Qin W, Sun L, Qi S, Yang D, Qin Z, Yuan H. 2010. Study of inhibitory effects and action mechanism of the novel fungicide pyrimorph against Phytophthora capsici. Journal of agricultural and food chemistry 58:2720–2725.
64. Reuveni M. 2003. Activity of the new fungicide benthiavalicarb against Plasmopara viticola and its efficacy in controlling downy mildew in grapevines. European Journal of Plant Pathology 109:243–251.
65. Stein J, Kirk W. 2003. Variations in the sensitivity of Phytophthora infestans isolates from different genetic backgrounds to dimethomorph. Plant disease 87:1283–1289.
66. Blum M, Boehler M, Randall E, Young V, Csukai M, Kraus S, Moulin F, Scalliet G, Avrova AO, Whisson SC. 2010. Mandipropamid targets the cellulose synthase-like PiCesA3 to inhibit cell wall biosynthesis in the oomycete plant pathogen, Phytophthora infestans. Molecular plant pathology 11:227–243.
67. Kuhn PJ, Pitt D, Lee SA, Wakley G, Sheppard AN. 1991. Effects of dimethomorph on the morphology and ultrastructure of Phytophthora. Mycological Research 95:333–340.
68. Toffolatti SL, Maffi D, Serrati L, Vercesi A. 2011. Histological and ultrastructural studies on the curative effects of mandipropamid on Plasmopara viticola. Journal of phytopathology 159:201–207.
69. Li T, Cai M, Wang W, Dai T, Zhang C, Zhang B, Shen J, Wang Y, Liu X. 2022. PcCesA1 is involved in the polar growth, cellulose synthesis, and glycosidic linkage crosslinking in the cell wall of Phytophthora capsici. International Journal of Biological Macromolecules 208:720–730.
70. Velivelli SL, Czymmek KJ, Li H, Shaw JB, Buchko GW, Shah DM. 2020. Antifungal symbiotic peptide NCR044 exhibits unique structure and multifaceted mechanisms of action that confer plant protection. Proceedings of the National Academy of Sciences 117:16043–16054.
71. Chen W, Cao P, Liu Y, Yu A, Wang D, Chen L, Sundarraj R, Yuchi Z, Gong Y, Merzendorfer H. 2022. Structural basis for directional chitin biosynthesis. Nature 610:402–408.

Conclusions and research perspectives

Phytopathogenic oomycetes pose significant challenges in agriculture, therefore innovative approaches for their study and control are required. In this study, we aimed to set a step forward in overcoming current limitations associated with traditional methodologies employed to characterize oomycete pathogens and their interaction with the plant as well as to validate a novel strategy for developing new-generation fungicides.

In the first study, we employed advanced techniques such as flow cytometry and fluorescence-activated cell sorting to analyze the composition and efficiency of *P. viticola's* inoculum. The proposed approach provided new insights into asexual spore behavior, advancing our understanding of infection dynamics. In this context, we also introduced a single-sporangia infection assay. Although specific to *P. viticola*, the proposed assay carries substantial potential for broader applications, thanks to the higher resolution and accuracy offered by cytometry compared to traditional methods. Expanding the application of this technique to related phytopathogenic oomycete species can unravel insights into infection mechanisms associated with other species. In particular, the integration with single-cell omics approaches opens new horizons for comprehensive molecular investigations aiming to deciphering virulence mechanisms, host-pathogen interactions, and evolutionary adaptations. Lastly, the high resolution and accuracy of the method, could provide a robust platform to assess the response of different pathogens to antifungal agents, thus accelerating fungicide discovery meanwhile providing insights into their mode of action.

In the second study, we introduced an accessible and open-source solution for disease severity estimation at the laboratory level using digital imagery and supervised machine learning. The research demonstrates the pipeline's effectiveness across diverse plant-pathogen systems, highlighting its adaptability and robustness. By addressing the limitations of existing tools, our study presented a user-friendly experience, empowering plant pathologists to perform computer vision tasks without requiring extensive technical expertise. In the next years, the widespread accessibility of computational resources, as well as rapid progress in machine learning and imaging technologies implementation will collectively mark a new era in phytopathometry. In this context, it is imperative for plant pathologists to assume a leading role in the development of these tools. Future developments of our platform will focus on enhancing its capabilities, in order to tackle complex disease scenarios, ensuring the pipeline remains responsive to evolving research needs and that these advancements remain accessible to a wider community.

In the third study, we evaluated the potential of peptide aptamers as anti-oomycetes compounds. In particular, the study identified and characterized two peptides with remarkable antimicrobial

activity towards several related phytopathogenic species. Moreover, the research also provided valuable insights into their effects on cellular structures and on mode of action. Although the preliminary results achieved look promising, further investigation on peptide specificity as well as eco-toxicity studies are required to fulfill the regulatory requirements. However, the wide application of such molecules in plant disease control needs to develop suitable formulations to ensure stability in the plant environment. For this reason, it is mandatory to assess the effectiveness of molecules arisen from this study under application conditions, either in greenhouse or field trials. Moreover, improvement on biotechnological platforms for peptide production are required to reduce the high cost of synthesis.